Supporting Information

A Lewis Acid-Controlled Enantiodivergent Epoxidation of Aldehydes

Aliakbar Mohammadlou,[§] Chetan Joshi,[‡] Brendyn P. Smith,[§] Li Zheng,[§] Stephanie A. Corio,[‡] Virginia M. Canestraight,[§] Saeedeh Torabikohlbouni,[§] S. Maryamdokht Taimoory,[†] Babak Borhan,[§] Richard Staples,[§] Mathew J. Vetticatt,[‡]* and William D. Wulff[§]*.

[§]Department of Chemistry, Michigan State University, East Lansing, MI 48824.

[†]Department of Chemistry, University of Michigan, Ann Arbor, MI 48109

[‡]Department of Chemistry, Binghamton University, Binghamton, NY 13902

vetticatt@binghamton.edu

wulff@chemistry.msu.edu

Table of Content

1. General Experimental

All reactions were performed in flame-dried glassware under an atmosphere of nitrogen unless otherwise indicated. Unless otherwise specified, all solvents were strictly dried before use: dichloromethane were distilled over calcium hydride under nitrogen; tetrahydrofuran, and toluene were distilled from sodium and benzophenone. Hexanes and ethyl acetate were ACS grade and used as purchased.

Melting points were recorded on a Thomas Hoover capillary melting point apparatus and are uncorrected. Varian Unity Plus 500 MHz spectrometer was used to record the ^{1}H NMR and ^{13}C NMR spectra using $CDCl_3$ as solvent. The residual peak of $CDCl_3$ or TMS was used as the internal standard for both ^{1}H NMR (δ = 7.26 ppm for $CDCl_3$ or δ = 0 ppm for TMS) and ^{13}C NMR (δ = 77.0 ppm). Chemical shifts were reported in parts per million (ppm). Analytical thin-layer chromatography (TLC) was performed on Silicycle silica gel plates with F-254 indicator. Visualization was by short wave (254 nm) and long wave (365 nm) ultraviolet light, or by staining with phosphomolybdic acid in ethanol. Column chromatography was performed with silica gel 60 (230 – 450 mesh). HPLC analyses were performed using Agilent 1100 or 1260 HPLC System with CHIRALCEL® OD-H and PIRKLE COVALENT (*R,R*) WHELK-O 1 columns. HPLC grade hexanes (mixture of isomers) and 2-propanol were used for HPLC analyses. Optical rotations were obtained at a wavelength of 589 nm (sodium D line) using a 1.0 decimeter cell with a total volume of 1.0 ml. Specific rotations are reported in degrees per decimeter at 20 °C and the concentrations are given in gram per 100 mL in spectral grad $CHCl_3$ unless otherwise noted. IR spectra were

recorded on NaCl disc (for liquids) on a Nicolet IR/42 spectrometer. High Resolution Mass Spectrometry was performed in the Department of Chemistry at Michigan State University Mass Facility. Aldehydes were purchased from Sigma-Aldrich, Alfa-Aesar, Combi-Blocks or Oakwood and were purified by distillation or sublimation unless otherwise indicated. $AlMe_3$ was purchased from Sigma-Aldrich as a 2 M solution in toluene and was used as received. VANOL, VAPOL and their derivatives were made according to published procedures.[1-4]

2. Optimization of the epoxidation of 3-silyloxypropanal 2 with the VANOL-Boron catalyst

Epoxidation with VANOL-boron catalyst was subjected to re-optimization involving changes in the catalyst loading, temperature and the amount of DMSO used in catalyst generation (Table S1). The results reveal that the yield could not be enhanced to any satisfactory level unless the catalyst loading was increased to 20 mol% (entries 6-8). Interestingly, increasing the temperature from –40 to 0 °C did not result in any significant change in the yield although the amount of the β-ketoamide side-product 15 doubled (entries 4 vs 5 and 6 vs 7). Removing the DMSO from the catalyst preparation did enhance the yield but the asymmetric induction dropped from 66% to 56% ee (entries 6 vs 8). The use of the VAPOL ligand 17 did not give a useful reaction (entry 11). The *t*-butyldiphenylsilyl substituted aldehyde 2b did give a reasonable yield at 10 mol% catalyst (entries 4 vs 12) but the yield and induction were not improved at 20 mol% catalyst (entries 8 vs 13).

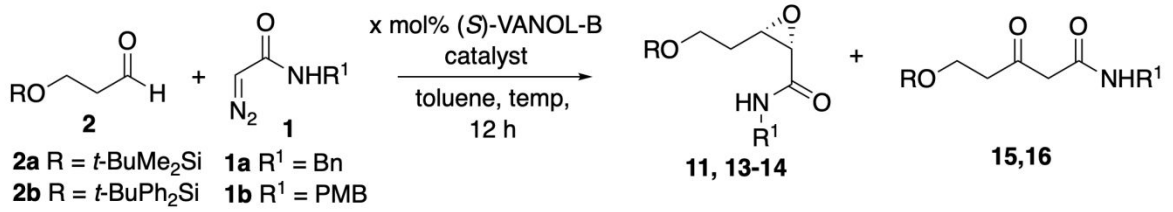

2a R = *t*-BuMe$_2$Si **1a** R^1 = Bn
2b R = *t*-BuPh$_2$Si **1b** R^1 = PMB

Optimization of the epoxidation of 3-silyloxypropanal **2** with the VANOL-Boron catalyst. [a]

entry	R	R^1	catalyst (x mol%)	Me$_2$SO (2x mol%)	temp (°C)	% conv [b]	epoxide	% yield epoxide [c]	%ee epoxide	% yield **15,16** [d]
1	TBS	Bn	5	0	–40	15	**11**	(12)	nd	nd
2	TBS	Bn	5	10	–40	10	**11**	(<5)	nd	nd
3	TBS	PMB	5	0	–40	9	**13**	(<5)	nd	nd
4	TBS	PMB	10	20	0	16	**13**	(11)	nd	nd
5	TBS	PMB	10	20	–40	9	**13**	(<5)	nd	nd
6	TBS	PMB	20	40	0	99	**13**	47	66	34 [e]
7	TBS	PMB	20	40	–40	72	**13**	51	65	17 [e]
8	TBS	PMB	20	0	0	90	**13**	63	78	4 [e]
9 [f]	TBS	PMB	20	0	0	80	**13**	47	78	32 [e]
10 [g]	TBS	PMB	20	0	0	95	**13**	46	30	10 [e]
11 [h]	TBS	PMB	10	0	0	21	**13**	(19)	nd	nd
12	TBDPS	PMB	10	20	0	87	**14**	44	50	24 [i]
13	TBDPS	PMB	20	0	0	99	**14**	65	52	34 [i]

[a] Unless otherwise specified, all reactions were carried out in toluene at 0.1 M in diazo compound **1** (0.5 mmol) with 1.2 equiv of **2**. The catalytst was prepared as indicated in Scheme 2. [b] Determined by ^{1}H NMR with Ph$_3$CH as internal standard. [c] Isolated yield. ^{1}H NMR yields are in given in parenthesis with Ph$_3$CH as internal standard. [d] Isolated yields. [e] Ketoamide **15**. [f] Reaction with 4 equiv of **2a**. [g] Catalyst prepared from (*R*)-VAPOL **17** and *ent*-**13** was formed. [h] Catalyst prepared from (*S*)-VAPOL **17** [i] Ketoamide **16.**

Table S1: Optimization of the epoxidation of 3-silyloxypropanal **2** with the VANOL-Boron catalyst.

3. Epoxidation reaction catalyzed by aluminum-lithium-VANOL catalyst S-1

Reacting 1.0 equiv of $LiAlH_4$ with 2.0 equiv of (*R*)-VANOL **10** produced heterobimetallic aluminum-lithium-VANOL complex (ALV) **S-1**. The BINOL version of this catalyst has been reported by Shibasaki to be effective in a number of asymmetric catalytic reactions.[5,6] Unfortunately, no product was observed after conducting the epoxidation of benzaldehyde with diazo acetamide **1c** the presence of 10 mol% ALV catalyst **S-1** (Scheme S1).

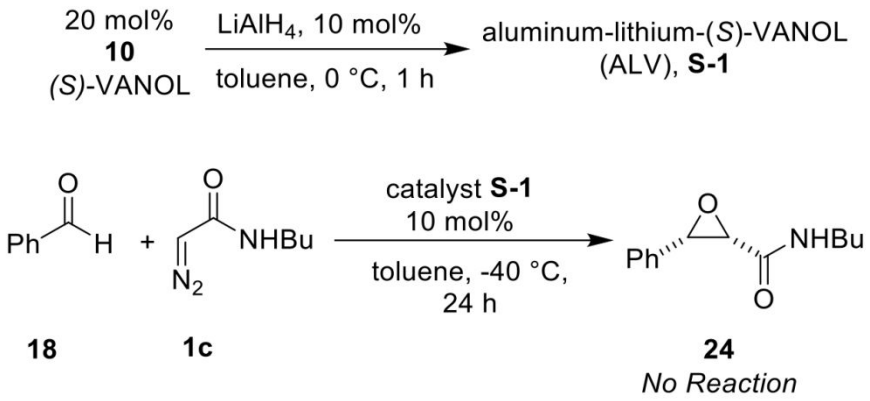

Scheme S1: Epoxidation reaction catalyzed by aluminum-lithium-(*S*)-VANOL

4. Temperature optimization in the epoxidation of benzaldehyde 18

Surprisingly, when the epoxidation reaction was performed with the aluminum catalyst **47** which was prepared from $AlMe_3$ (1.0 equiv.) and VANOL **10** (2.0 equiv.), a 19% yield (NMR) was obtained of the desired epoxide **24** at -40 ˚C (Table S2, entry 1). Further optimization of the temperature revealed the optimum temperature for this reaction to be 0 ˚C which gave the epoxide in 80% yield and 72% *ee* (Table S2, entry 3). Higher temperatures are detrimental to the yield of the reaction presumably due to a competing Roskamp reaction although a study of this was not pursued (entry 4). Interestingly, the enantiomeric excess of the epoxide was not affected by altering the temperature of the reaction.

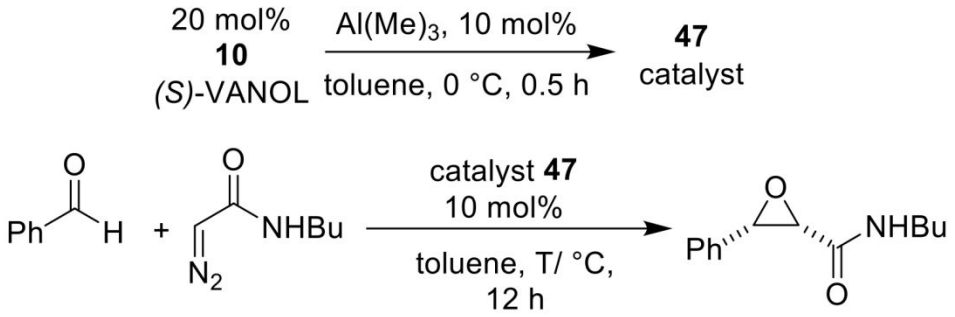

entry	T/°C	isolated yield%	ee%
1	-40 °C	19[1]	*not determined*
2	-20 °C	57	72
3	0 °C	80	72
4	25 °C	62	72

Unless otherwise specified, all of the reactions were done in toluene at 0 °C for 12 h with 0.5 mmol of diazo compound **1c** and 0.6 mmol of aldehyde. 1. NMR yield

Table S2: Temperature optimization in aluminum catalyzed epoxidation reaction.

5. Solvent and ligand optimization

Next, we turned our attention to the optimization of the solvent system. CH_2Cl_2 was as effective as toluene and produced epoxide **24** with comparable results (Table S3, entry 2). However, solvents containing heteroatoms such as THF and acetonitrile delivered the epoxide in poor yields (entry 3 and 4). These solvents are presumably coordinating to the catalyst and preventing the coordination of aldehyde, and thus stopping the reaction. BINOL did not perform well in this reaction and gave the epoxide in 60% yield and only 4% *ee* (entry 5). The catalyst generated from 7,7'-*t*Bu_2VANOL **S-2** produced epoxide **24** in higher *ee* compared with VANOL but in moderate

yield (entry 1 vs 6). We were delighted to observe excellent yield and excellent *ee* while conducting the reaction with the catalyst derived from the VAPOL ligand **17** (entry 7). Ligand **S-3** also performed excellently and afforded the epoxide in 88% yield and 99% *ee* (entry 8).

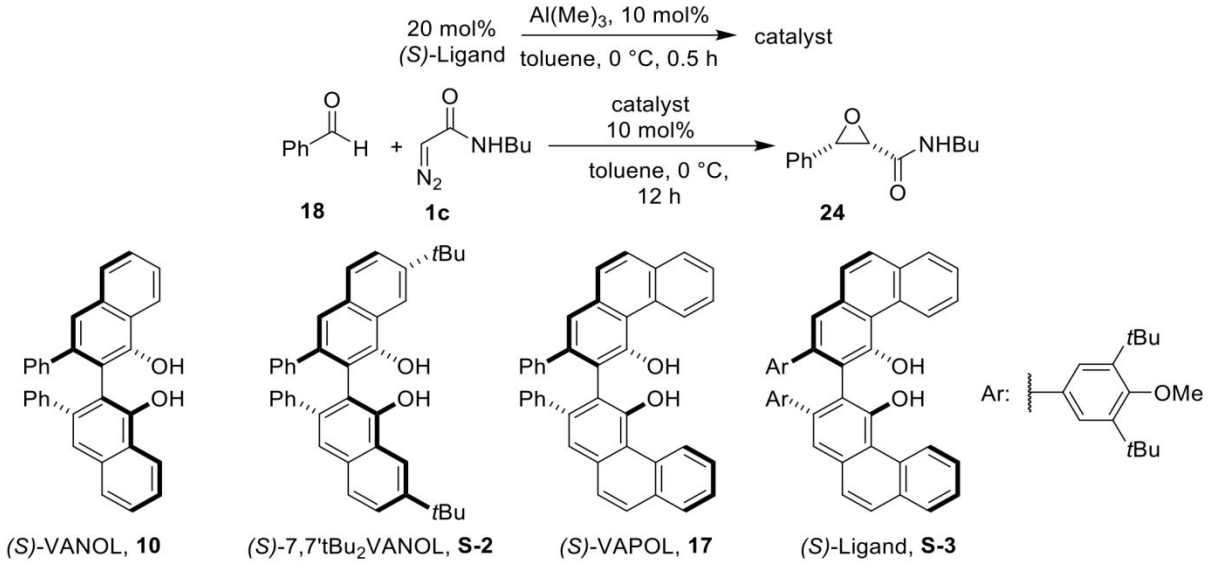

entry	Ligand	Solvent	isolated yield%	ee%
1	*(S)*-VANOL, **10**	toluene	80	72
2	*(S)*-VANOL, **10**	DCM	80	72
3	*(S)*-VANOL, **10**	THF	46	84
4	*(S)*-VANOL, **10**	MeCN	6[1]	*N.D.*
5	*(S)*-BINOL	toluene	60	4
6	*(S)*-7,7'tBu$_2$VANOL, **S-2**	toluene	46	84
7	*(S)*-VAPOL, **17**	toluene	81	98
8	*(S)*-Ligand, **S-3**	toluene	88	99

Unless otherwise specified, all of the reactions were done in toluene at 0 °C for 12 h with 0.5 mmol of diazo compound **1c** and 0.6 mmol of aldehyde.
1. NMR yield

Table S3: Optimization of the epoxidation of 3-silyloxypropanal **2** with the VANOL-Boron catalyst.

6. Optimization of catalyst loading and diazo compound

Decreasing the catalyst loading to 5 mol% produced similar results (Table S4, entry 1 vs 2). With 2.5 mol% catalyst loading, the reaction worked fine albeit with a slight deterioration in *ee* and yield (entry 3). However, conducting the reaction with 1 mol% catalyst loading resulted in only 30% NMR yield (entry 4).

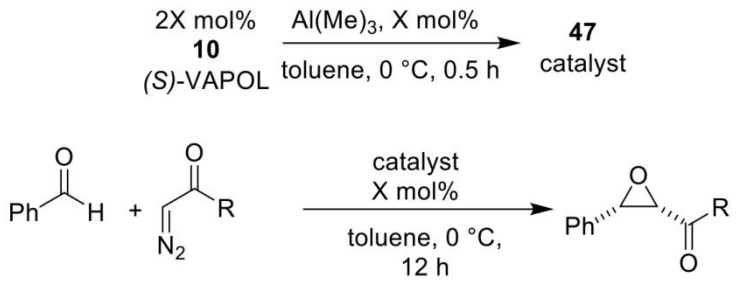

18 **1** **24**

entry	R	cat. loading%	Isolated yield%	ee%
1	**1c**, NHBu	10	81	98
2	**1c**, NHBu	5	86	97
3	**1c**, NHBu	2.5	61	95
4[1]	**1c**, NHBu	1	30[2]	*not determined*
6[3]	**1a**, NHBn	5	84	99
7[3]	**S-4**, NHPh	5	59	99
8[3]	**S-5**, OEt	5	*not determined*	*not determined*

Unless otherwise specified, all of the reactions were done in toluene at 0 °C for 12 h with 0.5 mmol of diazo compound **1** and 0.6 mmol of aldehyde. 1. The reaction was quenched after 21 h. 2. NMR yield. 3. The reaction was quenched after 3 h

Table S4: Study of catalyst loading and diazo compound.

Different diazo compounds were also evaluated during the course of epoxidation and it turned out that the N-benzyl diazo acetamide **1a** is the optimum reagent (entry 6). The reaction with N-phenyl diazo acetamide **S-4** produced epoxide with high enantioinduction but with lower yield presumably because of its poor solubility in toluene (Table S4, entry 7). In contrast, no product was detected when the reaction was carried out with ethyl diazo acetate **S-5** instead the alkylated VAPOL ligand was observed in the crude mixture of the reaction.

7. The effect of DMSO in aluminum catalyzed epoxidation of aldehyde 18

Previously, we have demonstrated that DMSO had a profound effect on the epoxidation of aldehydes with diazo acetamides. The effect of DMSO was also examined in epoxidation reaction catalyzed by aluminum catalyst (Scheme S2). The reaction was conducted in the presence of 10 mol% DMSO, interestingly, no change in the *ee* of the epoxide was observed although a slight decrease in yield was observed (Scheme S2, vs Table S3 entry 1).

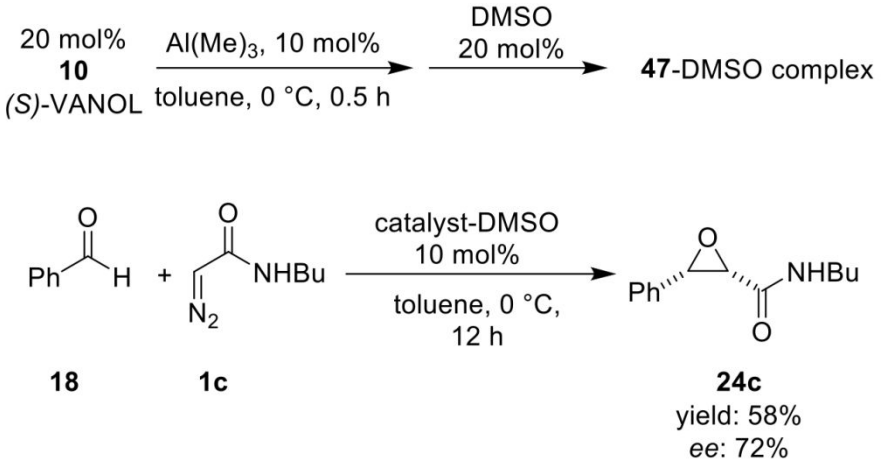

Scheme S2: Epoxidation reaction catalyzed by aluminum-VANOL-DMSO complex

8. General procedure 1: Asymmetric catalytic epoxidation reaction

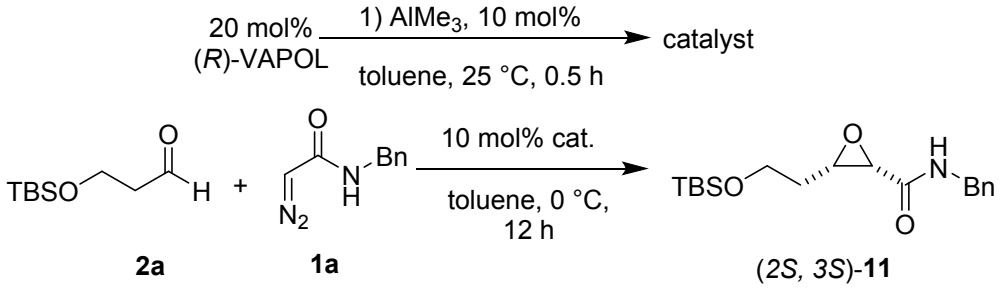

General procedure for preparation of catalyst stock solution: A flame dried 25 mL round bottom flask filled with nitrogen was charged with (*R*)-VAPOL (0.149 mmol, 82.0 mg) and toluene (3 mL). The resulting mixture was stirred at room temperature for 5 minutes until the ligand was fully dissolved then $AlMe_3$ (0.075 mmol, 38 µL, 2M solution in toluene) was added and the reaction mixture was stirred at room temperature for 30 minutes.

General procedure for the epoxidation reaction catalyzed with aluminum-VAPOL catalyst:

(2S,3S)-3-(2-((tert-butyldimethylsilyl)oxy)ethyl)-N-benzyl-oxirane-2-carboxamide ***11****:* Another flame dried round bottom flask filled with nitrogen was charged with *N*-benzyl diazo acetamide (0.49 mmol, 88 mg) **1a**, toluene (3 mL) and aldehyde 3-t-butyldimethylsilyloxypropanal (0.591 mmol, 127 µL) **2a**. The obtained cloudy mixture and the catalyst stock solution prepared from (*S*)-VAPOL were cooled down to 0 ˚C and stirred at 0 ˚C for 10 min. Then 2 mL of catalyst stock solution was transferred to the round bottom flask containing the starting materials using syringe and the obtained mixture was stirred at 0 ˚C for 12 h. Then the reaction was quenched by adding 1 mL of methanol followed by transferring the crude mixture of reaction to a 50 mL round bottom flask and evaporating the solvent under reduced pressure. The crude epoxide was purified via column chromatography (20 x 250 mm, 3:1 to 1:1 hexane: ethyl acetate as eluent) and epoxide **11**

was obtained as a yellowish oil in 80% (0.399 mmol, 142 mg) isolated yield. The enantiomeric excess of epoxide **11** was determined to be 96% with chiral HPLC (PIRKLE COVALENT (*R,R*) WHELK-O 1 column, 94:6 hexane/2-propanol at 228 nm, flow-rate: 1 mL/min): retention times: R_t = 18.9 min (major enantiomer, ent-**11**) and R_t = 21.6 min (minor enantiomer, **11**).

Spectral data for epoxide **11**: ^{1}H NMR (500 MHz, Chloroform-*d*) δ 0.05 (s, 6H), 0.89 (s, 9H), 1.64 (ddt, *J* = 14.2, 7.4, 5.8 Hz, 1H), 1.81 (dtd, *J* = 14.3, 6.5, 4.9 Hz, 1H), 3.36 (dt, *J* = 7.5, 4.8 Hz, 1H), 3.57 (d, *J* = 4.8 Hz, 1H), 3.76 (t, *J* = 6.2 Hz, 2H), 4.39 – 4.52 (m, 2H), 6.49 (t, *J* = 6.1 Hz, 1H), 7.21 – 7.32 (m, 3H), 7.28 – 7.37 (m, 2H). ^{13}C{^{1}H} NMR (126 MHz, Chloroform-*d*) δ -5.34, -5.31, 15.39, 18.35, 25.96, 31.19, 43.09, 55.10, 56.41, 60.00, 127.84, 128.01, 128.89, 137.67, 167.34. IR: 3305brs, 2928w, 1660s, 1096s, 881s, 775s, 729m, 698s. HRMS (ESI-TOF) *m/z* 336.2039, [(M+H$^+$); calcd for $C_{18}H_{30}NO_3Si$: 336.1994].

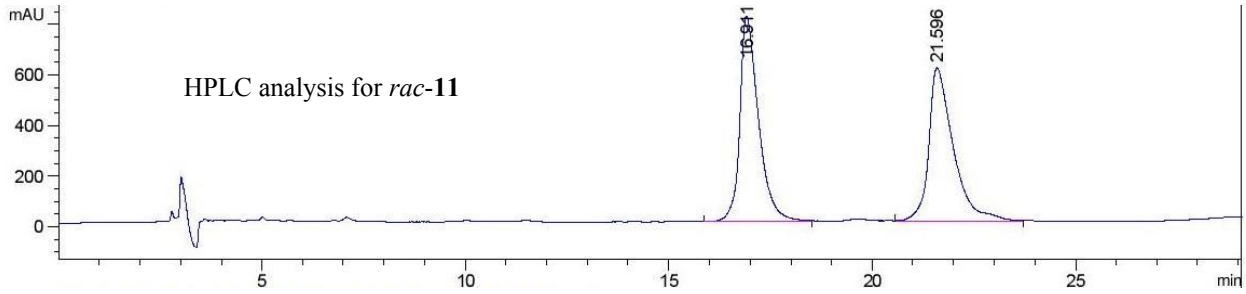

Peak #	RetTime [min]	Type	Width [min]	Area [mAU*s]	Height [mAU]	Area %
1	16.911	BV	0.4665	2.60566e4	811.68579	50.6110
2	21.596	BV	0.5764	2.54275e4	604.91522	49.3890

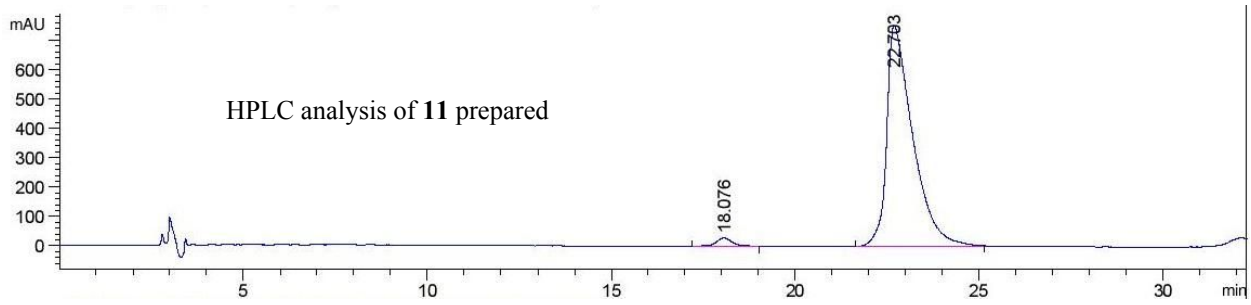

Peak #	RetTime [min]	Type	Width [min]	Area [mAU*s]	Height [mAU]	Area %
1	18.076	BB	0.4658	954.87958	28.87431	2.4896
2	22.703	VV	0.6621	3.73994e4	752.14655	97.5104

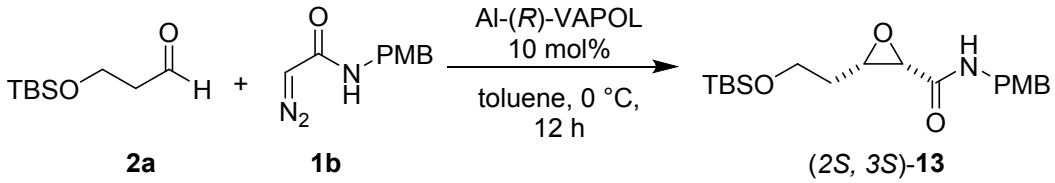

2a **1b** (*2S, 3S*)-**13**

*(2S,3S)-3-(2-((tert-butyldimethylsilyl)oxy)ethyl)-N-(4-methoxybenzyl)oxirane-2-carboxamide **13**: (Table 1, entry 7):* Epoxide **13** was synthesized from aldehyde **2a** (0.591 mmol, 127 µL) and diazo compound **1b** (0.499 mmol, 103 mg) catalyzed by aluminum-(*R*)-VAPOL catalyst prepared with the general procedure with a 12 h reaction time. The crude product was purified via column chromatography (20 x 250 mm, 3:1 to 1:1 hexane: ethyl acetate as eluent) and epoxide **13** was obtained as a yellowish oil in 87% (0.435 mmol, 159 mg) isolated yield. The enantiomeric excess of epoxide **13** was determined to be 95% with chiral HPLC (PIRKLE COVALENT (*R,R*) WHELK-O 1 column, 90:10 hexane/2-propanol at 228 nm, flow-rate: 1 mL/min): retention times: R_t = 19.24 min (major enantiomer, ent-**13**) and R_t = 25.98 min (minor enantiomer, **13**).

Spectral data for epoxide **13**: ^{1}H NMR (500 MHz, Chloroform-*d*) δ 0.03 (m, 6H), 0.88 (s, 9H), 1.61 (ddt, *J* = 14.2, 7.5, 5.8 Hz, 1H), 1.71 – 1.84 (m, 1H), 3.34 (dt, *J* = 7.5, 4.8 Hz, 1H), 3.55 (d, *J* = 4.8 Hz, 1H), 3.71 – 3.81 (m, 5H), 4.38 (d, *J* = 5.9 Hz, 2H), 6.40 (t, *J* = 6.2 Hz, 1H), 6.82 – 6.89 (m, 2H), 7.15 – 7.23 (m, 2H). ^{13}C{^{1}H}NMR (126 MHz, Chloroform-*d*) δ -5.45, -5.42, 18.24, 25.85, 31.06, 42.43, 54.97, 55.27, 56.27, 59.89, 114.11, 129.25, 129.26, 129.64, 167.08. HRMS (ESI-TOF) *m/z* 366.2136, [(M+H^{+}); calcd for $C_{19}H_{32}NO_4Si$: 366.2100]. IR: 3310 brs, 2950w, 1654s, 1512s, 1247s, 1094s, 830s, 778s. $[\alpha]^{20}_{D}$ (*c* 1.0, $CHCl_3$): 0.0481.

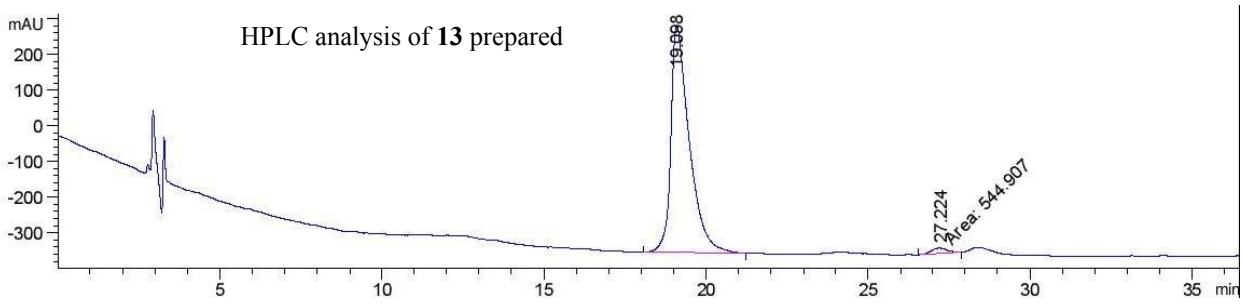

Peak #	RetTime [min]	Type	Width [min]	Area [mAU*s]	Height [mAU]	Area %
1	19.100	BB	0.5447	3385.00781	88.79678	97.9873
2	27.146	MM	0.5293	69.52958	2.18919	2.0127

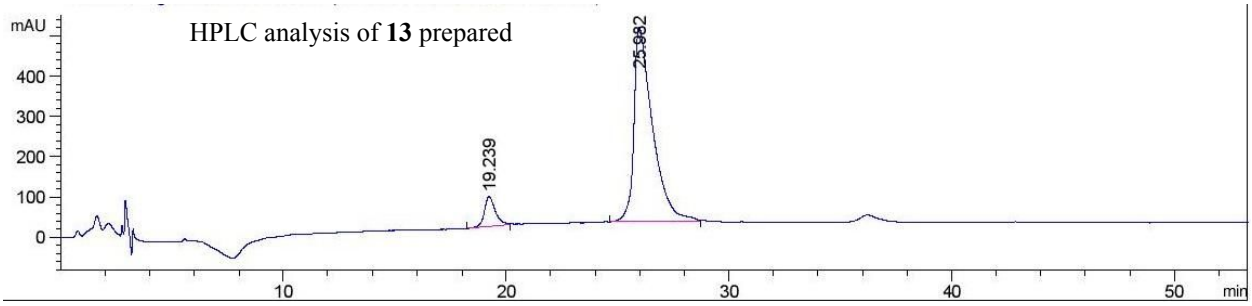

Peak #	RetTime [min]	Type	Width [min]	Area [mAU*s]	Height [mAU]	Area %
1	19.239	BV	0.4904	2550.96973	74.71109	8.2485
2	25.982	VV	0.7682	2.83755e4	483.83984	91.7515

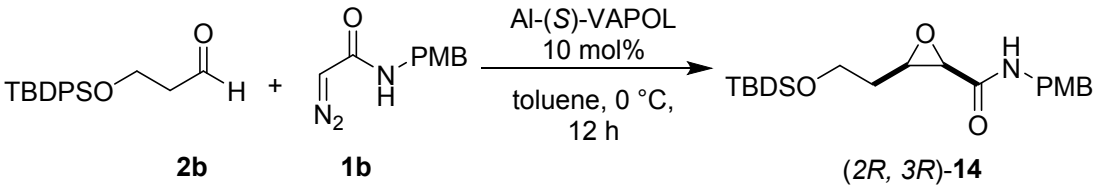

2b **1b** (*2R, 3R*)-**14**

(2R,3R)-3-(2-((tert-butyldiphenylsilyl)oxy)ethyl)-N-(4-methoxybenzyl)oxirane-2-carboxamide ***14*** *(Table 1, entry 8):* Epoxide **14** was synthesized from aldehyde **2b** (0.599 mmol, 188 mg) and diazo compound **1b** (0.499 mmol, 103 mg) catalyzed by aluminum-(*S*)-VAPOL catalyst prepared with the general procedure with a 12 h reaction time. The crude product was purified via column chromatography (20 x 250 mm, 3:1 to 1:1 hexane: ethyl acetate as eluent) and epoxide **14** was obtained as a yellowish oil in 77% (0.385 mmol, 188) isolated yield. The enantiomeric excess of epoxide **14** was determined to be 94% with chiral HPLC (PIRKLE COVALENT (*R,R*) WHELK-O 1 column, 93:7 hexane/2-propanol at 228 nm, flow-rate: 1 mL/min): retention times: R_t = 33.7 min (minor enantiomer, ent-**14**) and R_t = 48.8 min (major enantiomer, **14**).

Spectral data for epoxide **14**: ^{1}H NMR (500 MHz, Chloroform-*d*) δ 1.07 (s, 9H), 1.07, 1.56 – 1.67 (m, 1H), 1.89 (dddd, *J* = 14.3, 7.1, 5.9, 4.5 Hz, 1H), 3.40 – 3.54 (m, 1H), 3.57 (d, *J* = 4.8 Hz, 1H), 3.78 (s, 3H), 3.77 – 3.87 (m, 2H), 4.37 (d, *J* = 5.9 Hz, 2H), 6.37 (t, *J* = 5.9 Hz, 1H), 6.81 – 6.90 (m, 2H), 7.14 – 7.21 (m, 2H), 7.36 – 7.43 (m, 4H), 7.40 – 7.48 (m, 2H), 7.63 – 7.70 (m, 4H). ^{13}C{^{1}H}NMR (126 MHz, Chloroform-*d*) δ 15.41, 19.28, 26.90, 30.98, 42.52, 55.09, 55.37, 56.41, 60.96, 65.98, 114.23, 127.84, 127.85, 129.35, 129.75, 129.85, 129.87, 133.51, 133.54, 135.64, 159.24, 167.19. HRMS (ESI-TOF) *m/z* 490.243, [(M+H$^+$); calcd for $C_{29}H_{36}NO_4Si$: 490.2413]. $[\alpha]^{20}_D$ (*c* 1.0, $CHCl_3$): -0.403.

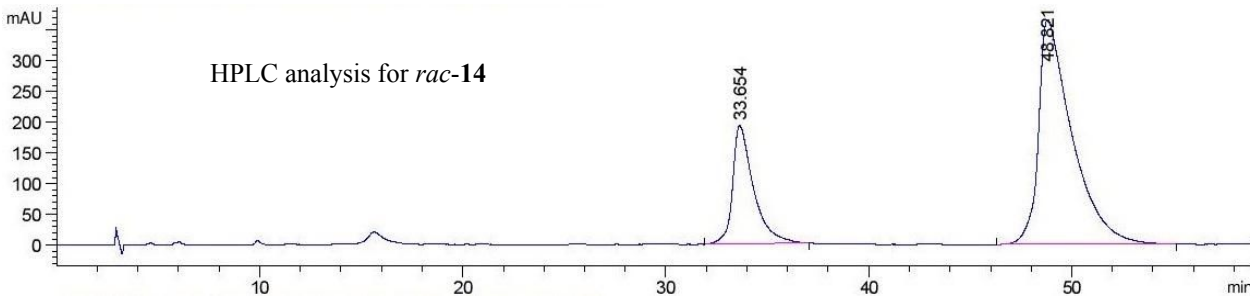

Peak #	RetTime [min]	Type	Width [min]	Area [mAU*s]	Height [mAU]	Area %
1	33.654	BB	1.0054	1.38466e4	192.46220	24.6439
2	48.821	BB	1.4985	4.23401e4	366.29782	75.3561

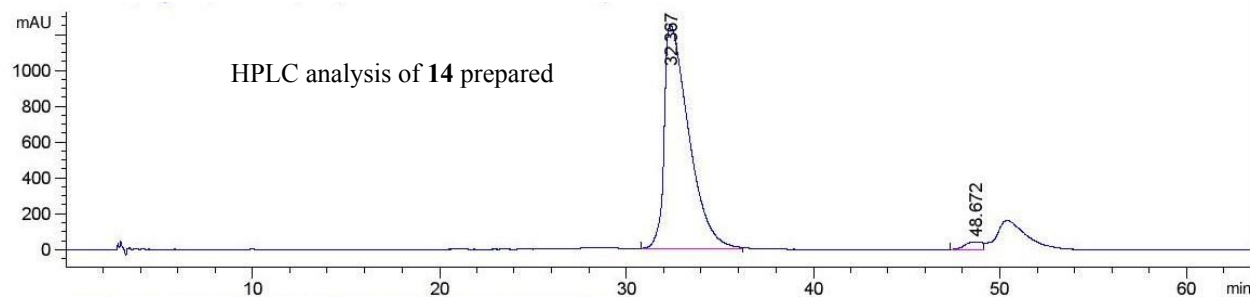

Peak #	RetTime [min]	Type	Width [min]	Area [mAU*s]	Height [mAU]	Area %
1	32.367	VV	1.0856	1.14078e5	1253.65527	97.7220
2	48.672	BV	0.7357	2659.27246	42.51522	2.2780

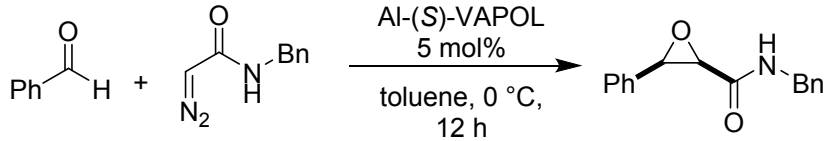

18 **1a** (*2R, 3R*)-**24a**

*(2R,3R)-3-phenyl-N-benzyl-oxirane-2-carboxamide **24a**:* Epoxide **24a** was synthesized from benzaldehyde **18** (0.59 mmol, 62 µL) and diazo compound **1a** (0.49 mmol, 88 mg) catalyzed by aluminum-(*S*)-VAPOL catalyst prepared with the general procedure with a 12 h as the reaction

time. The crude product was purified via column chromatography (20 x 250 mm, 3:1 to 1:1 hexane: ethyl acetate as eluent) and epoxide **24a** was obtained as a white solid in 97% (0.485 mmol, 123 mg) isolated yield. The enantiomeric excess of epoxide **24a** was determined to be 99% with chiral HPLC (PIRKLE COVALENT (*R,R*) WHELK-O 1 column, 90:10 hexane/2-propanol at 228 nm, flow-rate: 1 mL/min): retention times: R_t = 31.4 min (minor enantiomer, ent-**24a**) and R_t = 43.24 min (major enantiomer, **24a**).

Spectral data for epoxide **24a**: ^{1}H NMR (500 MHz, Chloroform-*d*) δ 7.40 – 7.27 (m, 5H), 7.24 – 7.13 (m, 3H), 6.75 – 6.69 (m, 2H), 6.19 (s, 1H), 4.38 – 4.27 (m, 2H), 4.07 (dd, *J* = 14.9, 4.9 Hz, 1H), 3.85 (d, *J* = 4.8 Hz, 1H). ^{13}C{^{1}H}NMR (126 MHz, Chloroform-*d*) ^{13}C NMR (126 MHz, Chloroform-*d*) δ 42.80, 56.46, 58.40, 126.67, 127.42, 127.53, 128.63, 128.66, 133.15, 137.11, 166.24. These spectral data are in good agreement with literature values.[7]

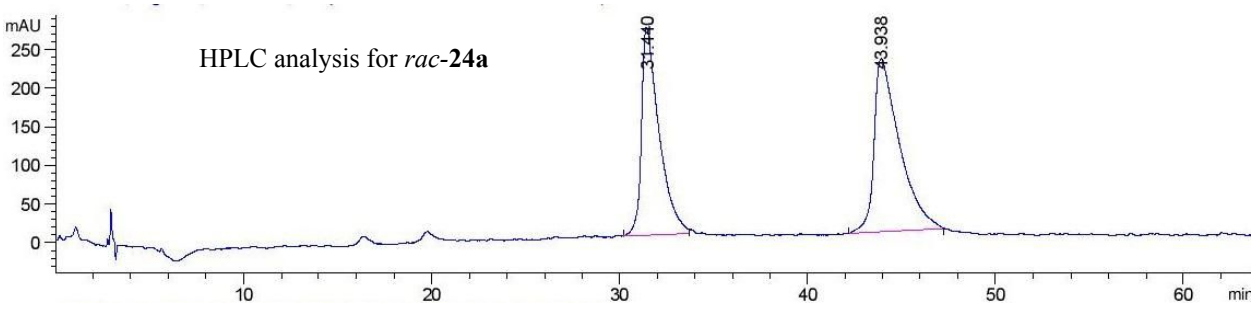

Peak #	RetTime [min]	Type	Width [min]	Area [mAU*s]	Height [mAU]	Area %
1	31.440	VV	0.8574	1.76355e4	269.50815	45.2891
2	43.938	BV	1.1202	2.13044e4	224.28755	54.7109

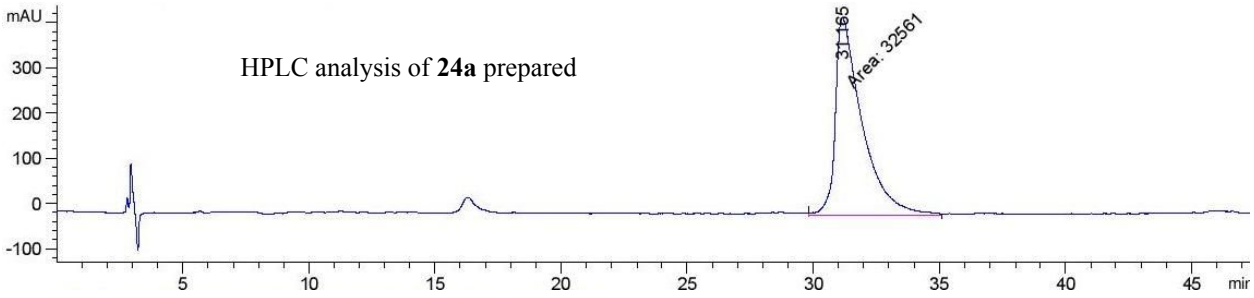

Peak #	RetTime [min]	Type	Width [min]	Area [mAU*s]	Height [mAU]	Area %
1	31.165	MM	1.2377	3.25610e4	438.44531	100.0000

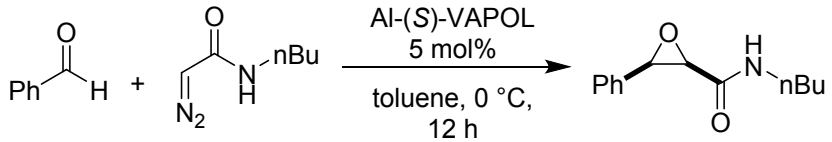

18 **1c** (*2R, 3R*)-**24c**

*(2R,3R)-3-phenyl-N-(n-butyl)oxirane-2-carboxamide **24c**:* Epoxide **24c** was synthesized from benzaldehyde **18** (0.59 mmol, 62 μL) and diazo compound **1c** (0.50 mmol, 74 mg) catalyzed by aluminum-(*S*)-VAPOL catalyst prepared with the general procedure with a 12 h reaction time. The crude product was purified via column chromatography (20 x 250 mm, 3:1 to 1:1 hexane: ethyl acetate as eluent) and epoxide **24c** was obtained as a white solid in 86% (0.43 mmol, 94 mg) isolated yield. The enantiomeric excess of epoxide **24c** was determined to be 97% with chiral HPLC (PIRKLE COVALENT (*R,R*) WHELK-O 1 column, 93:7 hexane/2-propanol at 228 nm, flow-rate: 1 mL/min): retention times: R_t = 24.63 min (minor enantiomer, ent-**24c**) and R_t = 31.46 min (major enantiomer, **24c**).

Spectral data for epoxide **24c**: ^{1}H NMR (500 MHz, Chloroform-*d*) δ 0.65 (t, J = 7.5 Hz, 3H), 0.80-1.00 (m, 4H), 2.75-2.83 (m, 1H), 2.98-3.07 (m, 1H), 3.70 (d, J = 5.0 Hz, 1H), 4.24 (d, J = 5.5 Hz, 1H), 5.85 (brs, 1H), 7.20-7.32 (m, 5H); ^{13}C{^{1}H}NMR (126 MHz, Chloroform-*d*) δ 13.62, 19.67, 31.23, 38.26, 56.34, 58.12, 126.54, 128.36, 128.43, 133.23, 166.02. These spectral data are in good agreement with literature values.[7]

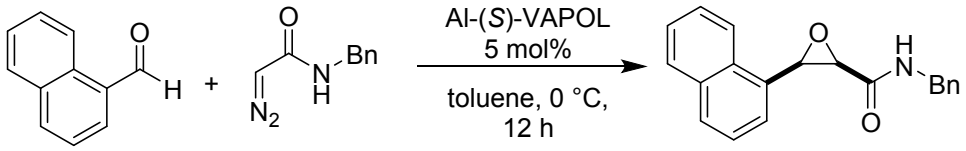

19 **1a** (*2R, 3R*)-**25a**

(2R, 3R)-3-(naphthalene-1-yl)-N-benzyl-oxirane-2-carboxamide ***25a****:* Epoxide **25a** was synthesized from 1-naphthalencarboxaldehyde **19** (0.60 mmol, 82 μL) and diazo compound **1a** (0.50 mmol, 88 mg) catalyzed by aluminum-(*S*)-VAPOL catalyst prepared with the general procedure with a 12 h reaction time. The crude product was purified via column chromatography (20 x 250 mm, 3:1 to 1:1 hexane: ethyl acetate as eluent) and epoxide **25a** was obtained as a white solid in 93% isolated yield (0.465 mmol, 141 mg). The enantiomeric excess of epoxide **25a** was determined to be 99% with chiral HPLC (PIRKLE COVALENT (*R,R*) WHELK-O 1 column, 85:15 hexane/2-propanol at 228 nm, flow-rate: 1 mL/min): retention times: R_t = 22.25 min (minor enantiomer, ent-**25a**) and R_t = 64.47 min (major enantiomer, **25a**). mp: 92-93 ˚C.

Spectral data for epoxide **25a**: ^{1}H NMR (500 MHz, Chloroform-*d*) δ 3.94 (dd, *J* = 15.0, 4.9 Hz, 1H), 4.10 (d, *J* = 4.7 Hz, 1H), 4.22 (dd, *J* = 15.0, 7.1 Hz, 1H), 4.72 (d, *J* = 4.7 Hz, 1H), 6.06 (d, *J* = 6.1 Hz, 1H), 6.43 – 6.49 (m, 2H), 6.98 – 7.05 (m, 2H), 7.07 – 7.14 (m, 1H), 7.33 (dd, *J* = 8.2, 7.0 Hz, 1H), 7.48 (dt, *J* = 7.1, 1.2 Hz, 1H), 7.56 (dddd, *J* = 19.5, 8.1, 6.8, 1.4 Hz, 2H), 7.83 (dd, *J*

= 8.3, 1.2 Hz, 1H), 7.87 – 7.93 (m, 1H), 8.10 – 8.16 (m, 1H). $^{13}C\{^{1}H\}$NMR (126 MHz, Chloroform-*d*) δ 42.66, 56.40, 57.75, 123.76, 124.66, 125.12, 126.58, 127.07, 127.18, 127.22, 128.46, 128.67, 129.16, 129.42, 131.18, 133.44, 137.05, 166.44. IR: 3334brs, 1651s, 1528s, 772m, 742s, 762s, 606s. HRMS (ESI-TOF) *m/z* 304.1404, [(M+H$^+$); calcd for $C_{20}H_{18}NO_2$: 304.1337]. $[\alpha]^{20}_D$ (*c* 1.0, $CHCl_3$): 1.2002.

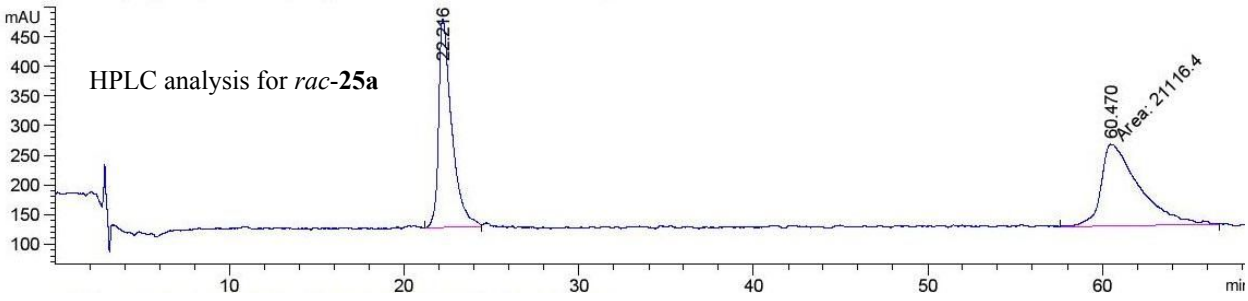

Peak #	RetTime [min]	Type	Width [min]	Area [mAU*s]	Height [mAU]	Area %
1	22.216	VV	0.6780	1.84987e4	352.62619	46.6960
2	60.470	MM	2.5464	2.11164e4	138.21289	53.3040

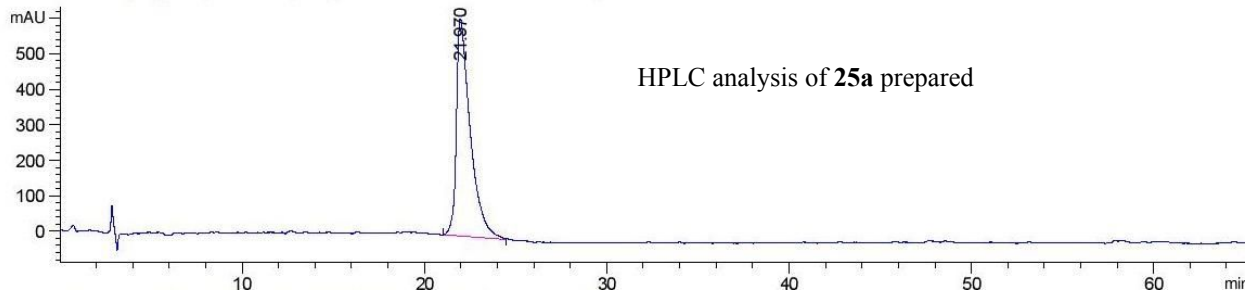

Peak #	RetTime [min]	Type	Width [min]	Area [mAU*s]	Height [mAU]	Area %
1	21.970	BV	0.7094	3.26369e4	612.77002	100.0000

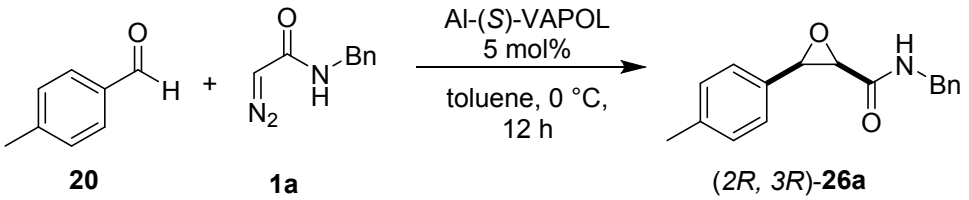

20 **1a** (*2R, 3R*)-**26a**

(2R, 3R)-3-(4-methyl-phenyl)-N-benzyl-oxirane-2-carboxamide ***26a****:* Epoxide **26a** was synthesized from aldehyde *para*-tolylaldehyde **20** (0.60 mmol, 71 μL) and diazo compound **1a** (0.50 mmol, 88 mg) catalyzed by aluminum-(*S*)-VAPOL catalyst prepared with the general procedure with a 12 h reaction time. The crude product was purified via column chromatography (20 x 250 mm, 3:1 to 1:1 hexane: ethyl acetate as eluent) and epoxide **26a** was obtained as a white solid in 76% isolated yield (0.379 mmol 102 mg). The enantiomeric excess of epoxide **26a** was determined to be 99% with chiral HPLC (PIRKLE COVALENT (*R,R*) WHELK-O 1 column, 90:10 hexane/2-propanol at 228 nm, flow-rate: 1 mL/min): retention times: R_t = 30.45 min (minor enantiomer, ent-**26a**) and R_t = 45.1 min (major enantiomer, **26a**). mp: 76-77 ˚C.

Spectral data for epoxide **26a**: ^{1}H NMR (500 MHz, Chloroform-*d*) δ 2.36 (s, 3H), 3.82 (d, *J* = 4.7 Hz, 1H), 4.04 (dd, *J* = 14.9, 4.9 Hz, 1H), 4.28 – 4.40 (m, 2H), 6.18 (t, *J* = 6.1 Hz, 1H), 6.68 – 6.74 (m, 2H), 7.09 (d, *J* = 7.9 Hz, 2H), 7.11 – 7.19 (m, 2H), 7.15 – 7.23 (m, 3H), 7.24 – 7.34 (m, 0H). ^{13}C{^{1}H}NMR (126 MHz, Chloroform-*d*) δ 21.41, 42.77, 56.49, 58.36, 126.56, 127.33, 127.55, 127.91, 128.47, 128.79, 129.29, 130.11, 137.18, 138.33, 166.39. IR: 3290brs, 1659s, 1532s, 696s. HRMS (ESI-TOF) *m/z* 268.1374, [(M+H$^+$); calcd for $C_{17}H_{18}NO_2$: 268.1337] $[\alpha]^{20}_D$ (*c* 1.0, $CHCl_3$): 0.273.

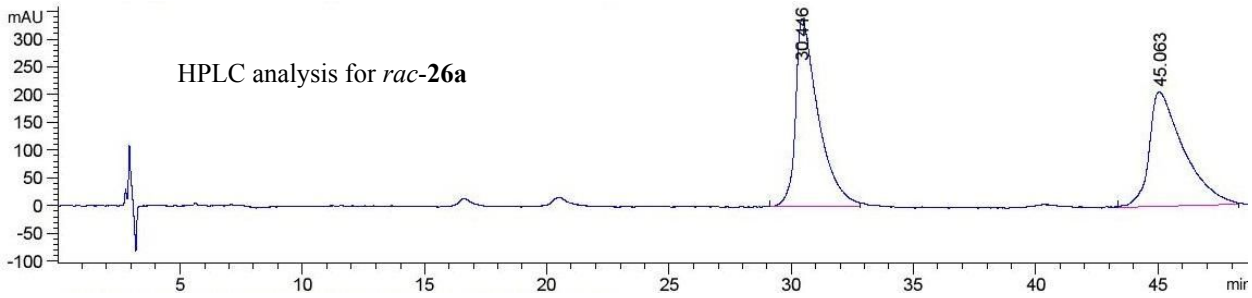

Peak #	RetTime [min]	Type	Width [min]	Area [mAU*s]	Height [mAU]	Area %
1	30.446	BV	0.8327	2.18385e4	338.48206	51.8648
2	45.063	VV	1.1596	2.02681e4	206.76707	48.1352

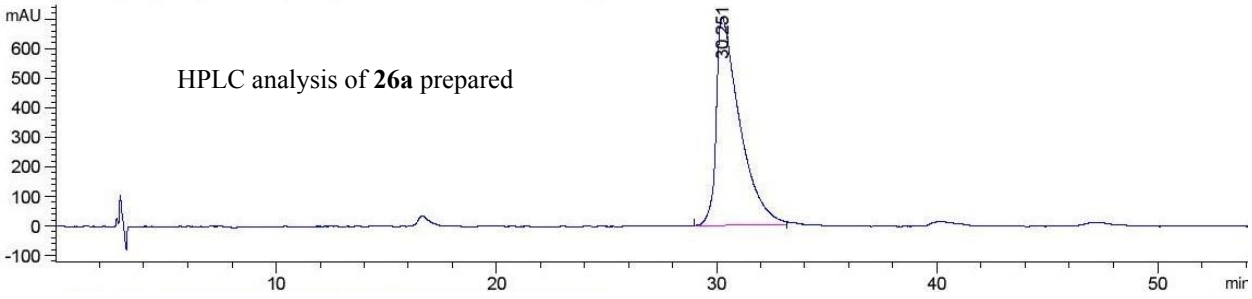

Peak #	RetTime [min]	Type	Width [min]	Area [mAU*s]	Height [mAU]	Area %
1	30.251	VV	0.8882	5.26027e4	706.88928	100.0000

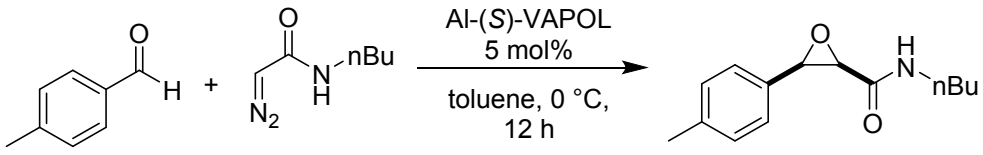

20 **1c** (*2R, 3R*)-**26c**

(2R, 3R)-3-(4-methyl-phenyl)-N-(n-butyl)-oxirane-2-carboxamide ***26c****:* Epoxide **26c** was synthesized from *para*-tolylaldehyde **20** (0.60 mmol, 71 μL) and diazo compound **1c** (0.50 mmol, 74 mg) catalyzed by aluminum-(*S*)-VAPOL catalyst prepared with the general procedure with a

12 h reaction time. The crude product was purified via column chromatography (20 x 250 mm, 3:1 to 1:1 hexane: ethyl acetate as eluent) and epoxide **26c** was obtained as a white solid in 66% isolated yield (0.330 mmol, 79.3 mg). The enantiomeric excess of epoxide **26c** was determined to be 93% with chiral HPLC (PIRKLE COVALENT (*R,R*) WHELK-O 1 column, 93:7 hexane/2-propanol at 228 nm, flow-rate: 1 mL/min): retention times: R_t = 25.13 min (minor enantiomer, ent-**26c**) and R_t = 37.54 min (major enantiomer, **26c**).

Spectral data for epoxide **26c**: ^{1}H NMR (500 MHz, Chloroform-*d*) δ 0.65 (t, J = 7.0 Hz, 3H), 0.80-0.88 (m, 2H), 0.91-0.99 (m, 2H), 2.25 (s, 3H), 2.74-2.82 (m, 1H), 3.01-3.10 (m, 1H), 3.67 (d, J = 4.5 Hz, 1H), 4.20 (d, J = 4.5 Hz, 1H), 5.84 (brs, 1H), 7.06 (d, J = 7.5 Hz, 2H), 7.16 (d, J = 8.0 Hz, 2H); ^{13}C{^{1}H}NMR (126 MHz, Chloroform-*d*) δ 13.66, 19.70, 21.20, 31.32, 38.29, 56.37, 58.11, 126.47, 129.02, 130.24, 138.21, 166.17. These spectral data are in good agreement with literature values.[7]

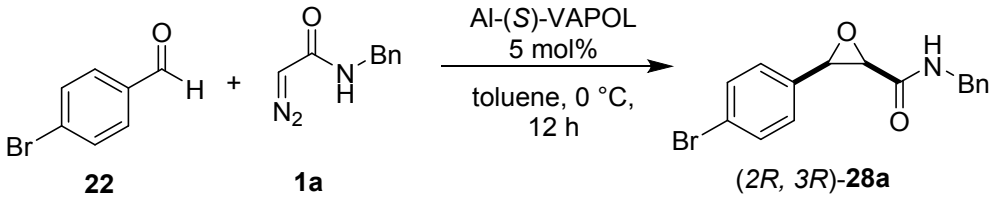

(2R, 3R)-3-(4-bromo-phenyl)-N-benzyl-oxirane-2-carboxamide ***28a****:* Epoxide **28a** was synthesized from *para*-bromobenzaldehyde **22** (0.591 mmol, 111 mg) and diazo compound **1a** (0.50 mmol, 88 mg) catalyzed by aluminum-(*S*)-VAPOL catalyst prepared with the general procedure with a 12 h reaction time. The crude product was purified via column chromatography (20 x 250 mm, 3:1 to 1:1 hexane: ethyl acetate as eluent) and epoxide **28a** was obtained as a white solid in 90% isolated yield (0.395 mmol, 131 mg). The enantiomeric excess of epoxide **28a** was determined to be 99% with chiral HPLC (PIRKLE COVALENT (*R,R*) WHELK-O 1 column,

85:15 hexane/2-propanol at 228 nm, flow-rate: 1 mL/min): retention times: R_t = 21.26 min (minor enantiomer, ent-**28a**) and R_t = 29.18 min (major enantiomer, **28a**).

Spectral data for epoxide **28a**: ^{1}H NMR (500 MHz, Chloroform-*d*) δ 3.85 (d, *J* = 4.8 Hz, 1H), 4.00 (dd, *J* = 14.8, 4.6 Hz, 1H), 4.28 (d, *J* = 4.8 Hz, 1H), 4.44 (dd, *J* = 14.7, 7.5 Hz, 1H), 6.15 (t, *J* = 5.9 Hz, 1H), 6.70 – 6.76 (m, 2H), 7.16 – 7.29 (m, 5H), 7.36 – 7.43 (m, 2H). ^{13}C{^{1}H}NMR (126 MHz, Chloroform-*d*) δ 42.84, 56.38, 57.78, 122.83, 127.60, 127.65, 128.36, 128.72, 131.83, 132.13, 137.07, 165.79. These spectral data are in good agreement with literature values.[7]

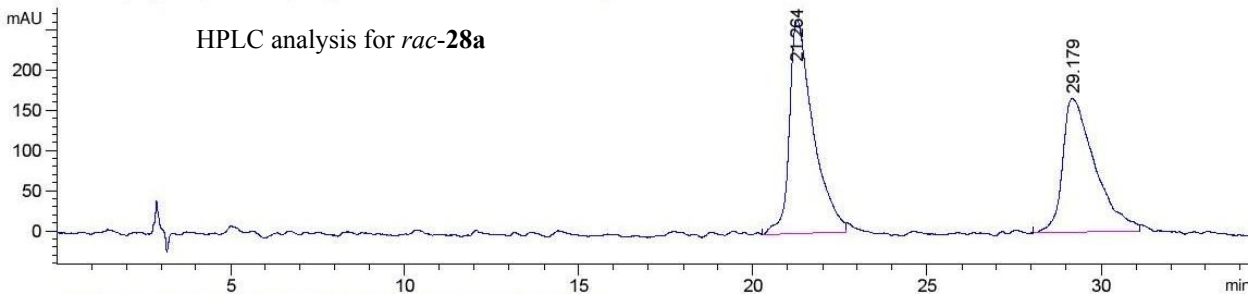

Peak #	RetTime [min]	Type	Width [min]	Area [mAU*s]	Height [mAU]	Area %
1	21.264	BV	0.6406	1.26518e4	266.14322	53.8332
2	29.179	VV	0.7707	1.08500e4	166.84195	46.1668

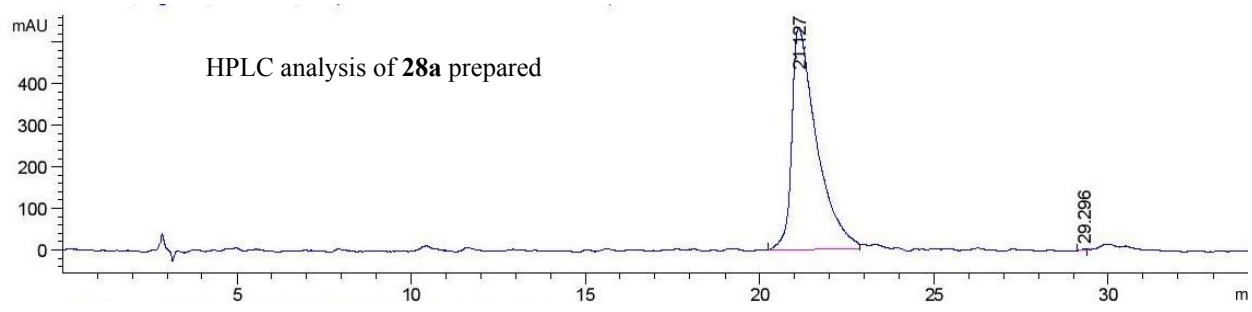

Peak #	RetTime [min]	Type	Width [min]	Area [mAU*s]	Height [mAU]	Area %
1	21.127	VV	0.6532	2.66842e4	535.65259	99.9119
2	29.296	BV	0.1308	23.53535	2.43379	0.0881

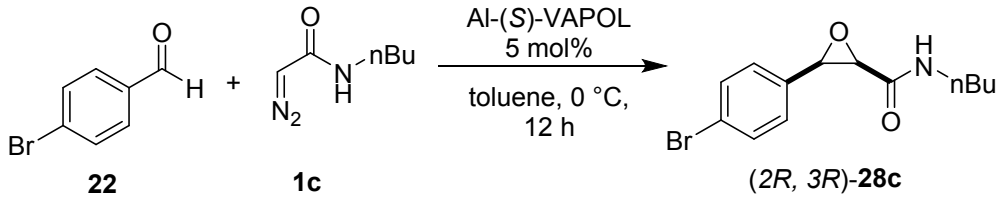

22 **1c** (*2R, 3R*)-**28c**

(2R, 3R)-3-(4-bromo-phenyl)-N-(n-butyl)-oxirane-2-carboxamide ***28c****:* Epoxide **28c** was synthesized from *para*-bromobenzaldehyde **22** (0.590 mmol, 111 mg) and diazo compound **1c** (0.50 mmol, 74 mg) catalyzed by aluminum-(*S*)-VAPOL catalyst prepared with the general procedure with a 12 h reaction time. The crude product was purified via column chromatography (20 x 250 mm, 3:1 to 1:1 hexane: ethyl acetate as eluent) and epoxide **28c** was obtained as a white solid in 77% isolated yield (0.385 mmol, 115 mg). The enantiomeric excess of epoxide **28c** was determined to be 85% with chiral HPLC (PIRKLE COVALENT (*R,R*) WHELK-O 1 column, 90:10 hexane/2-propanol at 228 nm, flow-rate: 1 mL/min): retention times: R_t = 18.05 min (minor enantiomer, ent-**28c**) and R_t = 26.19 min (major enantiomer, **28c**).

Spectral data for epoxide **28c**: ^{1}H NMR (500 MHz, Chloroform-*d*) δ 0.70 (t, J = 7.5 Hz, 3H), 0.86-0.95 (m, 2H), 0.99-1.06 (m, 2H), 2.77-2.85 (m, 1H), 3.02-3.12 (m, 1H), 3.71 (d, J = 4.5 Hz, 1H), 4.19 (d, J = 4.0 Hz, 1H), 5.87 (brs, 1H), 7.17 (d, J = 7.5 Hz, 2H), 7.40 (d, J = 7.5 Hz, 2H). ^{13}C{^{1}H}NMR (126 MHz, Chloroform-*d*) δ 13.67, 19.73, 31.36, 38.34, 56.29, 57.50, 122.57, 128.30, 131.52, 132.30, 165.64. These spectral data are in good agreement with literature values.[7]

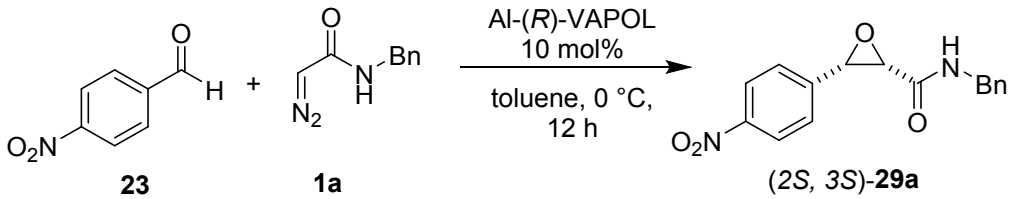

(2S,3S)-3-(4-nitro-phenyl)-N-benzyl-oxirane-2-carboxamide ***29a****:* Epoxide **29a** was synthesized from *para*-nitrobenzaldehyde **23** (0.590 mmol, 111 mg) and diazo compound **1a** (0.50 mmol, 74 mg) catalyzed by aluminum-(*R*)-VAPOL catalyst prepared with the general procedure with a 12 h reaction time. The crude product was purified via column chromatography (20 x 250 mm, 3:1 to 1:1 hexane: ethyl acetate as eluent) and epoxide **29a** was obtained as a white solid in 70% isolated yield (0.350 mmol, 105 mg). The enantiomeric excess of epoxide **29a** was determined to be 93% with chiral HPLC (PIRKLE COVALENT (*R,R*) WHELK-O 1 column, 85:15 hexane/2-propanol at 228 nm, flow-rate: 1 mL/min): retention times: R_t = 39.79 min (major enantiomer, ent-**29a**) and R_t = 48.53 min (minor enantiomer, **29a**). mp: 116-117 ˚C.

Spectral data for epoxide **29a**: ^{1}H NMR (500 MHz, Chloroform-*d*) δ 3.89 – 3.99 (m, 2H), 4.38 (d, *J* = 4.9 Hz, 1H), 4.44 (dd, *J* = 14.5, 7.9 Hz, 1H), 6.17 (s, 1H), 6.77 – 6.83 (m, 2H), 7.13 (ddt, *J* = 8.3, 6.5, 1.4 Hz, 2H), 7.15 – 7.23 (m, 1H), 7.40 – 7.47 (m, 2H), 7.99 – 8.06 (m, 2H). ^{13}C{^{1}H}NMR (126 MHz, Chloroform-*d*) δ δ 42.82, 56.41, 57.38, 123.71, 127.53, 127.80, 127.87, 128.63, 137.20, 139.94, 147.99, 165.03. IR: 3314brs, 1665s, 1512s, 1342s, 743m, 668s. HRMS (ESI-TOF) *m/z* 299.1056, [(M+H$^+$); calcd for $C_{16}H_{15}N_2O_4$: 299.1031] $[\alpha]^{20}_D$ (*c* 1.0, $CHCl_3$): 0.9559.

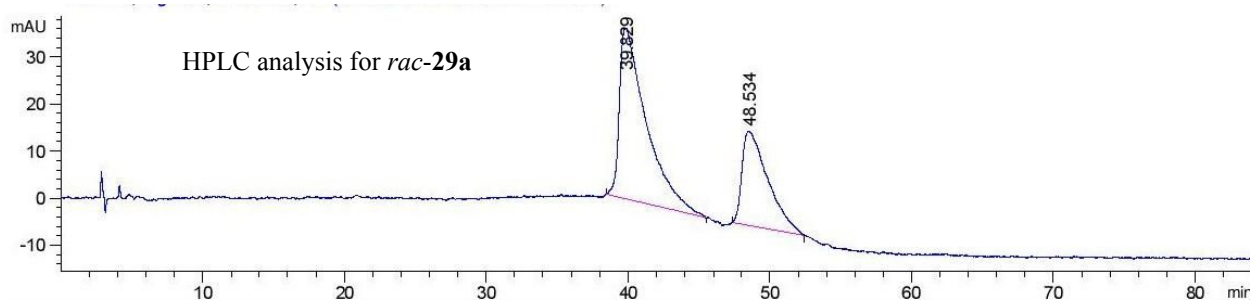

Peak #	RetTime [min]	Type	Width [min]	Area [mAU*s]	Height [mAU]	Area %
1	39.829	BB	1.5583	4810.85547	36.39244	65.2204
2	48.534	BB	1.4993	2565.44922	20.15129	34.7796

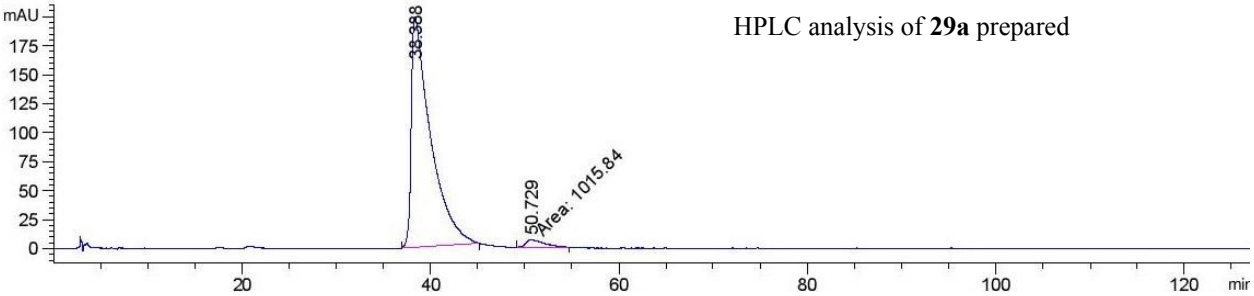

Peak #	RetTime [min]	Type	Width [min]	Area [mAU*s]	Height [mAU]	Area %
1	38.388	BB	1.8232	2.84159e4	199.09048	96.5485
2	50.729	MM	2.5603	1015.84143	6.61275	3.4515

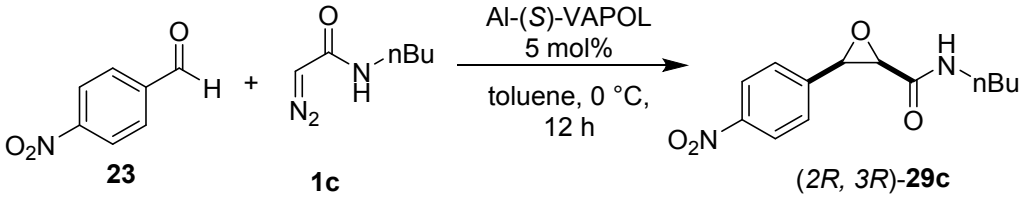

23 **1c** (*2R, 3R*)-**29c**

*(2R, 3R)-3-(4-nitro-phenyl)-N-benzyl-oxirane-2-carboxamide **29c**:* Epoxide **29c** was synthesized from *para*-nitrobenzaldehyde **23** (0.590 mmol, 111 mg) and diazo compound **1c** (0.50 mmol, 74

mg) catalyzed by aluminum-(*S*)-VAPOL catalyst prepared with the general procedure with a 12 h reaction time. The crude product was purified via column chromatography (20 x 250 mm, 3:1 to 1:1 hexane: ethyl acetate as eluent) and epoxide **29c** was obtained as a white solid in 36% isolated yield (0.18 mmol, 48 mg). The enantiomeric excess of epoxide **29c** was determined to be 71% with chiral HPLC (PIRKLE COVALENT (*R,R*) WHELK-O 1 column, 90:10 hexane/2-propanol at 228 nm, flow-rate: 1 mL/min): retention times: R_t = 50.34 min (minor enantiomer, ent-**29c**) and R_t = 57.11 min (major enantiomer, **29c**).

Spectral data for epoxide **29c**: ^{1}H NMR (500 MHz, Chloroform-*d*) δ 0.65 (t, J = 7.5 Hz, 3H), 0.84-0.94 (m, 2H), 0.98-1.06 (m, 2H), 2.82-2.90 (m, 1H), 2.98-3.07 (m, 1H), 3.80 (d, J = 5.0 Hz, 1H), 4.32 (d, J = 4.5 Hz, 1H), 5.97 (brs, 1H), 7.51 (d, J = 9.0 Hz, 2H), 8.15 (d, J = 8.5 Hz, 2H). ^{13}C{^{1}H}NMR (126 MHz, Chloroform-*d*) δ 13.51, 19.72, 29.69, 31.38, 38.43, 56.61, 57.24, 123.57, 127.68, 140.42, 147.93, 165.07. These spectral data are in good agreement with literature values.[7]

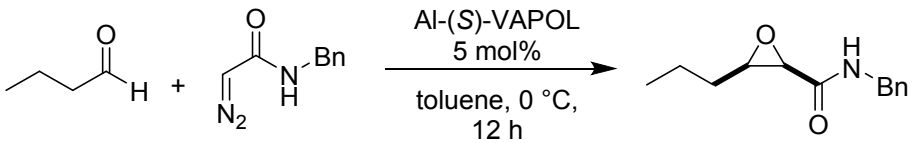

30 **1a** (*2R, 3R*)-**36a**

(2R,3R)-3-propyl-N-benzyl-oxirane-2-carboxamide ***36a****:* Epoxide **36a** was synthesized from butanal **30** (0.60 mmol, 55 μL) and diazo compound **1a** (0.50 mmol, 88 mg) catalyzed by aluminum-(*S*)-VAPOL catalyst prepared with the general procedure with a 12 h reaction time. The crude product was purified via column chromatography (20 x 250 mm, 5:1 to 1:1 hexane: ethyl acetate as eluent) and epoxide **36a** was obtained as a white solid in 62% isolated yield (0.31 mmol, 68 mg). The enantiomeric excess of epoxide **36a** was determined to be 89% with chiral HPLC (PIRKLE COVALENT (*R,R*) WHELK-O 1 column, 90:10 hexane/2-propanol at 228 nm, flow-

rate: 1 mL/min): retention times: R_t = 18.26 min (minor enantiomer, ent-**36a**) and R_t = 22.08 min (major enantiomer, **36a**).

Spectral data for epoxide **36a**: ^{1}H NMR (500 MHz, Chloroform-*d*) δ 0.82 (t, J = 7.0 Hz, 3H), 1.38 (m, 4H), 3.06 (d, *J* = 4.5 Hz, 1H), 3.43 (d, J = 4.5 Hz, 1H), 4.31 (dd, J = 14.5, 5.5 Hz, 1H), 4.43 (dd, J = 14.5, 6.0 Hz, 1H), 6.52 (brs, 1H), 7.17-7.25 (m, 5H). ^{13}C{^{1}H}NMR (126 MHz, Chloroform-*d*) δ 13.95, 19.51, 29.77, 43.07, 55.36, 58.68, 127.85, 128.05, 128.89, 137.80, 167.45. These spectral data are in good agreement with literature values.[7]

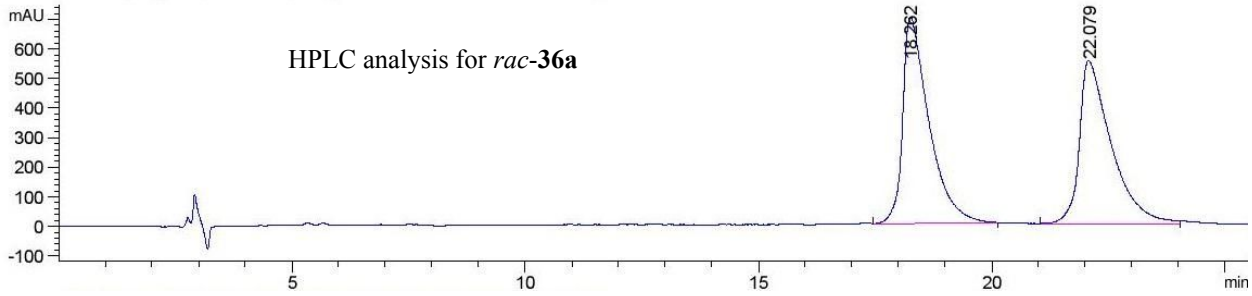

Peak #	RetTime [min]	Type	Width [min]	Area [mAU*s]	Height [mAU]	Area %
1	18.262	VV	0.5306	2.74908e4	699.40930	51.1894
2	22.079	BV	0.6446	2.62133e4	551.46143	48.8106

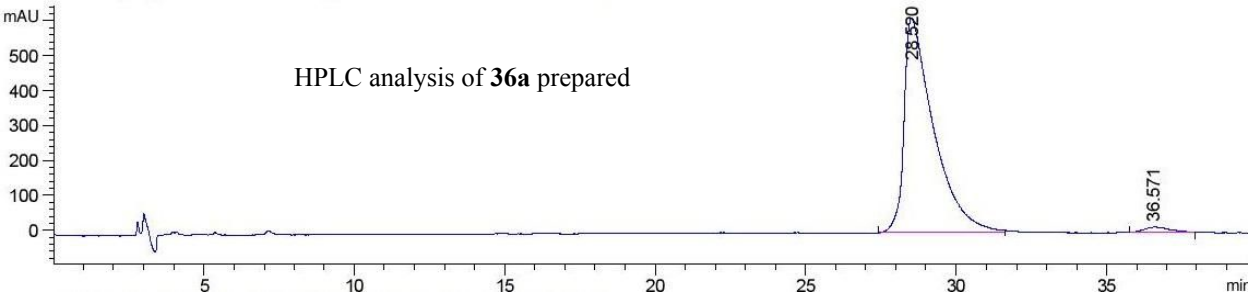

Peak #	RetTime [min]	Type	Width [min]	Area [mAU*s]	Height [mAU]	Area %
1	28.520	BV	0.9096	4.21920e4	615.58008	97.7047
2	36.571	VV	0.7598	991.16687	15.54709	2.2953

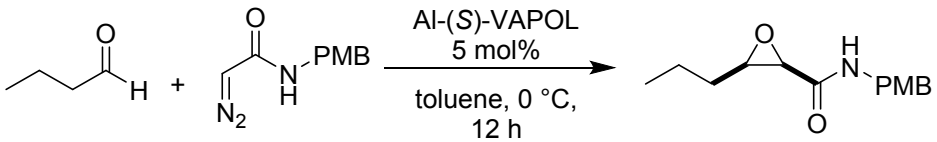

30 **1b** (*2R, 3R*)-**36b**

(2R, 3R)-3-propyl-N-(4-methoxybenzyl)-oxirane-2-carboxamide ***36b****:* Epoxide **36b** was synthesized from butanal **30** (0.60 mmol, 55 μL) and diazo compound **1b** (0.495 mmol, 103 mg) catalyzed by aluminum-(*S*)-VAPOL catalyst prepared under explained general procedure with a 12 h as the reaction time. The crude product was purified via column chromatography (20 x 250 mm, 3:1 to 1:1 hexane: ethyl acetate as eluent) and epoxide **36b** was obtained as a white solid in 50% isolated yield (0.25 mmol, 63 mg). The enantiomeric excess of epoxide **36b** was determined to be 86% with chiral HPLC (PIRKLE COVALENT (*R,R*) WHELK-O 1 column, 90:10 hexane/2-propanol at 228 nm, flow-rate: 1 mL/min): retention times: R_t = 16.42 min (minor enantiomer, ent-**36b**) and R_t = 19.3 min (major enantiomer, **36b**). mp: 62-64 ˚C

Spectral data for epoxide **36b**: ^{1}H NMR (500 MHz, Chloroform-*d*) δ 0.90 (ddd, *J* = 7.2, 5.4, 2.1 Hz, 3H), 1.39 – 1.53 (m, 4H), 3.16 (pd, *J* = 4.9, 4.0, 1.8 Hz, 1H), 3.51 (d, *J* = 4.8 Hz, 1H), 3.79 (s, 3H), 4.33 (dd, *J* = 14.5, 5.7 Hz, 1H), 4.45 (dd, *J* = 14.4, 6.2 Hz, 1H), 6.41 (s, 1H), 6.81 – 6.88 (m, 2H), 7.15 – 7.22 (m, 2H). ^{13}C{^{1}H}NMR (126 MHz, Chloroform-*d*) δ 13.95, 19.49, 29.72, 42.49, 55.32, 55.41, 58.62, 114.21, 129.39, 129.92, 159.24, 167.32. IR: 3270brs, 2963w, 1645s, 1511s, 1241s, 1031m, 605s, 569m. HRMS (ESI-TOF) *m/z* 250.1465, [(M+H$^+$); calcd for $C_{14}H_{20}NO_3$: 250.1443] $[\alpha]^{20}_D$ (*c* 1.0, $CHCl_3$): 0.1538.

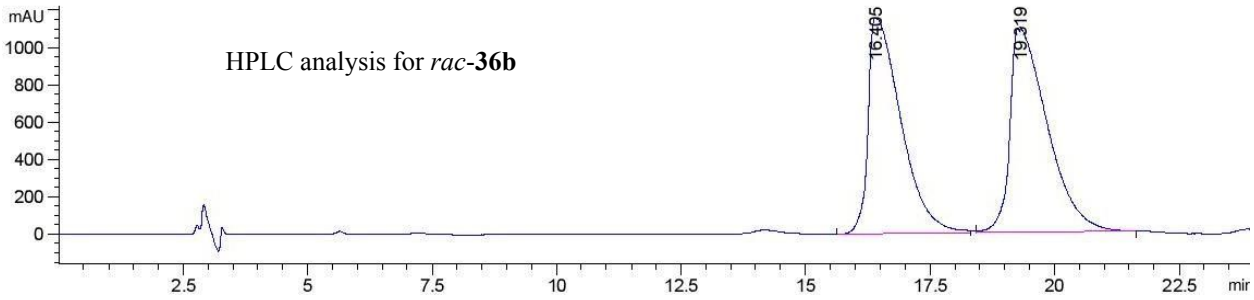

Peak #	RetTime [min]	Type	Width [min]	Area [mAU*s]	Height [mAU]	Area %
1	16.405	BV	0.5870	5.32234e4	1156.26392	48.0871
2	19.319	VB	0.6284	5.74579e4	1098.17993	51.9129

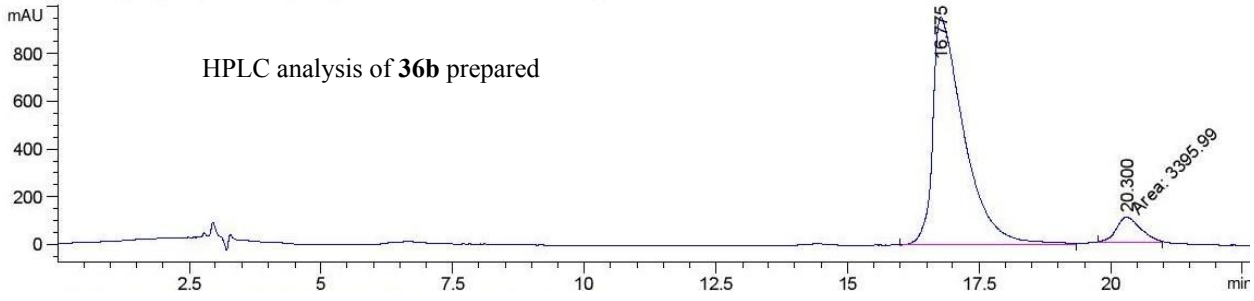

Peak #	RetTime [min]	Type	Width [min]	Area [mAU*s]	Height [mAU]	Area %
1	16.775	VV	0.5524	3.98856e4	956.76483	92.1537
2	20.300	MM	0.5416	3395.99268	104.50947	7.8463

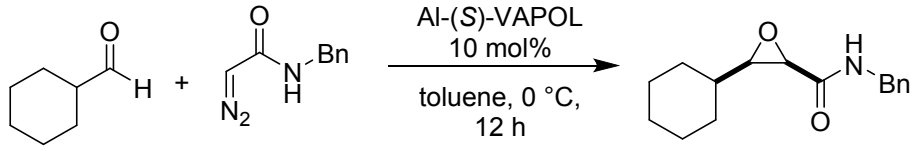

31 **1a** (*2R, 3R*)-**37a**

*(2R, 3R)-3-cyclohexyl-N-benzyl-oxirane-2-carboxamide **37a**:* Epoxide **37a** was synthesized from cyclohexanecarboxaldehyde **31** (0.60 mmol, 73 µL) and diazo compound **1a** (0.50 mmol, 88 mg) catalyzed by aluminum-(*S*)-VAPOL catalyst prepared with the general procedure with a 12 h

reaction time. The crude product was purified via column chromatography (20 x 250 mm, 3:1 to 1:1 hexane: ethyl acetate as eluent) and epoxide **37a** was obtained as a white solid in 68% isolated yield (0.34 mmol, 89 mg). The enantiomeric excess of epoxide **37a** was determined to be 88% with chiral HPLC (PIRKLE COVALENT (*R,R*) WHELK-O 1 column, 90:10 hexane/2-propanol at 228 nm, flow-rate: 1 mL/min): retention times: R_t = 16.42 min (minor enantiomer, ent-**37a**) and R_t = 19.29 min (major enantiomer, **37a**).

Spectral data for epoxide **37a**: ^{1}H NMR (500 MHz, Chloroform-*d*) δ 0.85-1.10 (m, 6H), 1.52-1.61 (m, 4H), 1.75 (d, J = 11.0 Hz, 1H), 2.79 (s, 1H), 3.45 (d, J = 3.5 Hz, 1H), 4.22 (dd, J = 14.5, 5.0 Hz, 1H), 4.55 (dd, J = 14.5, 7.0 Hz, 1H), 6.51 (brs, 1H), 7.18-7.25 (m, 5H. ^{13}C{^{1}H}NMR (126 MHz, Chloroform-*d*) δ 25.32, 26.10, 28.49, 30.56, 36.79, 42.99, 55.37, 62.92, 127.82, 128.06, 128.90, 137.99, 167.52. (one sp^3 carbon not located). These spectral data were in agreement with literature values.[7]

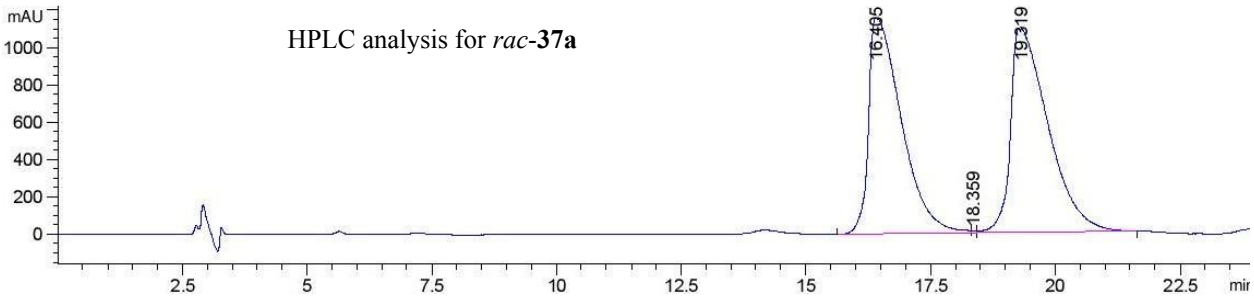

Peak #	RetTime [min]	Type	Width [min]	Area [mAU*s]	Height [mAU]	Area %
1	16.405	BV	0.5870	5.32234e4	1156.26392	48.0553
2	18.359	VV	0.0819	73.07272	11.54043	0.0660
3	19.319	VB	0.6284	5.74579e4	1098.17993	51.8787

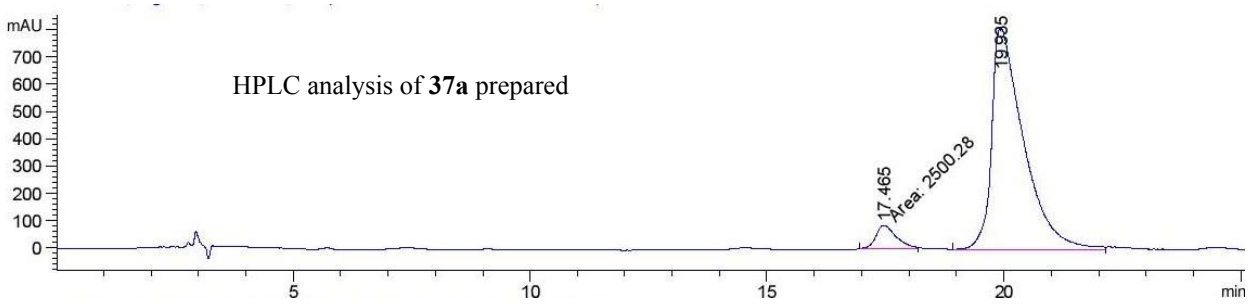

Peak #	RetTime [min]	Type	Width [min]	Area [mAU*s]	Height [mAU]	Area %
1	17.465	MM	0.4949	2500.28467	84.20614	6.1641
2	19.935	BV	0.6226	3.80618e4	815.42004	93.8359

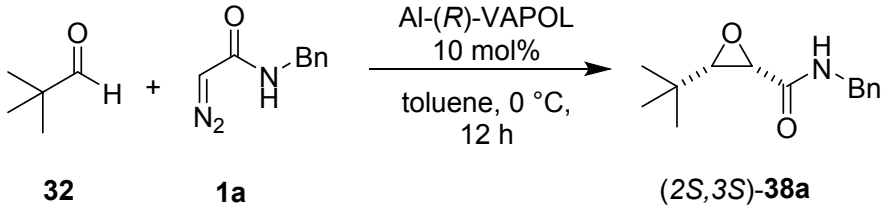

32 **1a** (*2S,3S*)-**38a**

*(2S,3S)-3-cyclohexyl-N-benzyl-oxirane-2-carboxamide **38a**:* Epoxide **38a** was synthesized from 2,2-dimethylpropanal **32** (0.60 mmol, 65 µL) and diazo compound **1a** (0.50 mmol, 88 mg) catalyzed by aluminum-(*R*)-VAPOL catalyst prepared under explained general procedure with a 12 h as the reaction time. The crude product was purified via column chromatography (20 x 250 mm, 3:1 to 1:1 hexane: ethyl acetate as eluent) and epoxide **38a** was obtained as a white solid in 50% isolated yield (0.250 mmol, 58.3 mg). The enantiomeric excess of epoxide **38a** was determined to be 99% with chiral HPLC (Daicel Chirapack OD-H column, 94:6 hexane/2-propanol at 228 nm, flow-rate: 1 mL/min): retention times: R_t = 7.14 min (major enantiomer, ent-**38a**) and R_t = 13.32 min (minor enantiomer, **38a**).

Spectral data for epoxide **38a**: ^{1}H NMR (500 MHz, Chloroform-*d*) δ 0.89 (s, 9H), 1.47 (d, J = 5.0 Hz, 1H), 1.37 (d, *J* = 5.0 Hz, 1H), 4.20 (dd, J = 14.0, 5.0 Hz, 1H), 4.48 (dd, J = 14.0, 6.0 Hz, 1H), 6.45 (brs, 1H), 7.20-7.30 (m, 5H). ^{13}C{^{1}H}NMR (126 MHz, Chloroform-*d*) δ 26.66, 31.97, 43.55, 56.13, 67.46, 127.94, 128.44, 128.91, 137.08, 167.41. These spectral data were in agreement with the literature values.[7]

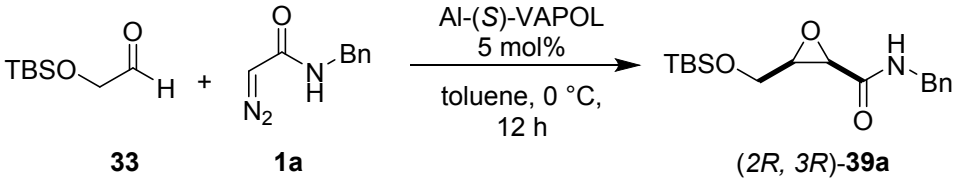

33 **1a** (*2R, 3R*)-**39a**

(2R,3R)-3-(2-((tert-butyldimethylsilyl)oxy)methyl)-N-benzyl-oxirane-2-carboxamide ***39a****:* Epoxide **39a** was synthesized from 2-((tert-butyldimethylsilyl)oxy)acetaldehyde **33** (0.590 mmol, 115 µL) and diazo compound **1a** (0.50 mmol, 88 mg) catalyzed by aluminum-(*S*)-VAPOL catalyst prepared with the general procedure with a 12 h reaction time. The crude product was purified via column chromatography (20 x 250 mm, 3:1 to 1:1 hexane: ethyl acetate as eluent) and epoxide **39a** was obtained as a yellowish oil in 78% isolated yield (0.390 mmol, 125 mg). The enantiomeric excess of epoxide **39a** was determined to be 56% with chiral HPLC (PIRKLE COVALENT (*R,R*) WHELK-O 1 column, 90:10 hexane/2-propanol at 228 nm, flow-rate: 1 mL/min): retention times: R_t = 20.67 min (minor enantiomer, ent-**39a**) and R_t = 22.98 min (major enantiomer, **39a**).

Spectral data for epoxide **39a**: ^{1}H NMR (500 MHz, Chloroform-*d*) δ -0.02 (s, 6H), 0.86 (s, 9H), 3.32 – 3.39 (m, 1H), 3.43 – 3.51 (m, 1H), 3.59 (d, *J* = 4.8 Hz, 1H), 3.88 (dd, *J* = 12.1, 3.2 Hz, 1H), 4.36 (dd, *J* = 14.6, 5.6 Hz, 1H), 4.53 (dd, *J* = 14.5, 6.5 Hz, 1H), 6.48 (d, *J* = 6.3 Hz, 1H), 7.23 – 7.33 (m, 3H), 7.30 – 7.37 (m, 2H). ^{13}C{^{1}H}NMR (126 MHz, Chloroform-*d*) δ -5.28, -5.26, 18.39, 25.91, 43.11, 54.16, 58.87, 61.35, 127.93, 128.08, 128.96, 137.56, 166.60. IR: 3299brs, 2930w,

1658s, 1512s, 1248s, 1092s, 1034m, 834s, 776m. HRMS (ESI-TOF) *m/z* 322.1872, [(M+H$^+$); calcd for $C_{17}H_{28}NO_3Si$: 322.1838]. $[\alpha]^{20}_D$ (*c* 1.0, $CHCl_3$): 0.252.

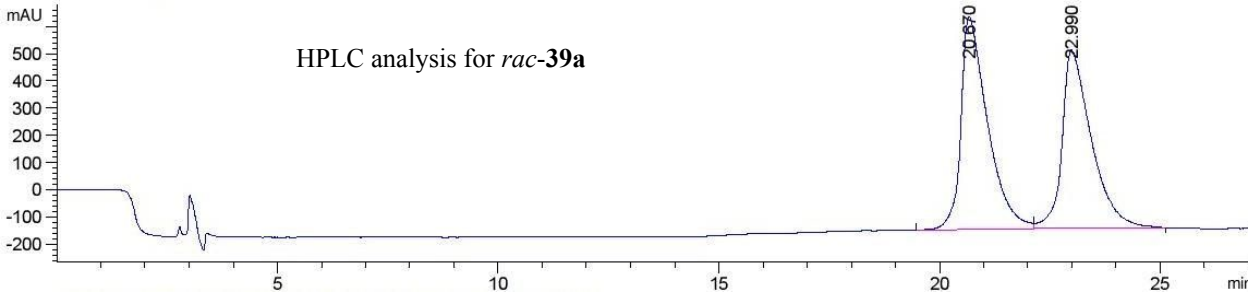

Peak #	RetTime [min]	Type	Width [min]	Area [mAU*s]	Height [mAU]	Area %
1	20.669	BB	0.5439	1214.69629	31.21845	51.6065
2	22.983	BB	0.5867	1139.07019	25.61986	48.3935

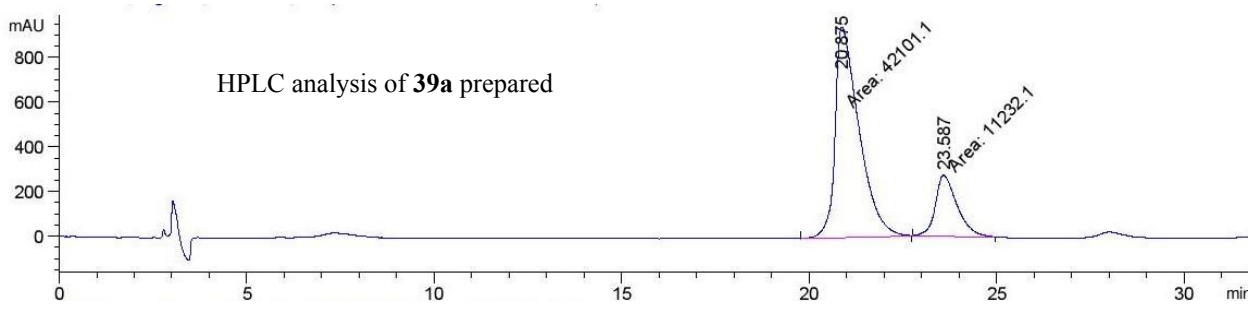

Peak #	RetTime [min]	Type	Width [min]	Area [mAU*s]	Height [mAU]	Area %
1	20.875	MM	0.7439	4.21011e4	943.29700	78.9397
2	23.587	MM	0.6821	1.12321e4	274.46686	21.0603

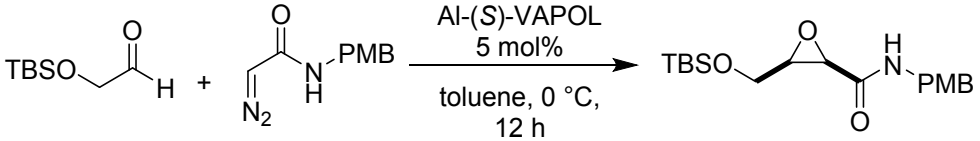

33 **1b** (*2R, 3R*)-**39b**

(2R,3R)-3-(2-((tert-butyldimethylsilyl)oxy)methyl)-N-(4-methoxy-phenyl)-oxirane-2-carboxamide ***39b****:* Epoxide **39b** was synthesized from 2-((tert-butyldimethylsilyl)oxy)acetaldehyde **33** (0.590 mmol, 115 μL) and diazo compound **1b** (0.490 mmol, 103 mg) catalyzed by aluminum-(*S*)-VAPOL catalyst prepared under explained general procedure with a 12 h as the reaction time. The crude product was purified via column chromatography (20 x 250 mm, 3:1 to 1:1 hexane: ethyl acetate as eluent) and epoxide **39b** was obtained as a yellowish oil in 73% isolated yield (0.365 mmol, 128 mg). The enantiomeric excess of epoxide **39b** was determined to be 50% with chiral HPLC (PIRKLE COVALENT (*R,R*) WHELK-O 1 column, 90:10 hexane/2-propanol at 228 nm, flow-rate: 1 mL/min): retention times: R_t = 19.69 min (minor enantiomer, ent-**39b**) and R_t = 23.44 min (major enantiomer, **39b**).

Spectral data for epoxide **39b**: ^{1}H NMR (500 MHz, Chloroform-*d*) δ 0.03 (s, 6H), 0.86 (s, 9H), 3.30 – 3.37 (m, 1H), 3.40 – 3.50 (m, 1H), 3.56 (d, *J* = 4.8 Hz, 1H), 3.79 (s, 2H), 3.86 (dd, *J* = 12.1, 3.1 Hz, 1H), 4.28 (dd, *J* = 14.4, 5.5 Hz, 1H), 4.46 (dd, *J* = 14.4, 6.5 Hz, 1H), 6.44 (t, *J* = 6.0 Hz, 1H), 6.81 – 6.88 (m, 2H), 7.13 – 7.23 (m, 2H). ^{13}C{^{1}H}NMR (126 MHz, Chloroform-*d*) δ -5.27, -5.25, 18.40, 25.91, 42.56, 54.15, 55.39, 58.86, 61.34, 114.31, 129.46, 129.70, 159.33, 166.49. IR: 3299brs, 2928w, 1661s, 1092s, 834s, 777m, 731w, 697m. HRMS (ESI-TOF) *m/z* 352.1964, [(M+H$^+$); calcd for $C_{18}H_{30}NO_4Si$: 352.1944]. $[\alpha]^{20}_D$ (*c* 1.0, $CHCl_3$): 0.1218.

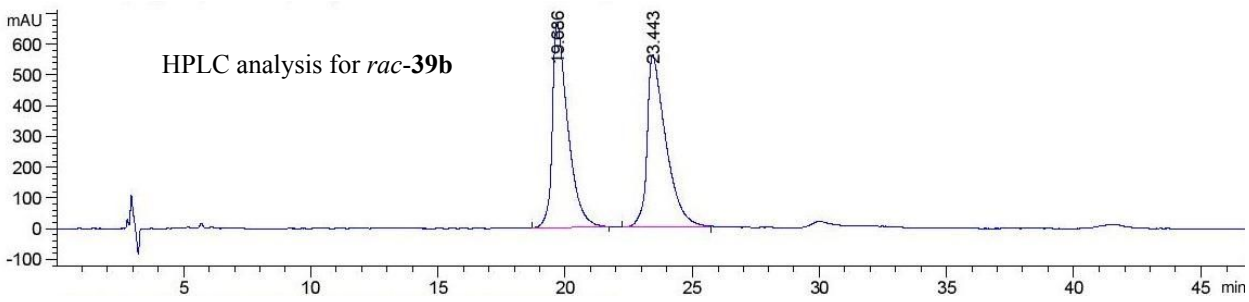

Peak #	RetTime [min]	Type	Width [min]	Area [mAU*s]	Height [mAU]	Area %
1	19.686	BV	0.5699	2.84904e4	670.26910	49.6251
2	23.443	BV	0.6699	2.89209e4	560.55884	50.3749

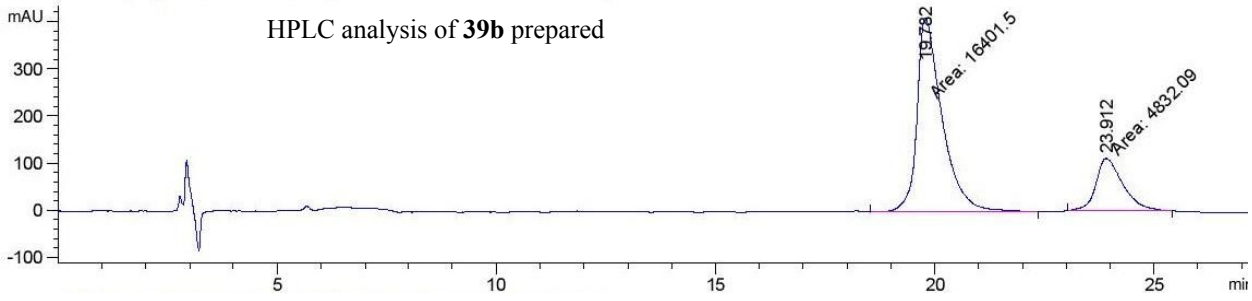

Peak #	RetTime [min]	Type	Width [min]	Area [mAU*s]	Height [mAU]	Area %
1	19.782	MM	0.6649	1.64015e4	411.10287	77.2432
2	23.912	MM	0.7238	4832.08936	111.26319	22.7568

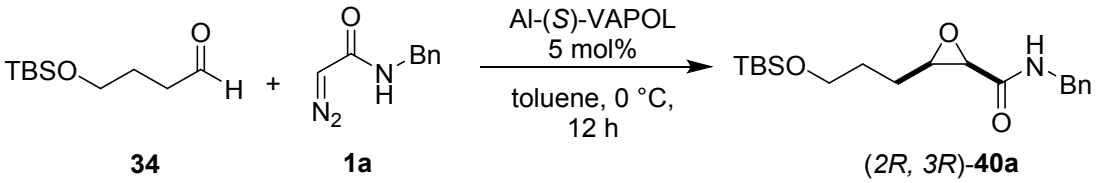

34 **1a** (*2R, 3R*)-**40a**

(2R,3R)-3-(2-((tert-butyldimethylsilyl)oxy)propyl)-N-benzyl-oxirane-2-carboxamide ***40a***:

Epoxide **40a** was synthesized from 4-((tert-butyldimethylsilyl)oxy)butanal **34** (0.590 mmol, 135 µL) and diazo compound **1b** (0.50 mmol, 88 mg) catalyzed by aluminum-(*S*)-VAPOL catalyst prepared with the general procedure with a 12 h reaction time. The crude product was purified via column chromatography (20 x 250 mm, 3:1 to 1:1 hexane: ethyl acetate as eluent) and epoxide **40a** was obtained as a yellowish oil in 84% isolated yield (0.420 mmol, 159 mg). The enantiomeric excess of epoxide **40a** was determined to be 50% with chiral HPLC (PIRKLE COVALENT (*R,R*)

WHELK-O 1 column, 90:10 hexane/2-propanol at 228 nm, flow-rate: 1 mL/min): retention times: R_t = 12.98 min (minor enantiomer, ent-**40a**) and R_t = 15.55 min (major enantiomer, **40a**).

Spectral data for epoxide **40a**: ^{1}H NMR (500 MHz, Chloroform-*d*) δ 0.01 (s, 6H), 0.88 (s, 9H), 1.52 – 1.65 (m, 2H), 1.66 (tdd, *J* = 10.3, 6.0, 2.0 Hz, 2H), 3.21 (td, *J* = 6.3, 4.8 Hz, 1H), 3.52 – 3.66 (m, 3H), 4.45 (qd, *J* = 14.7, 6.0 Hz, 2H), 6.48 (t, *J* = 6.2 Hz, 1H), 7.23 – 7.37 (m, 5H). ^{13}C{^{1}H}NMR (126 MHz, Chloroform-*d*) δ -5.22, 18.41, 24.55, 26.04, 29.32, 43.09, 55.48, 58.68, 62.39, 127.86, 128.04, 128.90, 137.74, 167.38. IR: 3301brs, 2928w, 1660s, 1095s, 833s, 774s, 698w. HRMS (ESI-TOF) *m/z* 350.2239, [(M+H$^+$); calcd for $C_{19}H_{32}NO_3Si$: 350.2151].

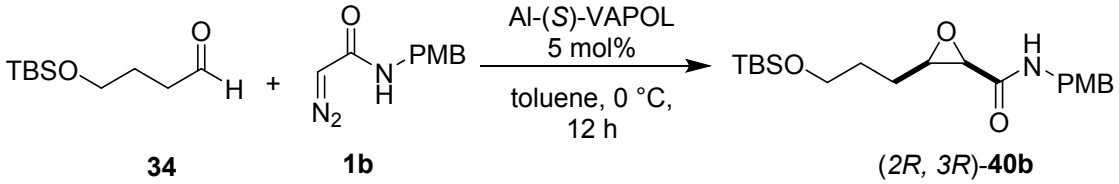

34 **1b** (*2R, 3R*)-**40b**

*(2R,3R)-3-(2-((tert-butyldimethylsilyl)oxy)propyl)-N-(4-methoxy-benzyl)-oxirane-2-carboxamide **40b**:* Epoxide **40b** was synthesized from 4-((tert-butyldimethylsilyl)oxy)butanal **34** (0.599 mmol, 135 μL) and diazo compound **1b** (0.499 mmol, 103 mg) catalyzed by aluminum-(*S*)-VAPOL catalyst prepared with the general procedure with a 12 h reaction time. The crude product was purified via column chromatography (20 x 250 mm, 3:1 to 1:1 hexane: ethyl acetate as eluent) and epoxide **40b** was obtained as a yellowish oil in 67% isolated yield (0.335 mmol, 127 mg). The enantiomeric excess of epoxide **40b** was determined to be 51% with chiral HPLC (PIRKLE COVALENT (*R,R*) WHELK-O 1 column, 90:10 hexane/2-propanol at 228 nm, flow-rate: 1 mL/min): retention times: R_t = 30.97 min (minor enantiomer, ent-**40b**) and R_t = 41.86 min (major enantiomer, **40b**).

Spectral data for epoxide **40b**: ^{1}H NMR (500 MHz, Chloroform-*d*) δ 0.01 (s, 6H), 0.87 (s, 9H), 1.50 – 1.62 (m, 2H), 1.59 – 1.70 (m, 2H), 3.20 (td, *J* = 6.3, 4.7 Hz, 1H), 3.53 (d, *J* = 4.8 Hz, 1H),

3.54 – 3.64 (m, 2H), 3.79 (s, 3H), 4.32 – 4.44 (m, 2H), 6.40 (t, *J* = 5.9 Hz, 1H), 6.81 – 6.88 (m, 2H), 7.15 – 7.22 (m, 2H). $^{13}C\{^{1}H\}$NMR (126 MHz, Chloroform-*d*) δ -5.23, 18.40, 24.53, 26.03, 29.32, 42.53, 55.39, 55.46, 58.64, 62.40, 114.23, 129.39, 129.85, 159.26, 167.25. IR: 3309brs, 2928w, 1662s, 1512s, 1247s, 1095s, 1035w, 833s, 774s, 731w. HRMS (ESI-TOF) *m/z* 380.2338, [(M+H$^+$); calcd for $C_{20}H_{34}NO_4Si$: 380.2257] $[\alpha]^{20}_D$ (*c* 1.0, $CHCl_3$): 0.054.

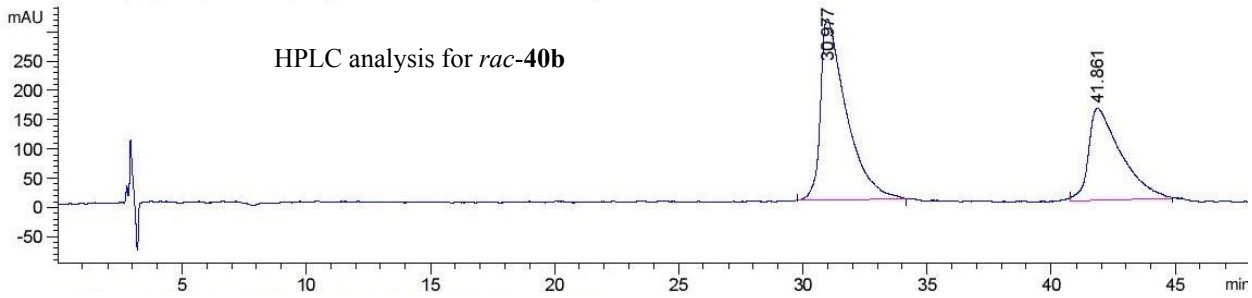

Peak #	RetTime [min]	Type	Width [min]	Area [mAU*s]	Height [mAU]	Area %
1	30.985	BB	0.9844	2.64967e4	365.23813	60.1958
2	41.866	BB	1.2704	1.75208e4	181.46814	39.8042

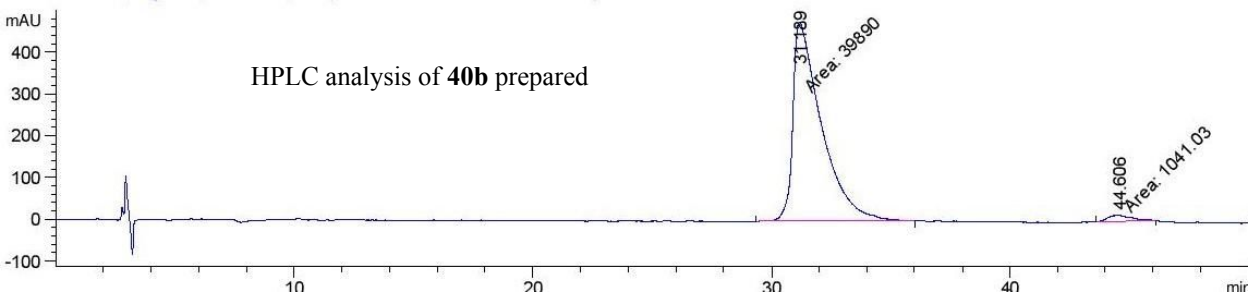

Peak #	RetTime [min]	Type	Width [min]	Area [mAU*s]	Height [mAU]	Area %
1	31.189	MM	1.3931	3.98900e4	477.21851	97.4566
2	44.606	MM	1.1951	1041.03369	14.51785	2.5434

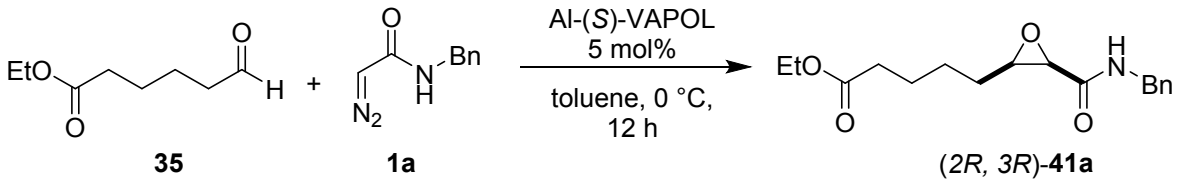

35 **1a** (*2R, 3R*)-**41a**

*Ethyl 5-((2S,3S)-3-(benzylcarbamoyl)oxiran-2-yl)pentanoate **41a**:* Epoxide **41a** was synthesized from ethyl 6-oxohexanoate **35** (0.60 mmol, 95 mg) and diazo compound **1a** (0.50 mmol, 88 mg) catalyzed by 5 mol% aluminum-(*S*)-VAPOL catalyst prepared with the general procedure with a 12 h reaction time. The crude product was purified via column chromatography (20 x 250 mm, 3:1 to 1:1 hexane: ethyl acetate as eluent) and epoxide **41a** was obtained as a yellowish oil in 75% isolated yield (0.370 mmol, 113 mg). The enantiomeric excess of epoxide **41a** was determined to be 76% with chiral HPLC (PIRKLE COVALENT (*R,R*) WHELK-O 1 column, 85:15 hexane/2-propanol at 228 nm, flow-rate: 1 mL/min): retention times: R_t = 33.45 min (minor enantiomer, ent-**41a**) and R_t = 39.6 min (major enantiomer, **41a**).

Spectral data for epoxide **41a**: ^{1}H NMR (500 MHz, Chloroform-*d*) δ 1.25 (t, *J* = 7.2 Hz, 4H), 1.49 (qdt, *J* = 9.9, 7.5, 3.6 Hz, 3H), 1.55 – 1.65 (m, 2H), 2.25 (t, *J* = 7.4 Hz, 2H), 3.12 – 3.20 (m, 1H), 3.54 (d, *J* = 4.7 Hz, 1H), 4.12 (q, *J* = 7.1 Hz, 2H), 4.41 (dd, *J* = 14.6, 5.8 Hz, 1H), 4.51 (dd, *J* = 14.6, 6.3 Hz, 1H), 6.48 (t, *J* = 5.8 Hz, 1H), 7.25 – 7.37 (m, 5H). ^{13}C{^{1}H}NMR (126 MHz, Chloroform-*d*) δ 14.36, 24.63, 25.65, 27.51, 34.06, 43.07, 55.33, 58.46, 60.43, 127.87, 128.06, 128.91, 137.77, 167.28, 173.44. IR: 3325brs, 2930w, 1729s, 1662s, 1572s, 1162s, 699s. HRMS (ESI-TOF) *m/z* 306.1732, [(M+H$^+$); calcd for $C_{17}H_{24}NO_4$: 306.1705] $[\alpha]^{20}_D$ (*c* 1.0, $CHCl_3$): 0.1193.

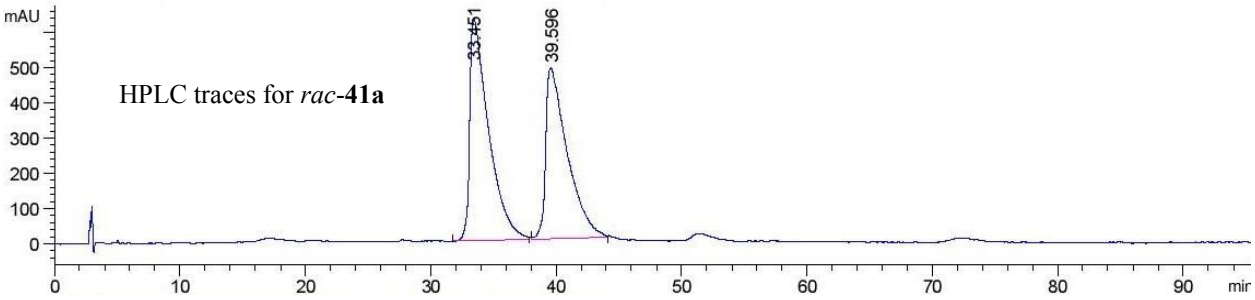

Peak #	RetTime [min]	Type	Width [min]	Area [mAU*s]	Height [mAU]	Area %
1	33.451	BV	1.2469	6.64301e4	633.74402	53.2155
2	39.596	VV	1.4269	5.84022e4	485.67450	46.7845

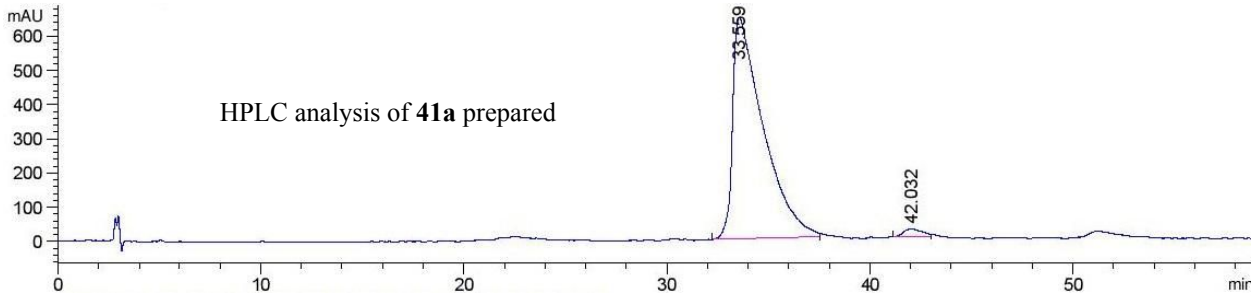

Peak #	RetTime [min]	Type	Width [min]	Area [mAU*s]	Height [mAU]	Area %
1	33.559	BV	1.3327	6.79210e4	647.01331	97.8536
2	42.032	BV	0.7346	1489.84741	23.92212	2.1464

9. Deprotection of TBS-alcohol

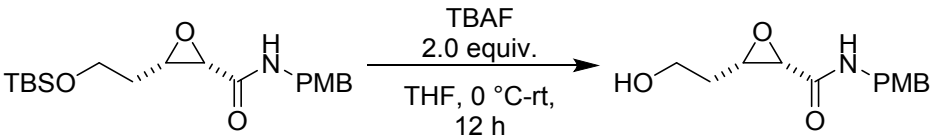

(*2R, 3R*)-**13** (*2R, 3R*)-**44**

*(2R,3R)-3-(2-hydroxyethyl)-N-(4-methoxybenzyl)oxirane-2-carboxamide **13**:* To a solution of epoxide **13** (0.490 mmol, 183 mg) in 5 mL THF in a 25 mL round bottom flask at 0 ˚C was added tetrabutylammonium fluoride (1 mmol, 1M solution in THF, 1 mL) and the resulting solution was

stirred at room temperature for 12 h. After removing the solvent under reduced pressure the resulting crude mixture was purified via column chromatography (20 x 250 mm, 1:1 hexane: ethyl acetate, pure ethyl acetate and 19:1 ethyl acetate: methanol) and compound **44** was obtained as a white solid in 84% yield (0.420 mmol, 106 mg). mp: 75-76 ˚C.

Spectral data for compound **44**: ^{1}H NMR (500 MHz, Chloroform-*d*) δ 1.70 – 1.82 (m, 2H), 3.34 (td, *J* = 6.4, 4.8 Hz, 1H), 3.57 (d, *J* = 4.8 Hz, 1H), 3.80 (s, 3H), 3.75 – 3.87 (m, 2H), 4.32 – 4.45 (m, 2H), 6.44 (s, 1H), 6.83 – 6.90 (m, 2H), 7.14 – 7.25 (m, 2H). ^{13}C{^{1}H}NMR (126 MHz, Chloroform-*d*) δ 30.91, 42.67, 54.93, 55.45, 56.62, 59.86, 114.30, 129.48, 129.68, 159.35, 167.33. IR: 3259brs, 1646s, 1511s, 1249s, 1031s, 806s, 572m. HRMS (ESI-TOF) *m/z* 274.1138, [(M+Na^{+}); calcd for $C_{13}H_{17}NO_4Na$: 273.0977], $[\alpha]^{20}_{D}$ (*c* 1.0, $CHCl_3$): 0.0161.

10. One pot alcohol tosylation and amide cyclization

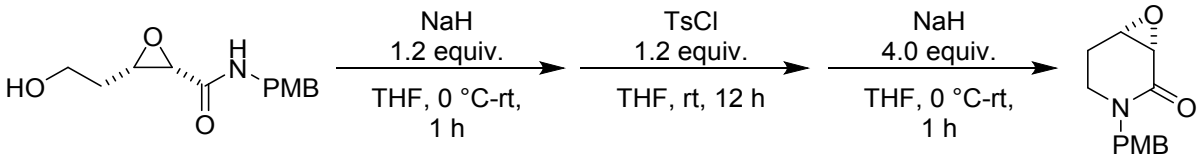

(*2S, 3S*)-**44** (*2S, 3S*)-**45**

*(1S,6S)-3-(4-methoxybenzyl)-7-oxa-3-azabicyclo[4.1.0]heptan-2-one **45**:* A flamed dried 25 mL round bottom flask was charged with compound **44** (0.499 mmol, 126 mg), and 5 mL THF. Then the resulting solution was cooled down to 0 ˚C, followed by addition of NaH (0.5 mmol, 60% dispersed in mineral oil, 20 mg). The reaction was warmed up to room temperature and stirred for an additional 1 h. Next, the reaction vessel was cooled down to 0 ˚C and freshly purified 4-toluenesulfonyl chloride (0.590 mmol, 115 mg) was slowly added. The resulting solution was warmed up to room temperature and stirred for another hour. After cooling down the temperature of the reaction to 0 ˚C, NaH (2.0 mmol, 60% dispersed in mineral oil, 80 mg) was added slowly

followed by gradual warming up to room temperature and stirring at ambient temperature for 1 h. Then, the reaction was quenched with careful addition of saturated aq NH_4Cl. The aqueous layer was separated and extracted three times with ethyl acetate. The combined organic layer was washed with brine, dried over Na_2SO_4 and purified via column chromatography (20 x 250 mm, 2:1 to 0:1 hexane: ethyl acetate). Compound **45** was obtained as pure white solid in 67% yield (0.33 mmol, 78 mg). The structure of this compound was confirmed unequivocally with x-ray structural analysis (CCDC number: 1972358). mp: 67-68 ˚C. mp of crystal: 68-69 ˚C.

Spectral data for compound **45**: ^{1}H NMR (500 MHz, Chloroform-*d*) δ 1.90 (ddd, *J* = 14.4, 12.7, 6.1 Hz, 1H), 2.23 (dq, *J* = 14.6, 2.7, 2.2 Hz, 1H), 2.86 – 2.95 (m, 1H), 3.28 (td, *J* = 12.6, 4.3 Hz, 1H), 3.53 (d, *J* = 4.1 Hz, 1H), 3.58 (t, *J* = 3.4 Hz, 1H), 3.78 (d, *J* = 2.0 Hz, 3H), 4.38 (d, *J* = 14.6 Hz, 1H), 4.59 (d, *J* = 14.5 Hz, 1H), 6.81 – 6.87 (m, 2H), 7.11 – 7.18 (m, 2H). ^{13}C{^{1}H}NMR (126 MHz, Chloroform-*d*) δ 24.22, 39.97, 49.91, 51.10, 53.17, 55.38, 114.16, 128.67, 129.39, 159.19, 166.79. IR: 1641s, 1512m, 1246s, 811m, 588m. HRMS (ESI-TOF) *m/z* 234.1153, [(M+H$^+$); calcd for $C_{13}H_{16}NO_3$: 234.1130], $[\alpha]^{20}_D$ (*c* 1.0, $CHCl_3$): 0.3521.

11. General method for the crystal growth of compound (2*S*, 3*S*)-45

The crystal of compound **II-186** was grown under following condition: 20 mg of compound **II-186** was dissolved in 5 mL of anhydrous diethylether in a 20 mL vial. Then the vial was covered with an aluminum foil which had holes in it. Slow evaporation of diethyl ether induced the subsequent crystal growth. CCDC number: 1972358.

12. PMB deprotection

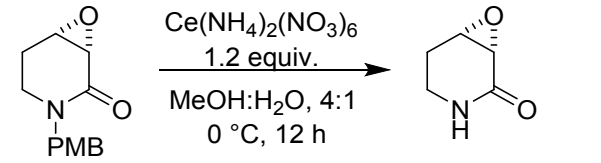

(−)-tedanalactam 5: To the stirring solution of compound **45** (0.490 mmol, 117 mg) in 12.5 mL methanol: water (4:1) at 0 ˚C was added $Ce(NH_4)_2(NO_3)_6$ (0.590 mmol, 329 mg) and the resulting mixture was stirred at 0 ˚C for 12 hour. The reaction was quenched with the addition of saturated NH_4Cl. The aqueous layer was separated and extracted three times with ethyl acetate. The combined organic layer was washed with brine, dried over Na_2SO_4 and purified via column chromatography (20 x 250 mm, 2:1 to 0:1 hexane: ethyl acetate then 19:1 ethyl acetate: methanol). Compound **5** was obtained as a yellow oil in 75% yield (0.375 mmol, 42.1 mg).

Spectral data for compound **5**: ^{1}H NMR (500 MHz, Chloroform-*d*) δ 1.95 – 2.07 (m, 1H), 2.28 (dddd, *J* = 14.6, 4.3, 2.8, 1.2 Hz, 1H), 3.03 (dtt, *J* = 12.3, 6.1, 1.4 Hz, 1H), 3.27 – 3.46 (m, 2H), 3.58 – 3.63 (m, 1H), 6.66 (s, 1H). ^{13}C{^{1}H}NMR (126 MHz, Chloroform-*d*) δ 23.64, 35.39, 50.78, 53.26, 169.28. HRMS (ESI-TOF) *m/z* 114.0584, [(M+H$^+$); calcd for $C_5H_7NO_2$: 114.0555], $[\alpha]^{20}_D$ (0.1 M, MeOH): −7.1. Literature value: $[\alpha]^{20}_D$ (0.1 M, MeOH): -7.9 These data matched with literature values.[8,9]

13. General procedure 2: mono-protection of diol:[10]

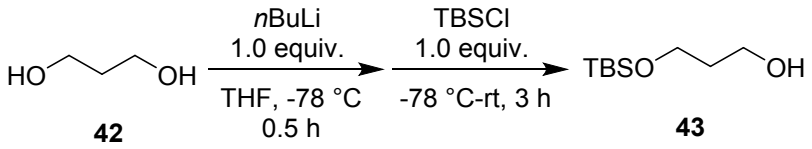

*3-((tert-butyldimehylsilyl)oxy)propan-1-ol **43**:* To a stirring solution of 1,3-propan-diol **42** (42 mmol, 3.0 mL) in 80 mL of THF at -78 ˚C was added *n*-BuLi (42 mmol, 2.5 M in hexane, 17 mL) and the resulting solution was stirred at the same temperature for 30 minutes. Then a solution of *t*BuMe$_2$SiCl (42.1 mmol, 6.33 *g*) in 10 mL THF was added to the stirring solution at -78 ˚C followed by warming up the reaction vessel to room temperature and stirring it at ambient temperature for 3 h. The reaction was quenched by slow addition of saturated NH_4Cl. Then the aqueous layer was separated, extracted three times with diethyl ether. The combined organic layer was washed with brine and dried over Na_2SO_4. After removing the solvent under reduced pressure, the crude mixture was purified via column chromatography (20 x 250 mm, 5:1 to 2:1 hexane: ethyl acetate) and the desired product **43** was obtained as a colorless oil in 90% isolated yield (38 mmol, 7.2 g). ^{1}H NMR (500 MHz, Chloroform-*d*) δ -0.02 (s, 6H), 0.86 (s, 9H), 1.73 (p, *J* = 5.7 Hz, 2H), 3.73 (m, 2H) 3.75 (dt, *J* = 5.2 Hz, 2H). ^{13}C{^{1}H}NMR (126 MHz, Chloroform-*d*) δ -5.51, 18.17, 25.86, 34.13, 62.47, 62.97. These data are in agreement with the literature values.[10]

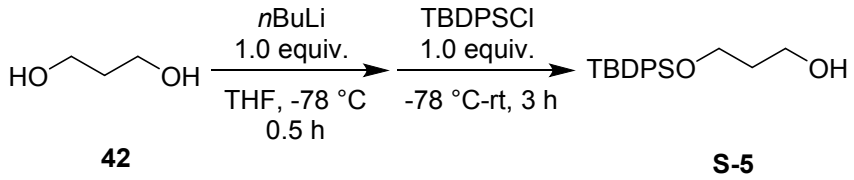

42 **S-5**

*3-((tert-butyldiphenylsilyl)oxy)propan-1-ol **S-5**:* Compound **S-5** was synthesized from 1,3-propan-diol **42** (42 mmol, 3.1 mL) and *t*BuPh$_2$SiCl (42.01 mmol, 11.54 g) with the general procedure 2. The resulting alcohol **S-5** was purified via column chromatography (20 x 250 mm, 5:1 to 2:1 hexane: ethyl acetate) and a white solid was afforded as the pure product in 87% yield (36.54 mmol, 11.49 g).

Spectral data for compound **S-5**: ^{1}H NMR (500 MHz, Chloroform-*d*) δ 1.07 (s, 9H), 1.83 (p, *J* = 5.7 Hz, 2H), 2.42 (s, 1H), 3.86 (t, *J* = 5.6 Hz, 4H), 7.37 – 7.45 (m, 4H), 7.42 – 7.49 (m, 2H), 7.67 – 7.75 (m, 4H). ^{13}C{^{1}H}NMR (126 MHz, Chloroform-*d*) δ 19.09, 26.83, 34.20, 62.06, 63.37, 127.77, 129.80, 133.20, 135.55. These data are in agreement with the literature values.[11]

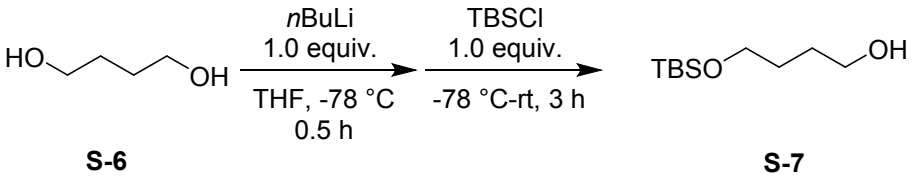

S-6 **S-7**

*4-((tert-butyldimethylsilyl)oxy)butan-1-ol **S-7**:* Compound **S-7** was synthesized from 1,3-butan-diol (34 mmol, 3.0 mL) and *t*BuMe$_2$SiCl (34 mmol, 5.1 g) with the general procedure 2. The resulting alcohol **S-7** was purified via column chromatography (20 x 250 mm, 5:1 to 2:1 hexane: ethyl acetate) and a colorless oil was afforded as the pure product in 76% yield (25.8 mmol, 5.28 g).

Spectral data for compound **S-7**: ^{1}H NMR (500 MHz, Chloroform-*d*) δ 0.06 (s, 6H), 0.89 (s, 9H), 1.57 – 1.70 (m, 4H), 3.60 – 3.69 (m, 4H). ^{13}C{^{1}H}NMR (126 MHz, Chloroform-*d*) δ -5.42, 18.28, 25.88, 29.88, 30.24, 62.74, 63.34. These data are in agreement with the literature values.[12]

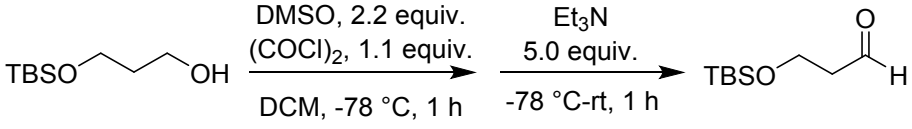

43 **2a**

14. General procedure 3: Swern oxidation:

*3-((tert-butyldimethylsilyl)oxy)propanal **2a**:* In a flamed dried 500 mL round bottom flask under N_2, DMSO (33 mmol, 2.3 mL) and CH_2Cl_2 (100 mL) were added. Then the reaction vessel was

cooled down to -78 ˚C and a solution of oxalyl chloride (16.5 mmol, 1.01 mL) in 10 mL CH_2Cl_2 was slowly added. After 10 minutes, alcohol **43** (15 mmol, 2.8 g) as a solution in 7.5 mL of CH_2Cl_2 was added slowly and the reaction mixture was stirred at -78 ˚C for 1 h. The reaction mixture was warmed up to room temperature after the addition of Et_3N (75 mmol, 10 mL) and it was quenched by the addition of saturated NH_4Cl. The organic layer was separated and washed with saturated $CuSO_4$ solution and brine. The resulting solution was dried over Na_2SO_4 and the solvent was removed under reduced pressure. Simple distillation (b.p. 65 ˚C, 1 mmHg) afforded pure aldehyde **2a** as a colorless oil in quantitative yield (15 mmol, 2.8 g).

Spectral data for compound **2a**: ^{1}H NMR (500 MHz, Chloroform-*d*) δ 0.06 (s, 6H), 0.86 (t, *J* = 1.2 Hz, 9H), 2.57 (tdd, *J* = 6.0, 2.2, 0.9 Hz, 2H), 3.97 (td, *J* = 6.0, 0.9 Hz, 2H), 9.78 (td, *J* = 2.0, 0.8 Hz, 1H). ^{13}C{^{1}H}NMR (126 MHz, Chloroform-*d*) δ -5.47, 18.19, 25.78, 46.53, 57.37, 202.01. These data are in good agreement with literature values.[13]

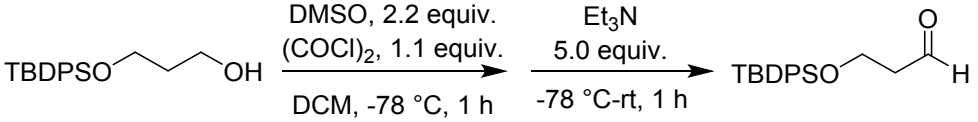

S-5 **2b**

*3-((tert-butyldiphenylsilyl)oxy)propanal **2b**:* Aldehyde **2b** was prepared from alcohol **S-5** (9.5 mmol, 3.1 g) with the general procedure 3 and purified via column chromatography (20 x 250 mm, 19:1 to 9:1 hexane: ethyl acetate) which afforded a white solid as the pure product in 78% yield (7.41 mmol , 2.32 g).

Spectral data for compound **2b**: ^{1}H NMR (500 MHz, Chloroform-*d*) δ 1.04 (s, 9H), 2.61 (td, *J* = 6.0, 2.2 Hz, 2H), 4.03 (t, *J* = 6.0 Hz, 2H), 7.36 – 7.44 (m, 4H), 7.41 – 7.49 (m, 2H), 7.63 – 7.70 (m, 4H), 9.83 (t, *J* = 2.2 Hz, 1H). ^{13}C{^{1}H}NMR (126 MHz, Chloroform-*d*) δ 19.13, 26.74, 46.37,

58.27, 127.76, 129.81, 133.21, 135.53, 201.95. These data are in agreement with the literature values.[14]

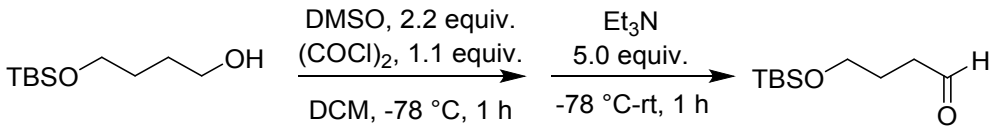

S-6 **34**

*4-((tert-butyldimethylsilyl)oxy)butanal **34**:* Aldehyde **34** was prepared from alcohol **S-6** (14.7 mmol, 3.01 g) with the general procedure 3 and purified via column chromatography (20 x 250 mm, 19:1 to 9:1 hexane: ethyl acetate) which afforded a colorless oil as the pure product in quantitative yield (14.7 mmol, 2.97 g).

Spectral data for compound **34**: ^{1}H NMR (500 MHz, Chloroform-*d*) δ 0.03 (s, 6H), 0.89 (s, 9H), 1.86 (tt, *J* = 7.0, 6.0 Hz, 2H), 2.51 (td, *J* = 7.1, 1.7 Hz, 2H), 3.65 (t, *J* = 6.0 Hz, 2H), 9.79 (t, *J* = 1.7 Hz, 1H). These data are in greement with the literature values.[12]

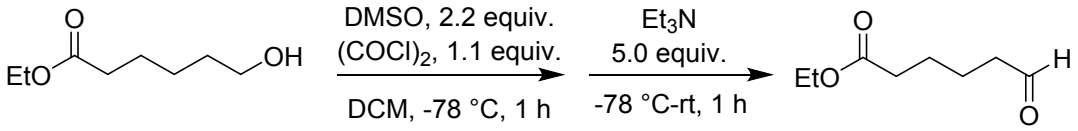

S-8 **35**

*ethyl 6-oxohexanoate **35***: Aldehyde **35** was prepared from ethyl 6-hydroxyhexanoate **S-8** (18 mmol, 3.0 mL) with the general procedure 3 and purified via simple distillation which afforded the pure product as a colorless oil in 80% yield (14.72 mmol, 2.328 g).

Spectral data for compound **35**: ^{1}H NMR (500 MHz, Chloroform-*d*) δ 1.21 (t, *J* = 7.1 Hz, 3H), 1.57 – 1.69 (m, 4H), 2.24 – 2.33 (m, 2H), 2.39 – 2.47 (m, 2H), 4.08 (q, *J* = 7.2 Hz, 2H), 9.73 (t, *J* = 1.6 Hz, 1H). ^{13}C{^{1}H}NMR (126 MHz, Chloroform-*d*) δ 14.19, 21.44, 24.32, 33.92, 43.46, 60.29, 173.18, 202.06. These data are in agreement with the literature value.[15]

15. Preparation of diazo compound

All diazo compounds were synthesized via standard procedure developed in our lab and the spectral data of these compounds were in agreement with the reported data in the literature.[7]

Spectral data for 2-diazo-N-(4-methoxybenzyl)acetamide **1a**: ^{1}H NMR (500 MHz, Chloroform-d) δ 5.16 (s, 1H), 6.95 (t, J = 7.5 Hz, 1H), 7.19 (t, J = 8.0 Hz, 2H), 7.55 (d, J = 8.0 Hz, 2H), 8.98 (s, 1H).^{13}C{^{1}H}NMR (126 MHz, Chloroform-d) δ 13.69, 19.97, 32.03, 39.83, 46.92, 165.32.

Spectral data for 2-diazo-N-(4-methoxybenzyl)acetamide **1b**: ^{1}H NMR (500 MHz, Chloroform-d) δ 3.79 (s, 3H), 4.38 (d, J = 5.7 Hz, 2H), 4.72 (s, 1H), 5.44 (s, 1H), 6.79 – 6.89 (m, 2H), 7.16 – 7.23 (m, 2H). ^{13}C{^{1}H}NMR (126 MHz, Chloroform-d) δ 43.68, 47.35, 55.45, 114.24, 129.29, 130.48, 159.22.

Spectral data for 2-diazo-N-(4-methoxybenzyl)acetamide **1c**: ^{1}H NMR (500 MHz, Chloroform-d) δ 0.89 (t, J = 7.3 Hz, 3H), 1.32 (dq, J = 14.7, 7.3 Hz, 2H), 1.46 (p, J = 7.3 Hz, 2H), 3.25 (brs, 2H), 4.73 (brs, 1H), 5.38 (brs, 1H); ^{13}C{^{1}H}NMR (126 MHz, Chloroform-d) δ 13.69, 19.97, 32.03, 39.83, 46.92, 165.32.

16. Determining the absolute stereochemistry of epoxide 11 with host-guest system

In Borhan group, several studies have proved that epoxide oxygen and amide functionalities can have binding interaction with porphyrin tweezers.[16] Tweezer C5-Zn-TPFP was employed for determination of absolute stereochemistry of substrate **11** (Figure S1). A proposed binding model was proposed to predict the helicity of the tweezers and therefore, the ECCD signal. It was assumed that one

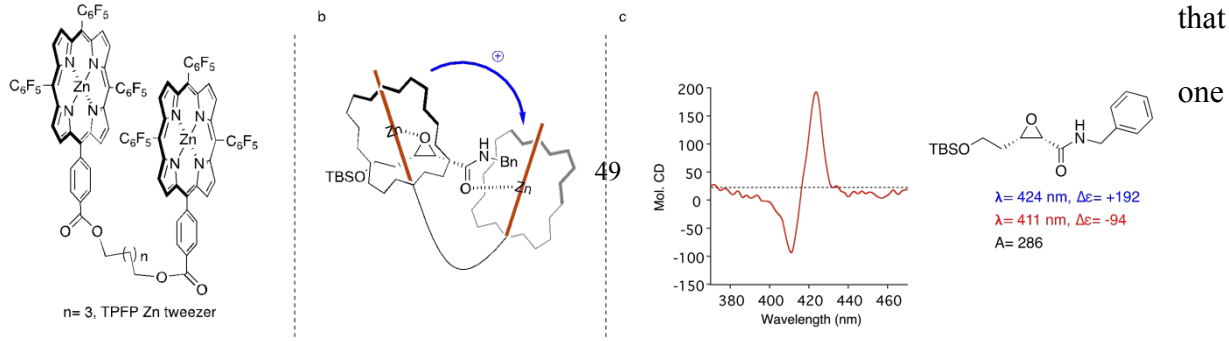

of the porphyrins binds to one of the pair electrons of epoxide from the same side of two hydrogens; therefore, the other porphyrin approaches to second binding site, carbonyl of amide, opposite side of the first porphyrin to avoid steric interaction (Figure S1-b). This binding approach between porphyrins and (*S*,*S*)-substrate **11** led to clockwise helical conformation and positive ECCD signal which is in agreement with the observed ECCD signals (Figure S1-c).

Figure S1: Structure of C5-Zn-TPFP. (b). binding model of substrate **11** and tweezer. (c). ECCD spectra.

16.1. Procedure for ECCD Measurement:

To hexanes (1 mL) in a 1.0 cm cell, 1 μL of a 1 mM stock solution of zinc porphyrin tweezer (C5-Zn-TPFP-Tz) in anhydrous CH_2Cl_2 was added to provide a 1 μM tweezer solution. The background spectrum was recorded from 480 nm to 350 nm at a scan rate of 100 nm/min at room temperature. Chiral guest molecule **11** was dissolved in anhydrous CH_2Cl_2 to afford a 10 mM solution then 0.2 to 100 μL of this solution was added to the cell with the tweezer solution affording the host-guest complex. CD spectra of samples measured with 10 accumulations, was subtracted from background and normalized based on the concentration to obtain the molecular CD (Mol. CD).

17. Computational Methods

All density functional theory (DFT) calculations presented in the manuscript were performed using M06-2X[18]/6-311++G**/PCM[19]//B3LYP[20]-D3[21]/6-31G*[22] (solvent = toluene) level of theory as implemented in *Gaussian 16*.[17] Ground state geometry optimization and transition structures (TSs) were located at the B3LYP-D3/6-31G* level of theory. All starting materials and intermediates were verified as true minima, and all the transition structures were characterized by one imaginary frequency. Single point energy calculations were performed using the M06-2X functional, a triple-ζ basis set 6-311++G**, and a PCM solvent model for toluene. Gibbs free energies were estimated at reaction temperatures, namely 233 K and 273 K for the boron-catalyzed and aluminum-catalyzed epoxidation of aldehydes, respectively. The Gibbs free energies were further corrected using Grimme's quasi-RRHO[23] approach. Intermediates along the reaction coordinate were located by performing a quick reaction coordinate analysis (QRC) from the respective transition structures (**Figure 1** in the manuscript). Cartesian coordinates of all computed starting materials, intermediates, and transition structures are included in the attached xyz file.

Extensive conformational analysis was conducted on the appropriate transition states in evaluation of the stereoselectivity-determining step. The lowest energy conformations of these transition states in both the boron-catalyzed and aluminum-catalyzed operational BLA pathways were modeled using B3LYP-D3/6-31G* and M06-2X/6-31G* to ensure an unbiased interpretation of the free energy differences. Single point energy calculations were performed using M06-2X/6-311++G** with a PCM solvent model for toluene. The relative energies between the modeled enantiomers remain almost consistent for each method employed.

For a systematic search on the enantiodivergent epoxidation of aldehydes, we utilized a reaction between **18** and **1a** (from the manuscript) as the model substrates. Various transition structures were explored for each of the different steps involved in the reaction pathway using B3LYP-D3/6-31G* level of theory, as implemented in *Gaussian 16.* The array of structures arises from the possibilities of (1) different arrangements of the catalyst's phenyl rings, (2) variable hydrogen bonding interaction between the hydroxyl group of one ligand to the oxygen atom of another ligand of the catalyst, and 3) various arrangements of the phenyl ring of aldehyde (**18**) and diazoacetamide (**1a**) (Figure S2 and Figure S3). Overall, 141 unique transition structures and intermediates were identified for this reaction.

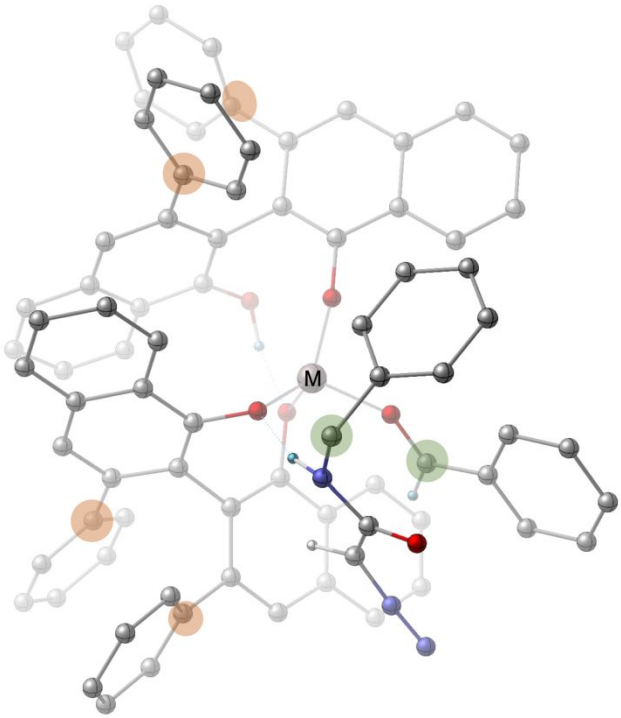

Figure S2: Showing rotatable bonds about which conformational search was performed for the BLA mechanism (M = B, Al).

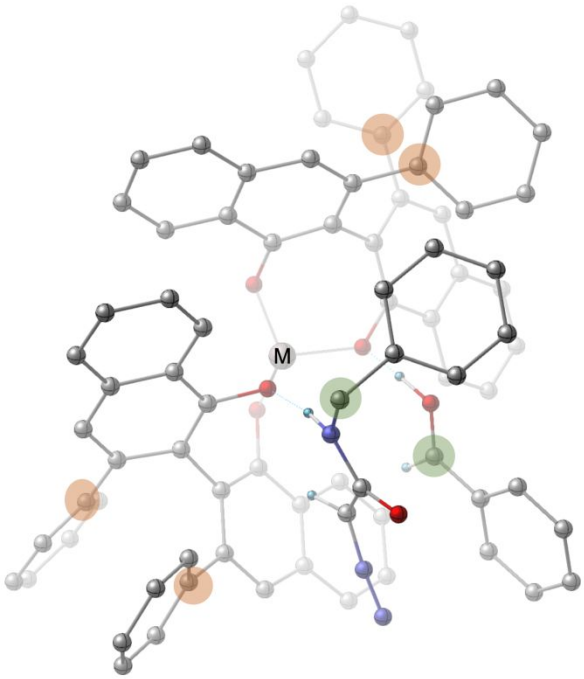

Figure S3: Showing rotatable bonds about which conformational search was performed for the BA mechanism (M = B, Al).

18. Brønsted Acid Assisted Lewis Acid Pathway for Boron

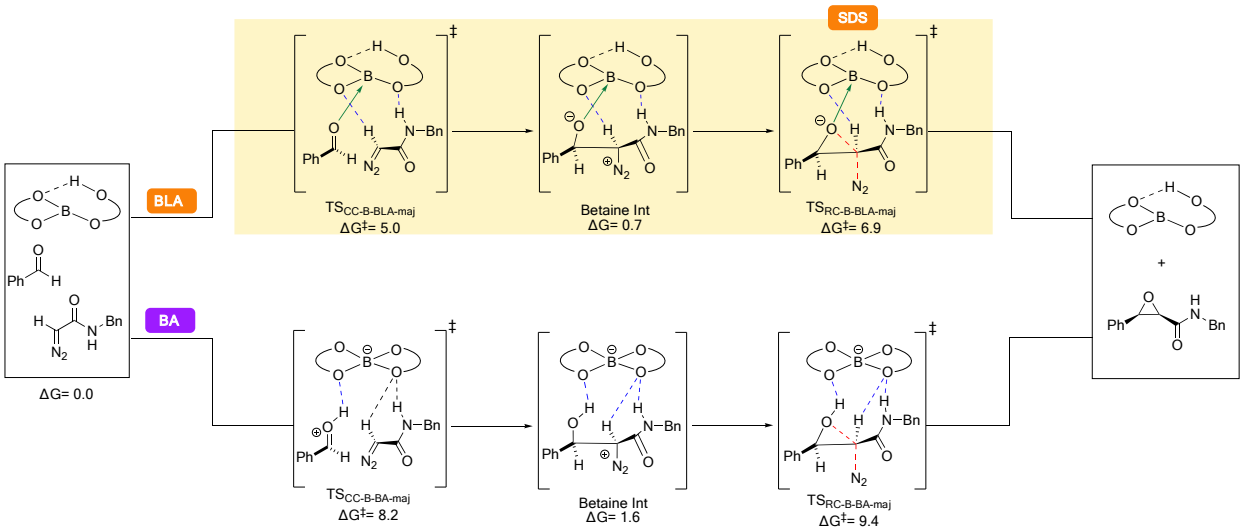

Figure S4: Free energies of key stationary points in the reaction coordinate leading to the major enantiomer of *cis*-epoxide **24a** for the reaction catalyzed by the (*R*)-VANOL boron catalyst computed at M06-2x/6-311++G** PCM (toluene)// B3LYP-D3/6-31G*. The BLA pathway is highlighted in yellow, and the selectivity-determining step (SDS) is indicated. All the reported energies for each transition state and intermediate are relative to the pre-reactive complex of the respective catalyst with benzaldehyde (**18**) and diazoacetamide **1a** in the BLA pathway, which is the lowest energy stationary point in either pathway for the catalyst.

To identify the rate- and selectivity-determining steps in the boron-catalyzed epoxidation of aldehydes, we modeled the key carbon-carbon bond forming and ring closing steps for the BLA pathway. The lowest-lying transition structures for the selectivity determining step of the BLA pathway are shown in **Figure 2** in the manuscript. The carbon-carbon bond forming distance is similar in the lowest-lying transition structures leading to major and minor enantiomers, specifically 1.85 Å in $\mathbf{TS_{CC\text{-}B\text{-}BLA\text{-}maj}}$ and 1.91 Å in $\mathbf{TS_{CC\text{-}B\text{-}BLA\text{-}min}}$. Both the TSs benefit from similar interactions: (a) a strong intramolecular hydrogen bonding interaction present between the hydroxyl group and oxygen atom of another ligand of the catalyst; (b) an intermolecular hydrogen bonding interaction present between the NH of diazo and the oxygen atom of the catalyst and (c)

a weaker non-covalent interaction present between the α-CH of diazo and the oxygen atom of the catalyst – shown in Figure S5.

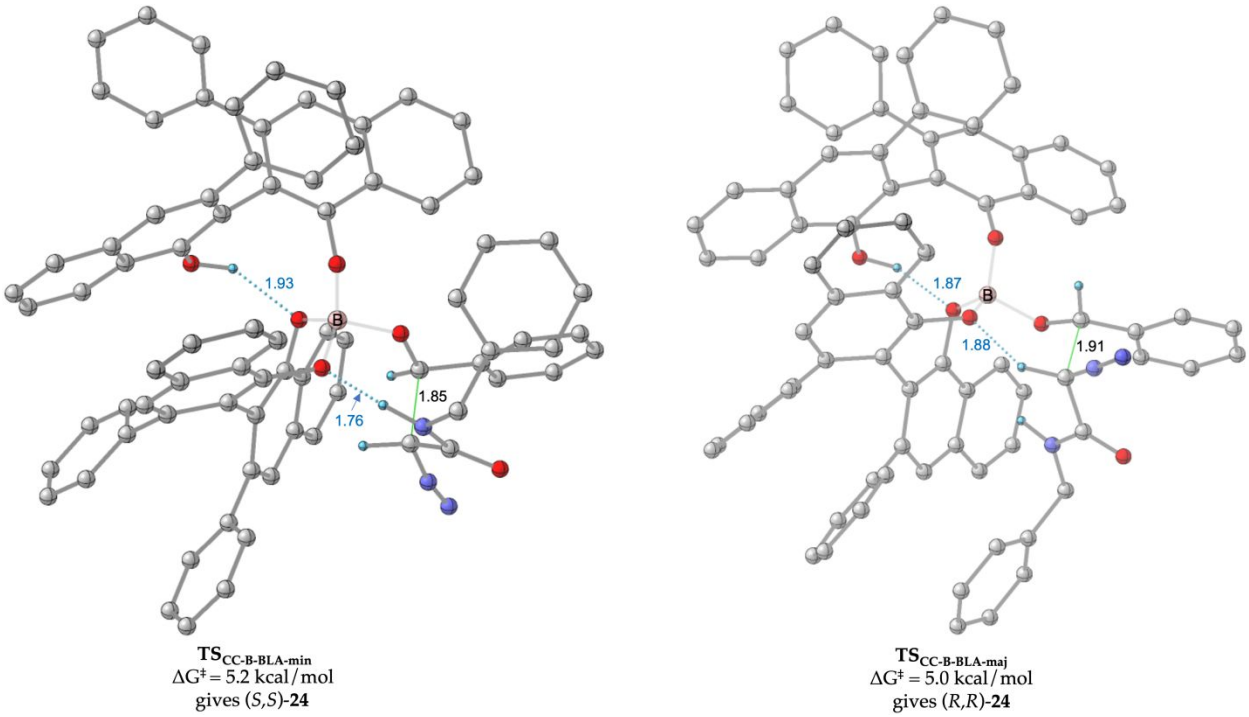

Figure S5: Lowest-lying transition structure for carbon-carbon bond formation ($TS_{CC-B-BLA}$) for BLA pathway for (*R*)-VANOL boron catalyst.

19. Brønsted Acid Pathway for Boron

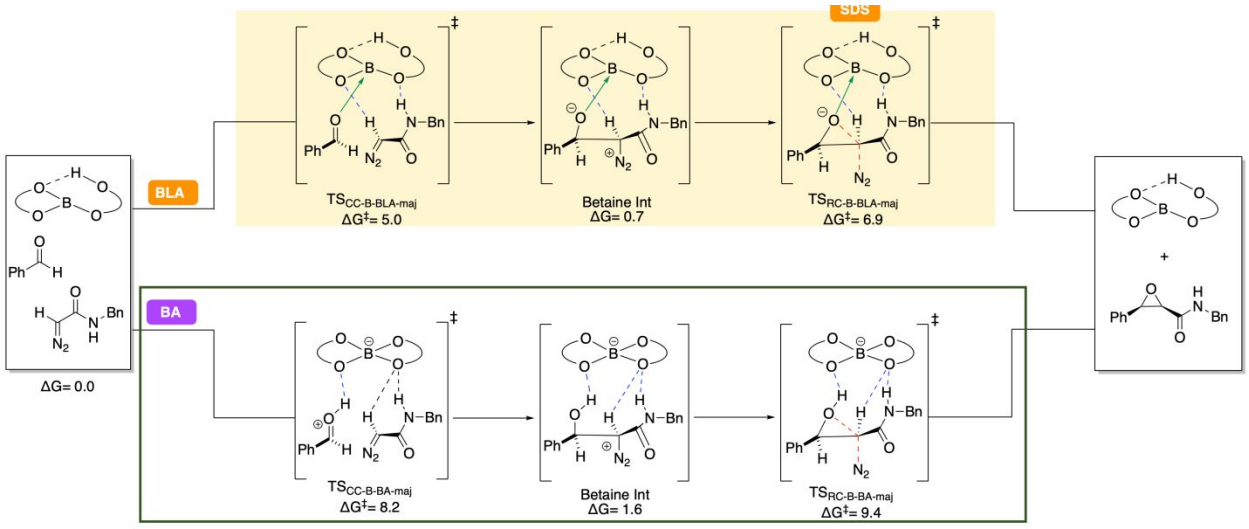

Figure S6: Free energies of key stationary points in the reaction coordinate leading to the major enantiomer of *cis*-epoxide **24a** for the reaction catalyzed by the (*R*)-VANOL boron catalyst computed at M06-2x/6-311++G** PCM (toluene)// B3LYP-D3/6-31G*. The BA pathway is highlighted in the green box, and the selectivity-determining step (SDS) is indicated. All the reported energies for each transition state and intermediate are relative to the pre-reactive complex of the respective catalyst with benzaldehyde (**18**) and diazoacetamide **1a** in the BLA pathway, which is the lowest energy stationary point in either pathway for the catalyst.

We initiated our DFT investigations by locating the transition structures for the key carbon-carbon bond-making ($\mathbf{TS_{CC}}$) and ring-closing step ($\mathbf{TS_{RC}}$) for the nucleophilic attack of **1a** to **18** for BLA, BA, and LA pathways. After careful analysis, BLA was found to be the operational pathway in the epoxidation reaction of the aldehydes, as described in the manuscript. The Brønsted acid (BA) pathway for the epoxidation of aldehydes was also explored (Figure S6-BA). It was expected that the catalyst structure would be comprised of a tetracoordinated boron along with protonated aldehyde coordinated to the oxygen atom of one ligand **(Scheme 4 in the manuscript)**. A similar mechanism to BLA was proposed for this pathway, involving initiation via the nucleophilic attack of the diazo acetamide to the aldehyde, followed by an S_N2-like ring closure.

Key transition structures $\mathbf{TS_{CC}}$ and $\mathbf{TS_{RC}}$ were modeled for the major and minor enantiomers of the *cis*-epoxide. The extent of the carbon-carbon bond forming distance was indistinguishable in both the modeled transition structures for the key carbon-carbon bond-making step (1.97 Å in $\mathbf{TS_{CC\text{-}B\text{-}BA\text{-}maj}}$ and 2.01 Å in $\mathbf{TS_{CC\text{-}B\text{-}BA\text{-}min}}$). A strong intermolecular hydrogen bonding interaction between NH and the oxygen atom of the catalyst (1.87 Å in $\mathbf{TS_{CC\text{-}B\text{-}BA\text{-}maj}}$ and 1.89 Å in $\mathbf{TS_{CC\text{-}B\text{-}BA\text{-}min}}$) and a non-covalent interaction present between α-CH and the oxygen atom the catalyst (2.22 Å in $\mathbf{TS_{CC\text{-}B\text{-}BA\text{-}maj}}$ and 2.36 Å in $\mathbf{TS_{CC\text{-}B\text{-}BA\text{-}min}}$) were observed in both the TSs (Figure S7). The lowest-lying TSs for the successive ring-closing step ($\mathbf{TS_{RC\text{-}B\text{-}BA\text{-}maj}}$ and $\mathbf{TS_{RC\text{-}B\text{-}BA\text{-}min}}$) retained similar interactions as their corresponding carbon-carbon bond-forming TSs (Figure S8). The C-O bond-forming distance (2.08 Å in $\mathbf{TS_{RC\text{-}B\text{-}BA\text{-}maj}}$ and 2.11 Å in $\mathbf{TS_{RC\text{-}B\text{-}BA\text{-}min}}$) and C-N bond-breaking distance (1.82 Å in $\mathbf{TS_{RC\text{-}B\text{-}BA\text{-}maj}}$ and 1.84 Å in $\mathbf{TS_{RC\text{-}B\text{-}BA\text{-}min}}$) were comparable in both the TSs. Given that the free energy barriers for the key TSs in the formation of the major enantiomer ($\mathbf{TS_{CC\text{-}B\text{-}BA\text{-}maj}}$ and $\mathbf{TS_{RC\text{-}B\text{-}BA\text{-}min}}$) were found to be significantly higher in energy compared to the lowest-lying TSs for the BLA pathway, this pathway was eliminated (Figure S6).

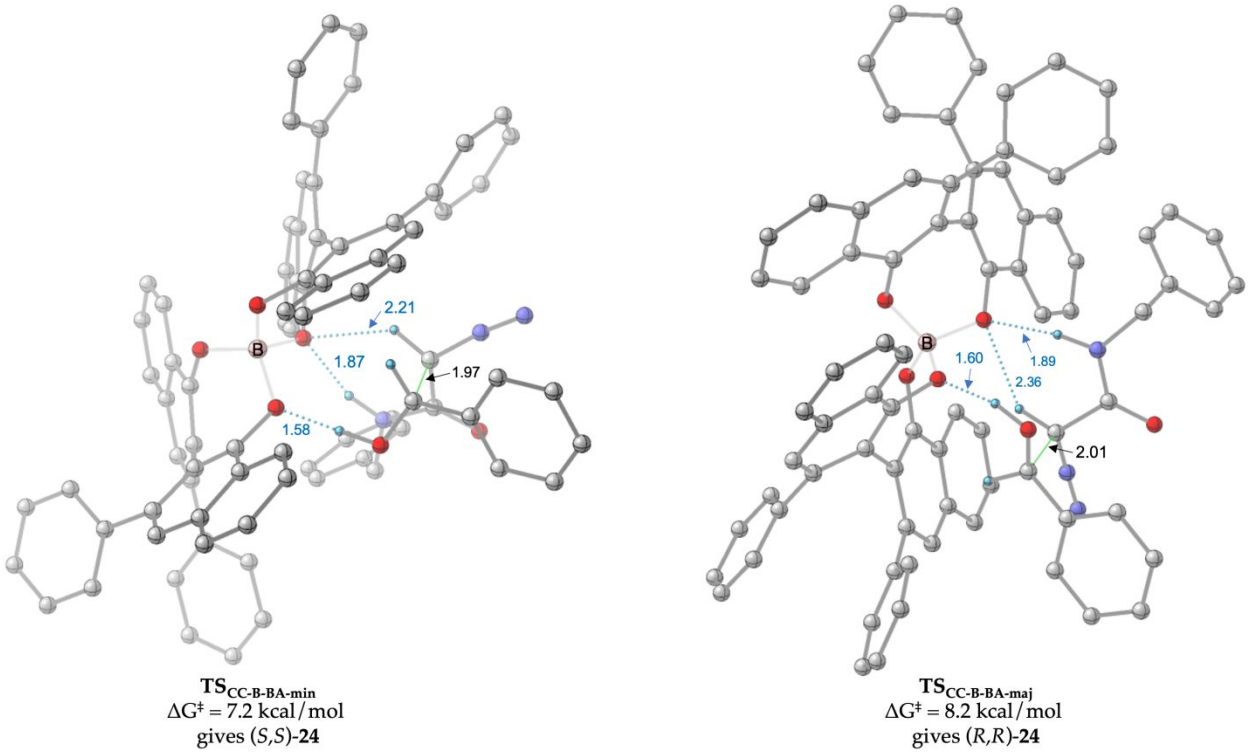

$TS_{CC\text{-}B\text{-}BA\text{-}min}$
$\Delta G^{\ddagger}$ = 7.2 kcal/mol
gives (*S*,*S*)-**24**

$TS_{CC\text{-}B\text{-}BA\text{-}maj}$
$\Delta G^{\ddagger}$ = 8.2 kcal/mol
gives (*R*,*R*)-**24**

Figure S7: Lowest-lying transition structure for carbon-carbon bond formation ($TS_{CC\text{-}B\text{-}BA}$) for BA pathway for (*R*)-VANOL boron catalyst.

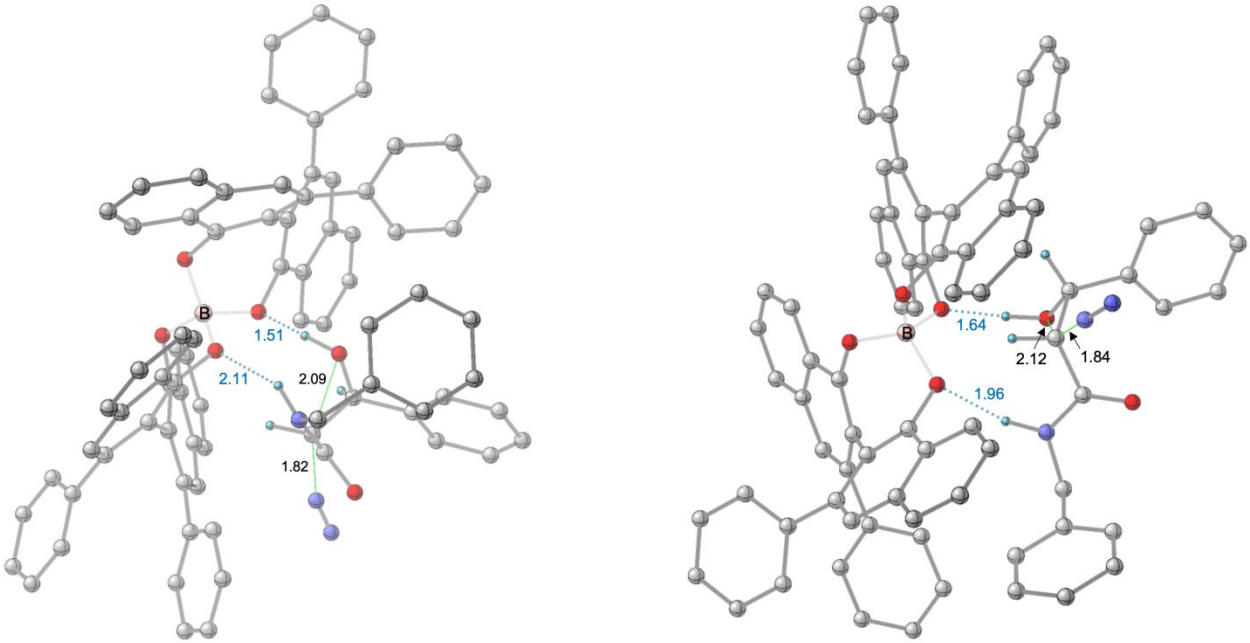

$TS_{RC\text{-}B\text{-}BA\text{-}min}$
$\Delta G^{\ddagger}$ = 9.2 kcal/mol
gives (*S*,*S*)-**24**

$TS_{RC\text{-}B\text{-}BA\text{-}maj}$
$\Delta G^{\ddagger}$ = 9.4 kcal/mol
gives (*R*,*R*)-**24**

Figure S8: Lowest-lying transition structure for ring-closing step ($TS_{RC\text{-}B\text{-}BA}$) for BA pathway for (*R*)-VANOL boron catalyst.

20. Brønsted Acid Assisted Lewis Acid Pathway for Aluminum

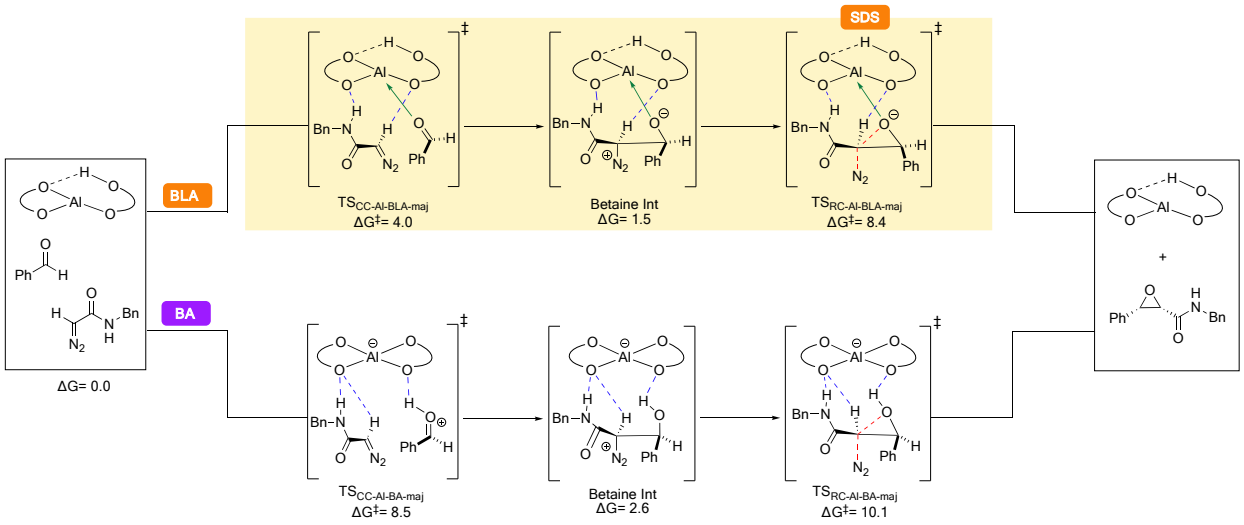

Figure S9: Free energies of key stationary points in the reaction coordinate leading to the major enantiomer of *cis*-epoxide **24a** for the reaction catalyzed by the (*R*)-VANOL aluminium catalyst computed at M06-2x/6-311++G** PCM (toluene)// B3LYP-D3/6-31G*. The BLA pathway is highlighted in yellow, and the selectivity-determining step (SDS) is indicated. All the reported energies for each transition state and intermediate are relative to the pre-reactive complex of the respective catalyst with benzaldehyde (**18**) and diazoacetamide **1a** in the BLA pathway, which is the lowest energy stationary point in either pathway for the catalyst.

To identify the rate- and selectivity-determining steps in the aluminum-catalyzed epoxidation of aldehydes, we modeled the key carbon-carbon bond forming and ring-closing steps for the BLA pathway. The lowest-lying transition structures for the selectivity determining step of the BLA pathway are shown in (**Figure 3 in the manuscript**). The carbon-carbon bond forming distance was found to be almost similar in the lowest-lying transition structures leading to the major and minor enantiomers, specifically 1.89 Å in $\mathbf{TS_{CC\text{-}Al\text{-}BLA\text{-}maj}}$ and 1.87 Å in $\mathbf{TS_{CC\text{-}Al\text{-}BLA\text{-}min}}$.

Both the TSs benefit from similar interactions: (a) a strong intramolecular hydrogen bonding interaction present between the hydroxyl group and oxygen atom of another ligand of the catalyst; (b) an intermolecular hydrogen bonding interaction present between the NH of diazo and the oxygen atom of the catalyst and (c) a weaker non-covalent interaction present between the α-CH of diazo and the oxygen atom of the catalyst – shown in Figure S10.

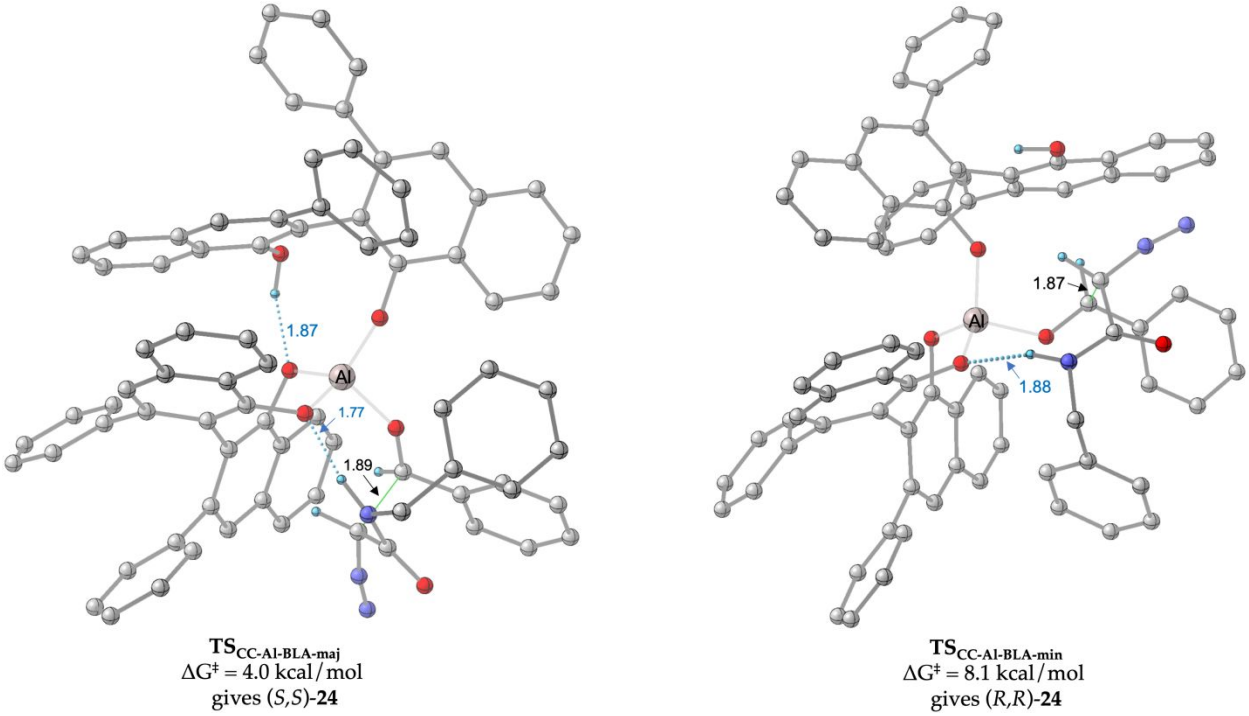

Figure S10: Lowest-lying transition structure for carbon-carbon bond formation ($TS_{CC-Al-BLA}$) for BLA pathway for (*R*)-VANOL aluminum catalyst.

21. Brønsted Acid Pathway for Aluminum

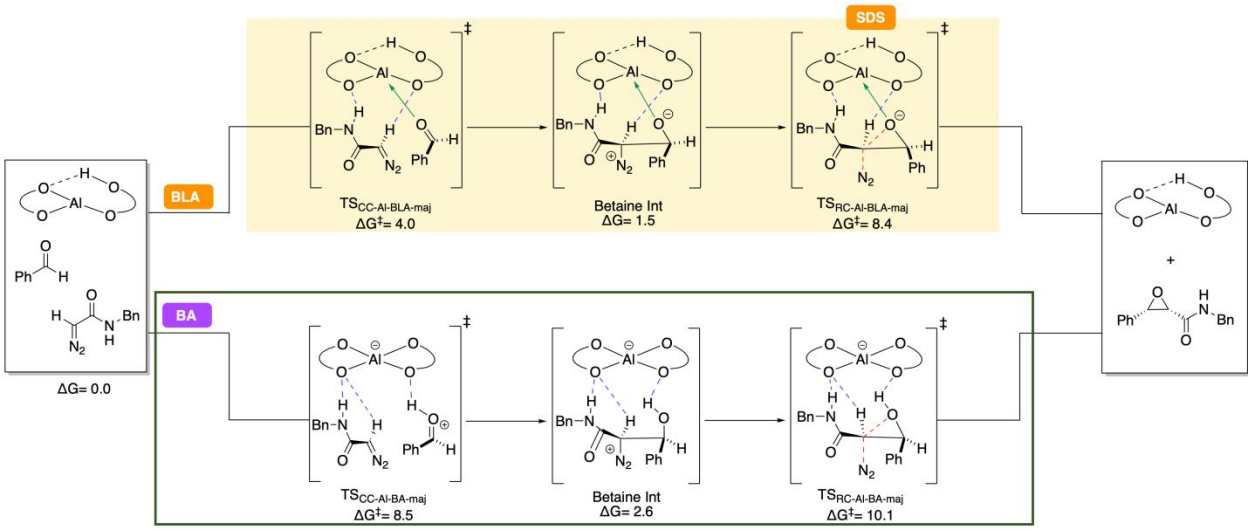

Figure S11: Free energies of key stationary points in the reaction coordinate leading to the major enantiomer of *cis*-epoxide **24a** for the reaction catalyzed by the (*R*)-VANOL aluminum catalyst computed at M06-2x/6-311++G** PCM (toluene)// B3LYP-D3/6-31G*. The BA pathway is highlighted in the green box, and the selectivity-determining step (SDS) is indicated. All the reported energies for each transition state and intermediate are relative to the pre-reactive complex of the respective catalyst with benzaldehyde (**18**) and diazoacetamide **1a** in the BLA pathway, which is the lowest energy stationary point in either pathway for the catalyst.

We initiated our DFT investigations by locating the transition structures for the key carbon-carbon bond-making ($\mathbf{TS_{CC}}$) and ring-closing step ($\mathbf{TS_{RC}}$) for the nucleophilic attack of **1a** to **18** for BLA, BA, and LA pathways. After careful analysis, BLA was found to be the operational pathway in the epoxidation reaction of the aldehydes, as described in the manuscript. The Brønsted acid (BA) pathway for the epoxidation of aldehydes was also explored. It was expected that the structure would be comprised of a tetracoordinated aluminium along with a protonated aldehyde coordinated to the oxygen atom of one ligand **(Scheme 4 in the manuscript)**. A similar

mechanism to BLA was proposed for this pathway, involving initiation via the nucleophilic attack of the diazo acetamide to the aldehyde, followed by an S_N2-like ring closure (Figure S11-BA).

Key transition structures $\mathbf{TS_{CC}}$ and $\mathbf{TS_{RC}}$ were modeled for the major and minor enantiomers of the *cis*-epoxide. The extent of the carbon-carbon bond forming distance in $\mathbf{TS_{CC\text{-}Al\text{-}BA\text{-}maj}}$ is 2.03 Å whereas 1.96 in $\mathbf{TS_{CC\text{-}Al\text{-}BA\text{-}min}}$. A strong intermolecular hydrogen bonding interaction between NH and the oxygen atom of the catalyst (1.81 Å in $\mathbf{TS_{CC\text{-}Al\text{-}BA\text{-}maj}}$ and 1.82 Å in $\mathbf{TS_{CC\text{-}Al\text{-}BA\text{-}min}}$) and a weak non-covalent interaction present between α-CH and the oxygen atom the catalyst (2.44 Å in $\mathbf{TS_{CC\text{-}Al\text{-}BA\text{-}maj}}$ and 2.38 Å in $\mathbf{TS_{CC\text{-}Al\text{-}BA\text{-}min}}$) were observed in both TSs. The lowest-lying TSs for the successive ring-closing step ($\mathbf{TS_{RC\text{-}Al\text{-}BA\text{-}maj}}$ and $\mathbf{TS_{RC\text{-}Al\text{-}BA\text{-}min}}$) retained similar interactions as their corresponding carbon-carbon bond-forming TSs (Figure S12). The C-O bond-forming distance (2.10 Å in $\mathbf{TS_{RC\text{-}Al\text{-}BA\text{-}maj}}$ and 2.11 Å in $\mathbf{TS_{RC\text{-}Al\text{-}BA\text{-}min}}$) and C-N bond-breaking distance (1.86 Å in $\mathbf{TS_{RC\text{-}Al\text{-}BA\text{-}maj}}$ and 1.83 Å in $\mathbf{TS_{RC\text{-}Al\text{-}BA\text{-}min}}$) were comparable in both the TSs (Figure S13). Given that the free energy barriers for the key TSs in the formation of the major enantiomer ($\mathbf{TS_{CC\text{-}Al\text{-}BA\text{-}maj}}$ and $\mathbf{TS_{RC\text{-}Al\text{-}BA\text{-}min}}$) were found to be significantly higher in energy compared to the lowest-lying TSs for the BLA pathway, this pathway was eliminated.

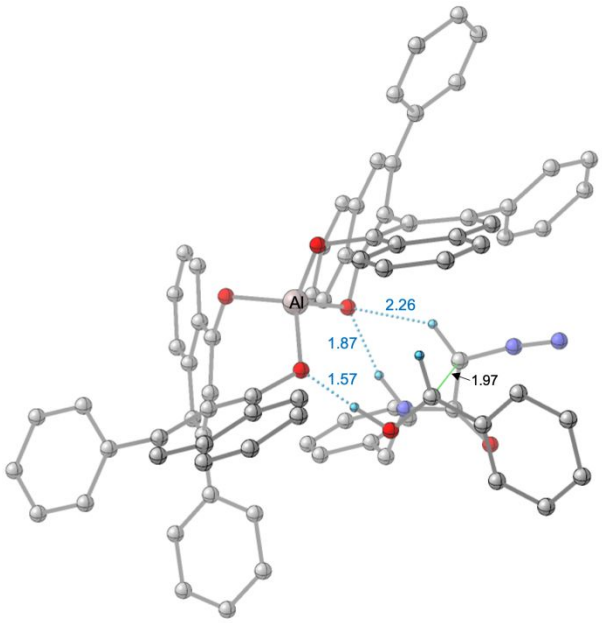

TS$_{\text{CC-Al-BA-maj}}$
$\Delta G^{\ddagger}$ = 8.5 kcal/mol
gives (*S*,*S*)-**24**

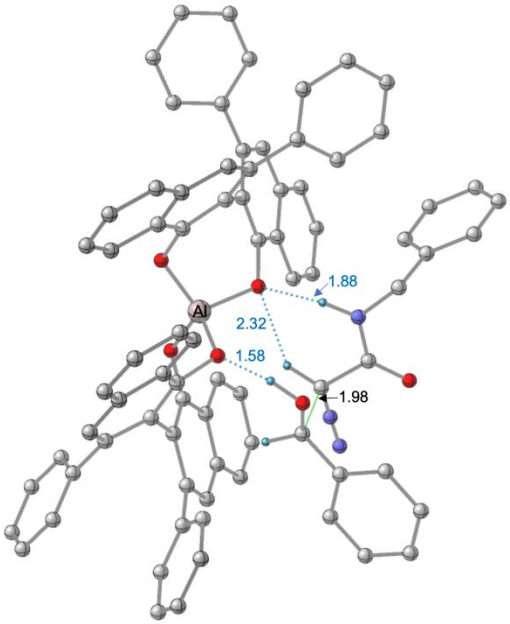

TS$_{\text{CC-Al-BA-min}}$
$\Delta G^{\ddagger}$ = 8.9 kcal/mol
gives (*R*,*R*)-**24**

Figure S12: Lowest-lying transition structure for carbon-carbon bond formation ($TS_{CC\text{-}Al\text{-}BA}$) for BA pathway for (*R*)-VANOL aluminum catalyst.

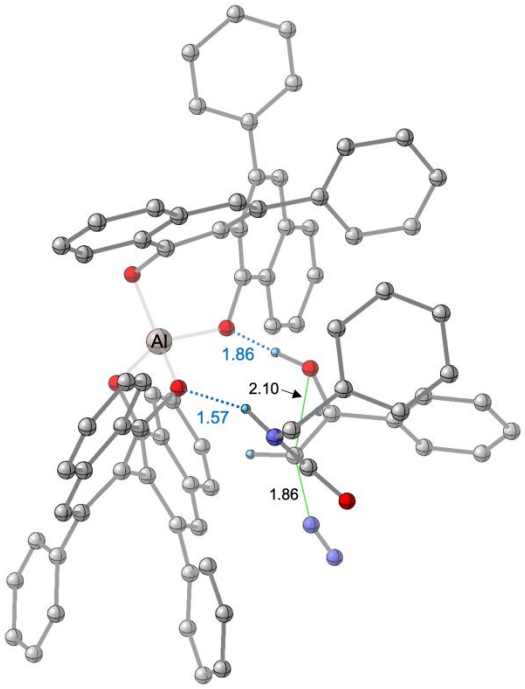

TS$_{\text{RC-Al-BA-maj}}$
$\Delta G^{\ddagger}$ = 10.1 kcal/mol
gives (*S*,*S*)-**24**

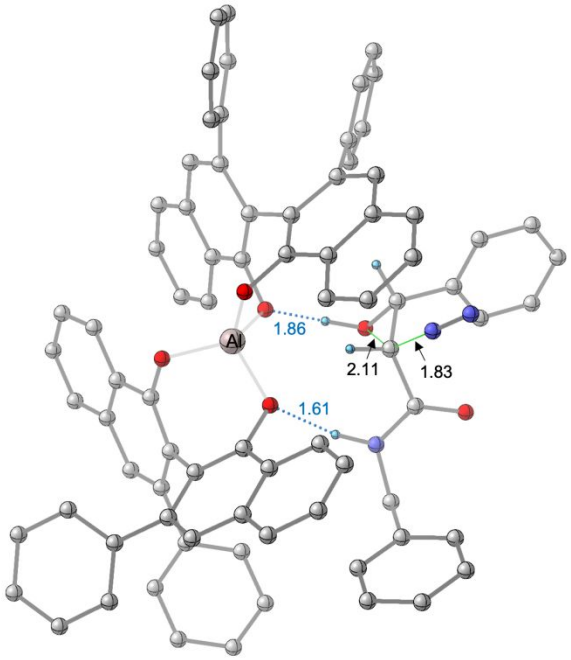

TS$_{\text{RC-Al-BA-min}}$
$\Delta G^{\ddagger}$ = 10.9 kcal/mol
gives (*R*,*R*)-**24**

Figure S13: Lowest-lying transition structure for ring-closing step ($TS_{RC\text{-}Al\text{-}BA}$) for BA pathway for (*R*)-VANOL aluminum catalyst.

22. Alternate Structure of VANOL-derived Boron Catalyst

An alternate conformation of the VANOL-derived boron catalyst was also explored. The proposed structure of the catalyst contains two tri-coordinated borons (VANOL-B-2). It is anticipated that the hydrogen-bearing oxygen atom in VANOL-B protonates the diazo acetamide in the reaction and further coordinates with another boron-ligated VANOL moiety to generate the catalyst with a 3:2 ratio of VANOL to boron (Figure S14).

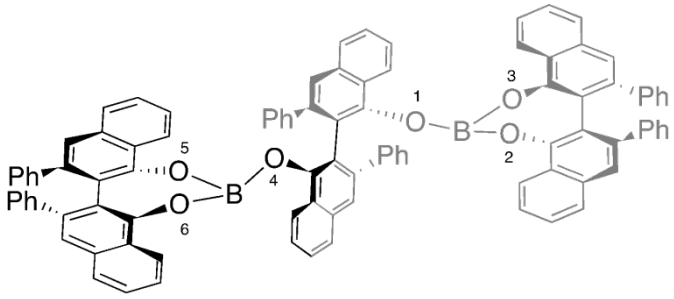

Figure S14: Proposed structure of 3:2 complex of VANOL-B-2 catalyst.

We modeled the carbon-carbon bond forming and ring-closing steps for the major enantiomer utilizing the VANOL-B-2 catalyst to establish the rate- and selectivity-determining steps. All the transition structures presented in this section for the (*R*)-VANOL-B-2 catalyzed reaction of **18** and **1a** were calculated using ONIOM(B3LYP/6-31+G*:AM1), as implemented in *Gaussian 16*. High-level single-point energy calculations were performed using M06-2X/6-

311++G** PCM (toluene). The division of layers for the ONIOM calculations is shown in Figure S15.

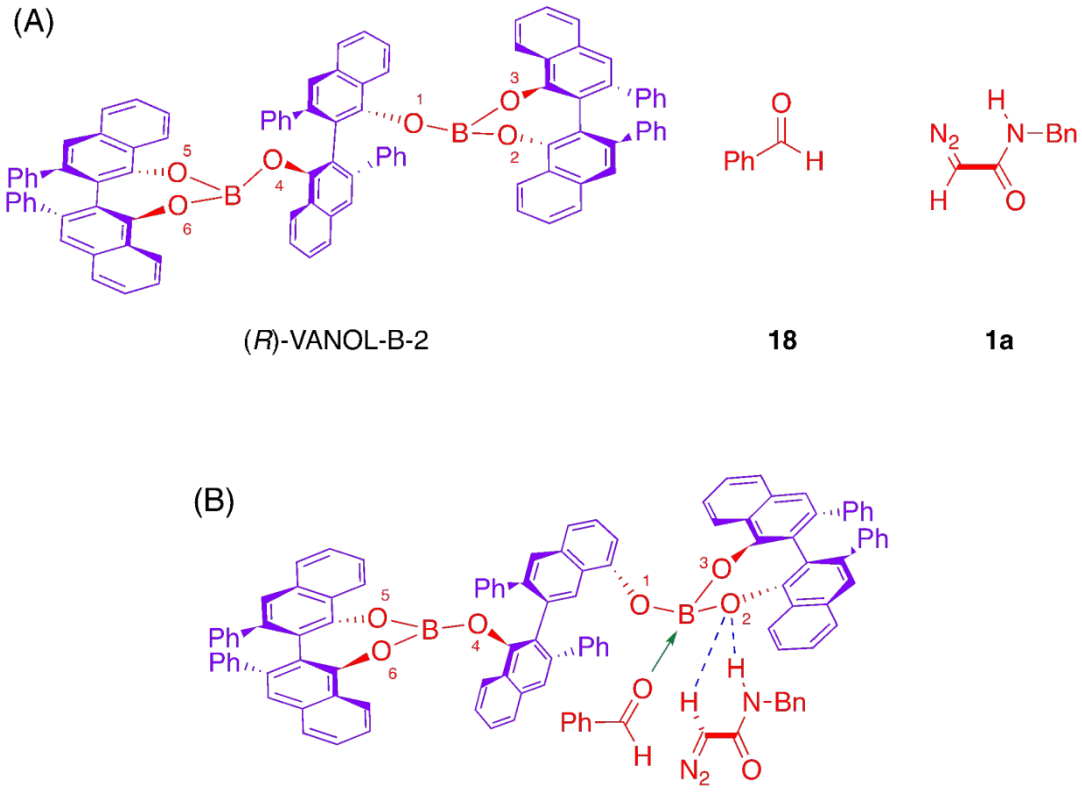

Figure S15: (A) Division of layers for ONIOM calculation. The portions highlighted in red are modeled using DFT calculation and portions highlighted in blue are calculated using the semi-empirical method (B) Interaction of VANOL-B-2 with aldehyde **18** and diazo acetamide **1a** in transition structure.

$\mathbf{TS_{CC\text{-}B\text{-}2\text{-}maj}}$ and $\mathbf{TS_{RC\text{-}B\text{-}2\text{-}maj}}$ are the lowest energy transition structures located for the major enantiomer for the carbon-carbon bond forming and ring-closing steps, respectively. Both the TSs experience similar interactions with the VANOL-B-2 catalyst. A hydrogen bonding interaction between NH of **1a** and O2 of the catalyst (2.01 Å in $\mathbf{TS_{CC\text{-}B\text{-}2\text{-}maj}}$ and 2.05 Å in $\mathbf{TS_{RC\text{-}}}$

$_{\text{B-2-maj}}$), an α-CH of **1a** and O3 (2.19 Å in $\mathbf{TS}_{\text{CC-B-2-maj}}$ and 2.23 Å in $\mathbf{TS}_{\text{RC-B-2-maj}}$), and an additional non-covalent interaction between the α-CH of **18** and O3 (2.45 Å in $\mathbf{TS}_{\text{CC-B-2-maj}}$ and 2.57 Å in $\mathbf{TS}_{\text{RC-B-2-maj}}$) are present, and more enhanced, in $\mathbf{TS}_{\text{CC-B-2-maj}}$ compared to $\mathbf{TS}_{\text{RC-B-2-maj}}$. This facilitates the stabilization and lowering of the barrier for catalysis for the respective transition structure. $\mathbf{TS}_{\text{RC-B-2-maj}}$ is found to be 7.0 kcal/mol higher in energy than $\mathbf{TS}_{\text{CC-B-2-maj}}$ and serves as the rate- and selectivity-determining step (Figure S16). Having established the selectivity-determining step, we modeled both the observed *cis*-epoxides for the ring-closing step (Figure S17). The extent of C-O bond formation (2.15 Å in $\mathbf{TS}_{\text{RC-B-2-min}}$ and 2.09 Å in $\mathbf{TS}_{\text{RC-B-2-maj}}$) and C-N bond breaking (1.86 Å in $\mathbf{TS}_{\text{RC-B-2-min}}$ and 1.82 Å in $\mathbf{TS}_{\text{RC-B-2-maj}}$) are almost indistinguishable. There is a similar degree of hydrogen bonding present between NH of **1a** and O2 (1.93 Å in $\mathbf{TS}_{\text{RC-B-2-min}}$ and 2.04 Å in $\mathbf{TS}_{\text{RC-B-2-maj}}$) in both the lowest lying transition structures located for the *cis*-epoxides. A stronger non-covalent interaction between α-CH of **1a** and O2 (2.23 Å) was observed in $\mathbf{TS}_{\text{RC-B-2-maj}}$ compared to $\mathbf{TS}_{\text{RC-B-2-min}}$ (2.48 Å). The computed free energy difference between the two competing *cis* enantiomers was found to be 1.0 kcal/mol, favoring $\mathbf{TS}_{\text{RC-B-2-maj}}$ leading to the experimentally observed enantiomer. A 79% ee at 233 K was predicted for these transition states, which is slightly lower than the experimentally observed ee of 99% for this reaction. Previously reported experimental studies on the Lewis acid boron complex does not support the formation of this catalyst conformation in the reaction.[7]

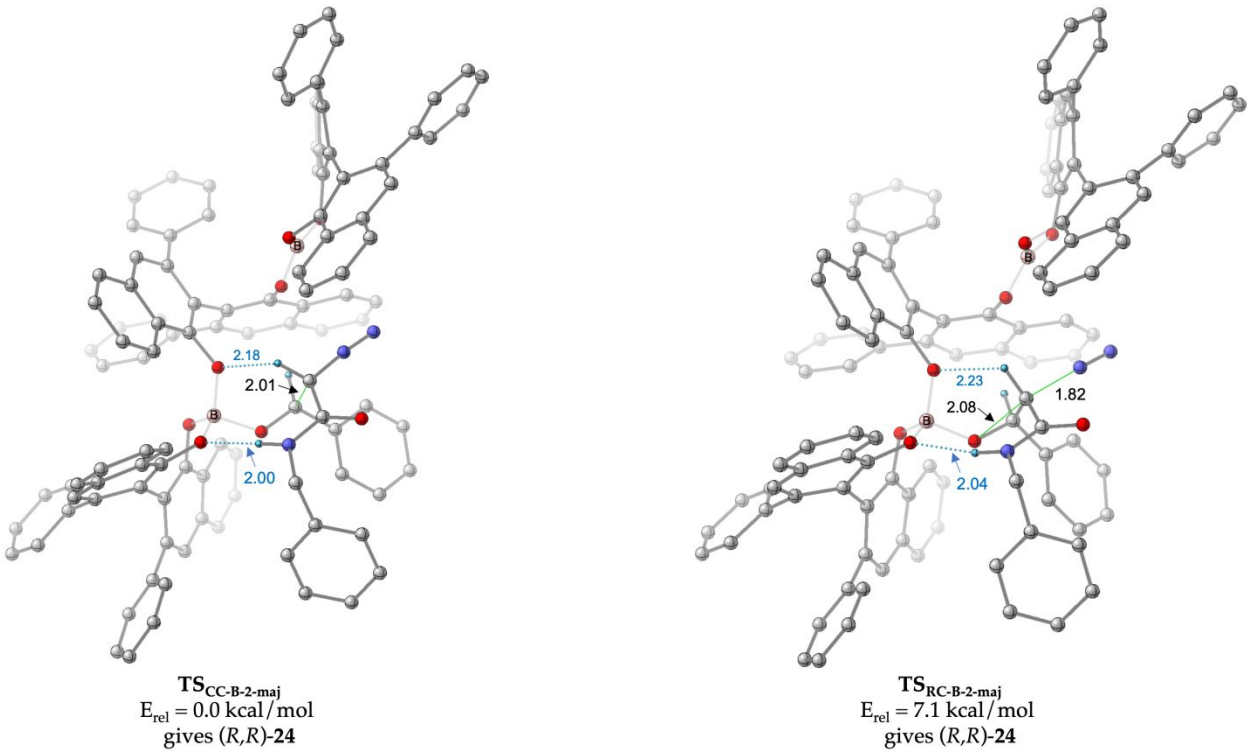

Figure S16: Determination of rate- and selectivity determining step. Lowest-lying transition structure for carbon-carbon bond forming and ring-closing TS for (*R*)-VANOL-B-2 catalyst.

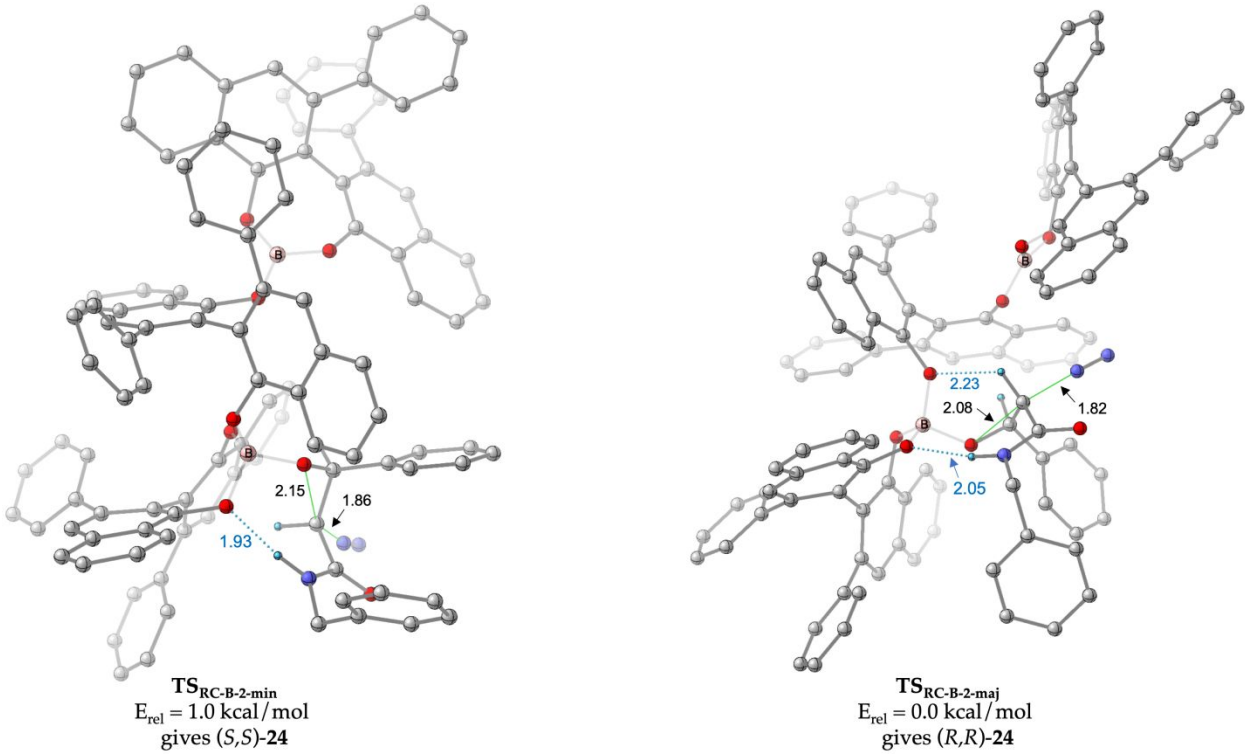

Figure S17: Lowest-lying transition structures for ring-closing step for (*R*)-VANOL-B-2 catalyst.

23. Pentacoordinated Aluminum

Another catalyst conformation of aluminum was also explored (Figure S18). This new conformation is comprised of a tetracoordinated aluminum with a protonated oxygen atom of one ligand. The aluminum was found in a nearly tetrahedral geometry in the located transition structures for the major enantiomer, with three of the Al-O bonds ranging from 1.78-1.83 Å and the hydrogen-bearing oxygen at 2.11 Å. All attempts to locate a similar conformation for boron resulted in a catalyst structure resembling that of the Brønsted Acid-assisted Lewis Acid pathway. The modeled TSs for the key carbon-carbon bond forming and ring-closing step experience similar stabilizing interactions between the reactant and catalyst compared to the TSs for the BLA pathway, as discussed earlier. A strong intermolecular hydrogen bonding interaction between the NH of diazo and the oxygen atom of the catalyst and a weak non-covalent interaction between the

α-CH of diazo and the oxygen atom of the catalyst was noted. Another intermolecular hydrogen bonding interaction between the hydrogen-bearing oxygen of the ligand and the carbonyl oxygen atom of the aldehyde was also observed. However, the free energy barriers for the lowest-lying transition structures for carbon-carbon bond formation and the subsequent ring-closing step were found significantly higher in energy compared to the lowest-energy carbon-carbon bond formation TS in the operational BLA pathway ($\mathbf{TS_{CC\text{-}Al\text{-}2\text{-}maj}}$ = 12.3 kcal/mol and $\mathbf{TS_{RC\text{-}Al\text{-}2\text{-}maj}}$ = 18.2 kcal/mol relative to the lowest transition structure located for $\mathbf{TS_{CC\text{-}Al\text{-}BLA\text{-}maj}}$). The key features and bond distances for the modeled TSs of this pathway are shown in Figure S19.

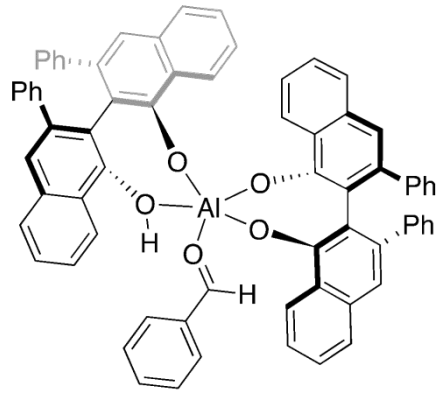

Figure S18: Modeled catalyst conformation for (*R*)-VANOL-Al-2 catalyst.

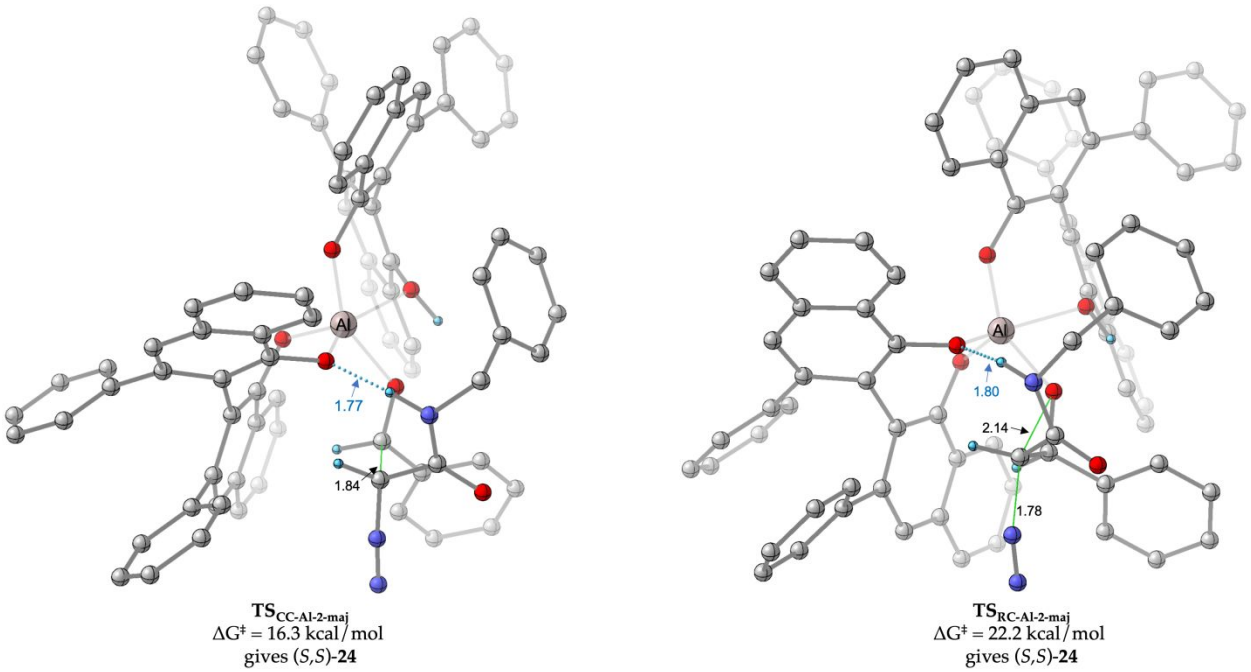

Figure S19: Lowest-lying transition structure for carbon-carbon bond forming and ring-closing step for major enantiomer.

24. Comparison of various computational methods

To ensure an unbiased interpretation of the relative free energy differences (ΔΔG‡) between the calculated transition structures for the selectivity-determining step, the lowest energy conformations for VANOL-derived boron and aluminum catalyzed epoxidation reactions were modeled using both B3LYP-D3/6-31G* and M06-2X/6-31G*. Single point energy calculations for these transition states along the BLA pathway were performed using M06-2X/6-311++G** and a PCM solvent model for toluene. The relative energies between the modeled enantiomers for the selectivity-determining step remain almost consistent for each metal employed. The ΔΔG‡ between the VANOL-derived aluminum catalyzed epoxidation transition structures was found to be 0.6 kcal/mol. This corresponds to a predicted ee of 50%, slightly lower than the experimentally observed ee of 81%, however an extensive conformational search was not performed with this

level of theory (Figure S20). The computed free energy difference ($\Delta\Delta G^{\ddagger}$) between the transition structures of the two enantiomers for the VANOL-derived boron catalyzed epoxidation was found to be 3.1 kcal/mol, predicting an ee > 99% - a value qualitatively consistent with the experimentally observed ee of 96% (Figure S21).

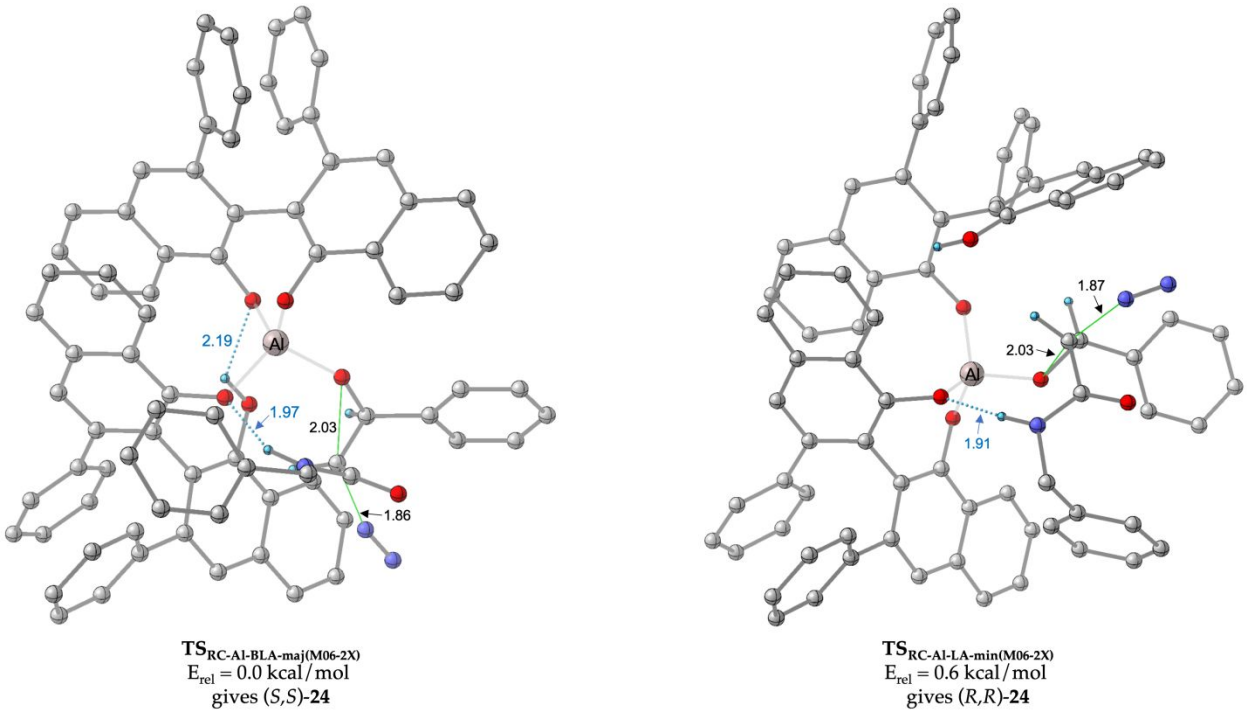

Figure S20: Lowest-lying transition structure for the ring-closing step ($TS_{RC\text{-}Al\text{-}BLA\text{-}M06\text{-}2X}$) for BLA pathway using M06-2X/6-311++G** PCM (toluene)//M06-2X/6-31G* at 273 K.

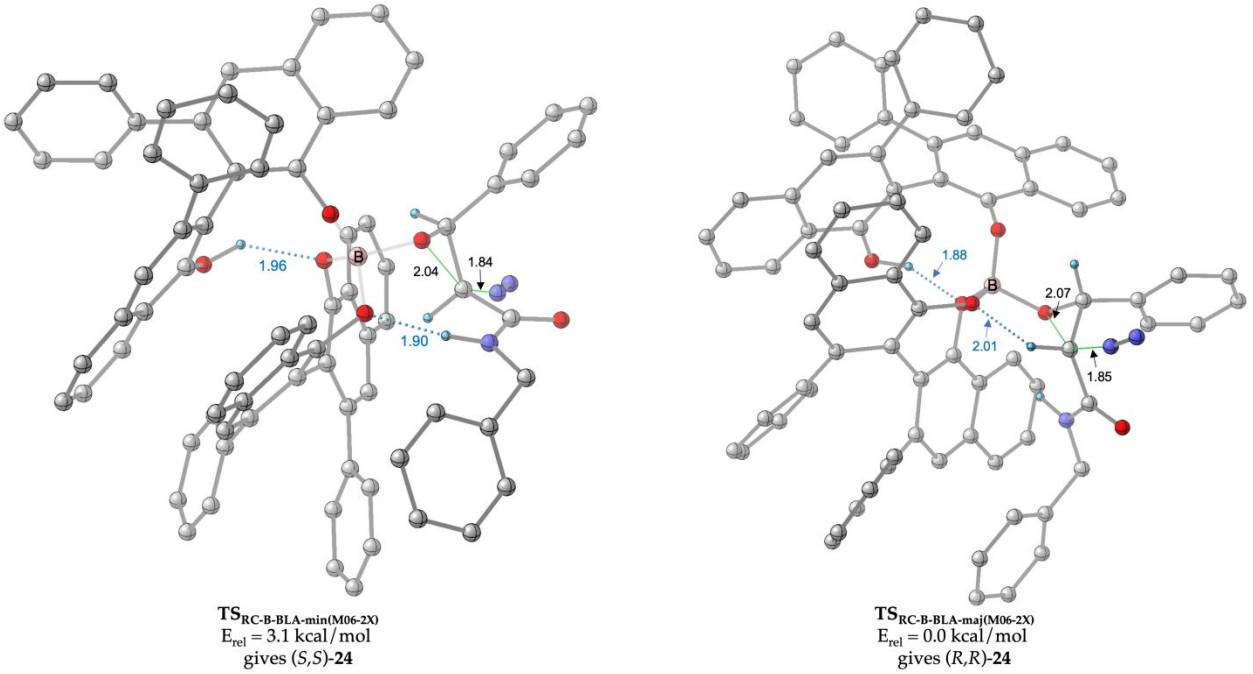

Figure S21: Lowest-lying transition structure for the ring-closing step ($TS_{RC\text{-}B\text{-}BLA\text{-}M06\text{-}2X}$) for BLA pathway using M06-2X/6-311++G** PCM (Toluene)//M06-2X/6-31G* at 233 K.

We also evaluated the relative free energy differences for the selectivity-determining step using B3LYP-D3(BJ)/6-311++G** PCM (Toluene)//B3LYP-D3/6-31G* as well as with ωB97-xD/6-311++G** PCM (Toluene)//B3LYP-D3/6-31G*. The qualitative trends remain the same regardless of the functional utilized (Table S5).

SP1: M06-2X//6-311++G** PCM (Toluene)//B3LYP-D3/6-31G* (in manuscript)
SP2: B3LYP-D3(BJ)/6-311++G** PCM (Toluene)//B3LYP-D3/6-31G*
SP3: ωB97-xD/6-311++G** PCM (Toluene)//B3LYP-D3/6-31G*

Boron catalyst TSs	SP1 (in manuscript)	SP2	SP3
$TS_{RC\text{-}B\text{-}BLA\text{-}maj}$	0.0	0.0	0.0
$TS_{RC\text{-}B\text{-}BLA\text{-}min}$	+3.2	+1.2	+1.7

Aluminum catalyst TSs	SP1 (in manuscript)	SP2	SP3
$TS_{RC\text{-}Al\text{-}BLA\text{-}maj}$	0.0	0.0	0.0
$TS_{RC\text{-}Al\text{-}LA\text{-}min}$	+1.8	+3.0	+4.4

Table S5: Relative free energy differences between the lowest energy transition structures leading to either enantiomer in both catalyst systems.

We further optimized the lowest energy transition structures leading to either enantiomer in both catalyst systems using B3LYP-D3/6-31G** (with additional polarization function) followed by single-point energy corrections using M06-2X/6-311++G** PCM (Toluene). The relative free energies and transition state geometries remained largely the same (Figure S22 and S23).

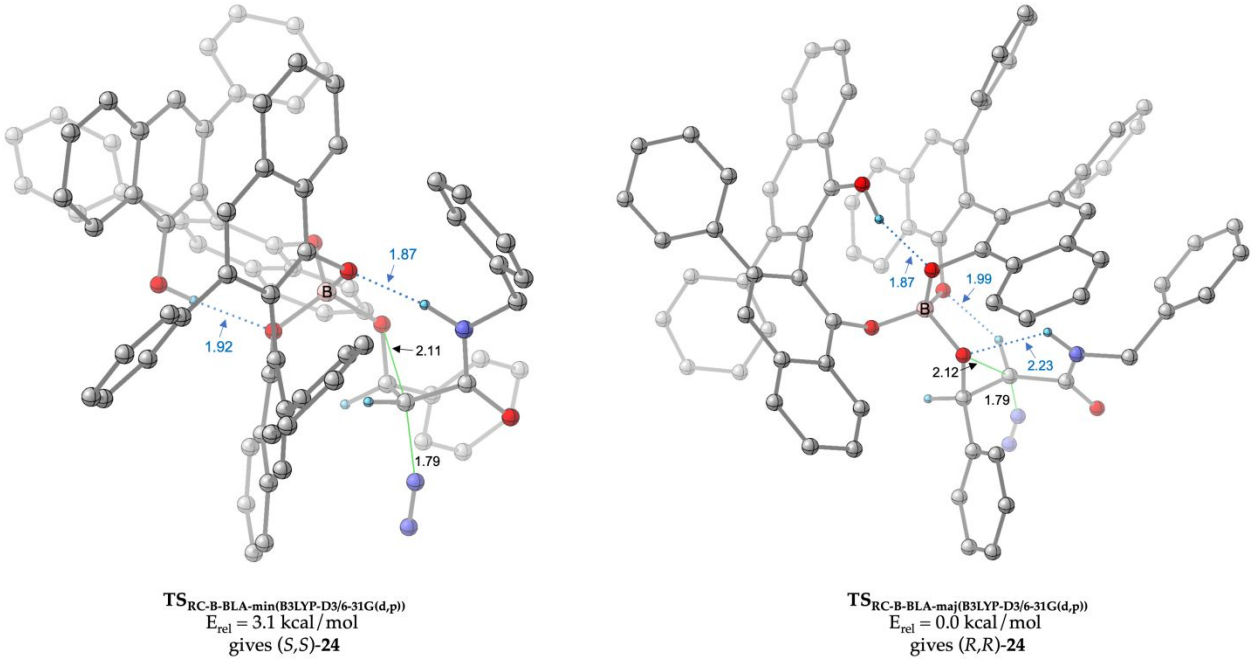

$TS_{RC\text{-}B\text{-}BLA\text{-}min(B3LYP\text{-}D3/6\text{-}31G(d,p))}$
E_{rel} = 3.1 kcal/mol
gives (*S*,*S*)-**24**

$TS_{RC\text{-}B\text{-}BLA\text{-}maj(B3LYP\text{-}D3/6\text{-}31G(d,p))}$
E_{rel} = 0.0 kcal/mol
gives (*R*,*R*)-**24**

Figure S22: Lowest-lying transition structure for the ring-closing step ($TS_{RC\text{-}B\text{-}BLA}$) for BLA pathway using M06-2X/6-311++G** PCM (Toluene)//B3LYP-D3/6-31G** at 233 K.

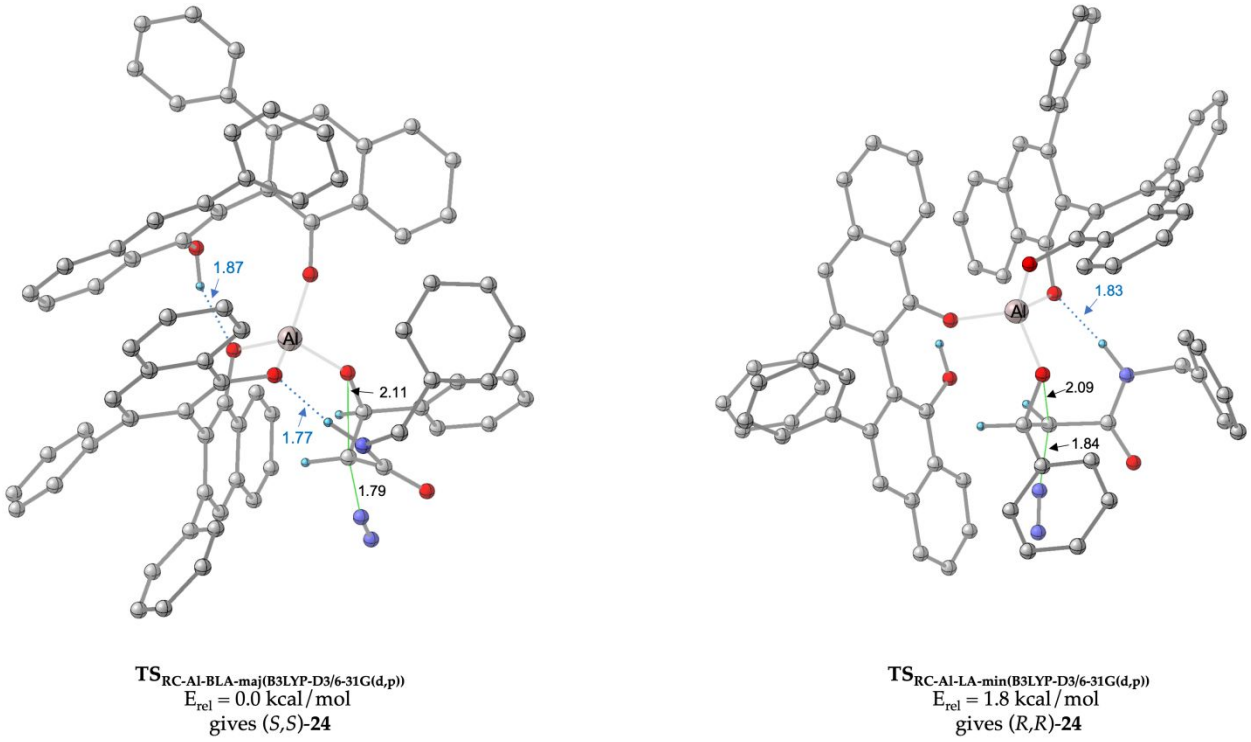

Figure S23: Lowest-lying transition structure for the ring-closing step ($TS_{RC\text{-}Al\text{-}BLA/LA}$) for BLA pathway using M06-2X/6-311++G** PCM (Toluene)//B3LYP-D3/6-31G** at 273 K.

Additionally, we also utilized B3LYP-D3/6-31G** CPCM (Toluene) (inclusion of implicit solvent model and polarization function) to optimize the lowest energy transition structures leading to either enantiomer in both catalyst systems followed by single-point energy calculations using M06-2X/6-311++G** PCM (Toluene). The relative free energies between the two enantiomers in both catalyst systems and transition state geometries also remained largely the same. The $\Delta\Delta G^{\ddagger}$ between the VANOL-derived aluminum catalyzed epoxidation transition structures was found to be 1.6 kcal/mol whereas the $\Delta\Delta G^{\ddagger}$ between the transition structures of the two enantiomers for the VANOL-derived boron catalyzed epoxidation was found to be 3.3 kcal/mol.

25. Analysis of key transition structures for selectivity-determining step for BLA pathway

Boron: We performed distortion-interaction analysis[24] on the transition structures for the selectivity-determining step, $\mathbf{TS_{RC\text{-}B\text{-}BLA\text{-}maj}}$ and $\mathbf{TS_{RC\text{-}B\text{-}BLA\text{-}min}}$, to qualitatively analyze their key differences and to assess the origin of the reaction's stereoselectivity (Table S6). In this analysis, the transition states were divided into two parts: (1) the Brønsted Acid-assisted Lewis acid complex, and (2) the diazo acetamide. Through these means, the transition state energy was decomposed into a distortion term, describing the energy required to distort the reactants from ground-state geometries into that of the TS, and an interaction term, describing the energy arising from interactions between these distorted fragments in the TS. From this analysis, it was observed that the TS leading to the (*R,R*)-**24** enantiomer ($\mathbf{TS_{RC\text{-}B\text{-}BLA\text{-}maj}}$) experiences fewer destabilizing distortions, 1.7 kcal/mol less compared to the TS leading to the minor (*S,S*)-**24** enantiomer ($\mathbf{TS_{RC\text{-}B\text{-}BLA\text{-}min}}$), with the diazo reactant distorting more compared to the catalyst fragment. Additionally, $\mathbf{TS_{RC\text{-}B\text{-}BLA\text{-}maj}}$ experiences 1.0 kcal/mol more energy from favorable interactions within the TS compared to $\mathbf{TS_{RC\text{-}B\text{-}BLA\text{-}min}}$. These results demonstrate that the difference in the enantioselectivity of the computed enantiomers is a consequence of distortion and interaction energies with both favoring in the TS leading to the (*R,R*)-**24** enantiomer ($\mathbf{TS_{RC\text{-}B\text{-}BLA\text{-}maj}}$). These results demonstrate that both distortion and interaction energy favor the major computed (*R,R*)-**24** enantiomer ($\mathbf{TS_{RC\text{-}B\text{-}BLA\text{-}maj}}$) in the boron-catalyzed reaction with the distortion component contributing to a greater degree.

Favors (*R,R*)-**24** ***[major]***				Favors (*S,S*)-**24** ***[minor]***				
	Distortion (kcal/mol)	Dist-Cat (kcal/mol)	Dist-Rct (kcal/mol)	**Interaction (kcal/mol)**	Int-Disp. (kcal/mol)	Int-ESP (kcal/mol)	Int-Rem. (kcal/mol)	**Overall (kcal/mol)**
$\mathbf{TS_{RC\text{-}B\text{-}BLA\text{-}maj}}$	82.6	44.5	38.1	-97.9	-4.2	-15.7		
$\mathbf{TS_{RC\text{-}B\text{-}BLA\text{-}min}}$	84.3	44.9	39.4	-96.9	-3.9	-21.3		
ΔΔE‡ ($\mathbf{TS_{RC\text{-}B\text{-}BLA\text{-}maj}}$ - $\mathbf{TS_{RC\text{-}B\text{-}BLA\text{-}min}}$)	**-1.7**	**-0.4**	**-1.3**	**-1.0**	**-0.3**	**+5.6**	**-6.3**	**-2.6**

Table S6: Components of the distortion/interaction analysis for the enantioselectivity-determining TS using M06-2x-D3/6-311++G** PCM (toluene).[25] Distortion of the catalyst (Cat) and reactant (Rct) as well as overall interaction energy, including dispersion (Disp.), electrostatic potential (ESP) and the remaining interactions such as electron repulsion and charge transfer (Rem.), are highlighted. Energy differences are reported in kcal/mol.

Aluminum: Similar analysis was carried out for the aluminum-catalyzed reaction to analyze the key differences between $\mathbf{TS_{RC\text{-}Al\text{-}BLA\text{-}maj}}$ leading to (*S,S*)-**24** and $\mathbf{TS_{RC\text{-}Al\text{-}BLA\text{-}min}}$ leading to (*R,R*)-**24** (Table S7). For this system, the ground state catalyst and reactant of the TS leading to the major (*S,S*)-**24** enantiomer ($\mathbf{TS_{RC\text{-}Al\text{-}BLA\text{-}maj}}$) undergo significantly less distortions to attain TS-like geometry, namely 5.5 kcal/mol less, compared to the TS leading to the minor (*R,R*)-**24** enantiomer ($\mathbf{TS_{RC\text{-}Al\text{-}BLA\text{-}min}}$) with the majority of this difference (3.2 kcal/mol) arising from the distortion of the diazo reactant. Although the distortion component of the energy decomposition analysis favors the TS leading to the major (*S,S*)-**24** enantiomer by 5.5 kcal/mol, the interaction component actually favors that of the minor (*R,R*)-**24** enantiomer. $\mathbf{TS_{RC\text{-}Al\text{-}BLA\text{-}min}}$ experiences 3.4 kcal/mol

more energy from interactions compared to $\mathbf{TS_{RC\text{-}Al\text{-}BLA\text{-}maj}}$. As such, the enantioselectivity for the computed aluminum-catalyzed system is determined by the degree of distortion needed to achieve transition state-like geometry, with fewer distortions necessitated in the TS leading to the major (*S,S*)-**24** product.

Favors (*R,R*)-**24** ***[minor]***				Favors (*S,S*)-**24** ***[major]***				
	Distortion (kcal/mol)	Dist-Cat (kcal/mol)	Dist-Rct (kcal/mol)	**Interaction (kcal/mol)**	Int-Disp. (kcal/mol)	Int-ESP (kcal/mol)	Int-Rem. (kcal/mol)	**Overall (kcal/mol)**
$\mathbf{TS_{RC\text{-}Al\text{-}BLA\text{-}maj}}$	83.4	44.7	38.7	-101.7	-4.6	-25.2		
$\mathbf{TS_{RC\text{-}Al\text{-}LA\text{-}min}}$	88.9	47.0	41.9	-105.1	-4.2	-24.4		
$\mathbf{\Delta\Delta E^{\ddagger}_{major}}$ $\mathbf{(TS_{RC\text{-}Al\text{-}BLA\text{-}maj} - TS_{RC\text{-}Al\text{-}LA\text{-}min})}$	**-5.5**	**-2.3**	**-3.2**	**+3.4**	**-0.4**	**-0.8**	**+4.6**	**-2.1**

Table S7: Components of the distortion/interaction analysis for the enantioselectivity-determining TS using M06-2x-D3/6-311++G** PCM (toluene). Distortion of the catalyst (Cat) and reactant (Rct) as well as overall interaction energy, including dispersion (Disp.), electrostatic potential (ESP) and the remaining interactions such as electron repulsion and charge transfer (Rem.), are highlighted. Energy differences are reported in kcal/mol.

Non-Covalent Interaction Plots: Non-covalent interaction (NCI) plots[26-28] were generated to illustrate the differing magnitude of dispersive energy between the catalyst and reactant fragments for both the boron-catalyzed and aluminum-catalyzed reactions (Figure S24). Comparing the boron-catalyzed transition states, $\mathbf{TS_{RC\text{-}B\text{-}BLA\text{-}maj}}$ and $\mathbf{TS_{RC\text{-}B\text{-}BLA\text{-}min,}}$ they exhibit similar amounts and types of dispersion interactions, primarily hydrogen bonding between the reactant fragment and the borate oxygen atoms. Comparing the aluminum-catalyzed transition states, the transition

state leading to the major (*S,S*)-**24** enantiomer (**$TS_{RC\text{-}Al\text{-}BLA\text{-}maj}$**) exhibits hydrogen-bonding with the aluminate oxygen atoms, CH—π interactions and van der Waal dispersions with the reactant fragment and the catalyst scaffold. The transition state leading to the minor (*R,R*)-**24** enantiomer (**$TS_{RC\text{-}Al\text{-}LA\text{-}min}$**) exhibits the aforementioned dispersion interactions in addition to a significant N_2—π interaction.

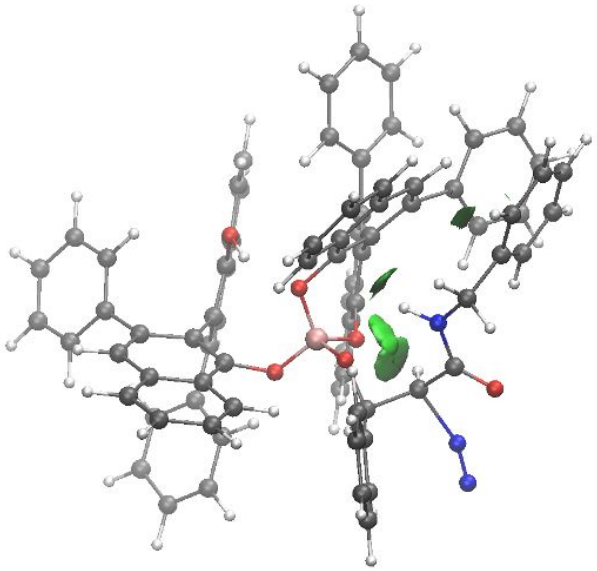

$TS_{RC\text{-}B\text{-}BLA\text{-}maj}$
gives (R,R)-**24**

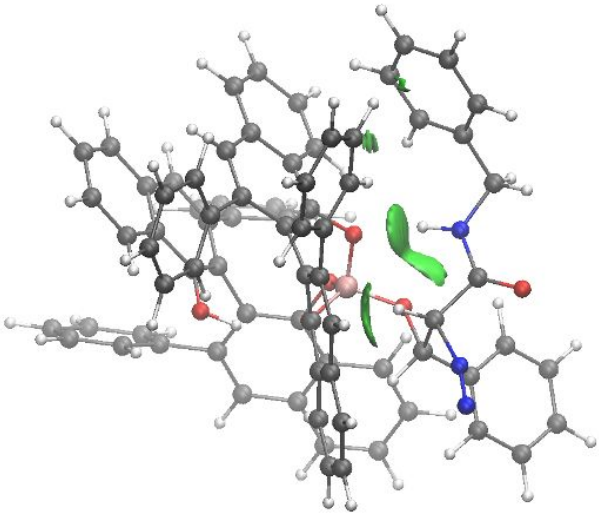

$TS_{RC\text{-}B\text{-}BLA\text{-}min}$
gives (S,S)-**24**

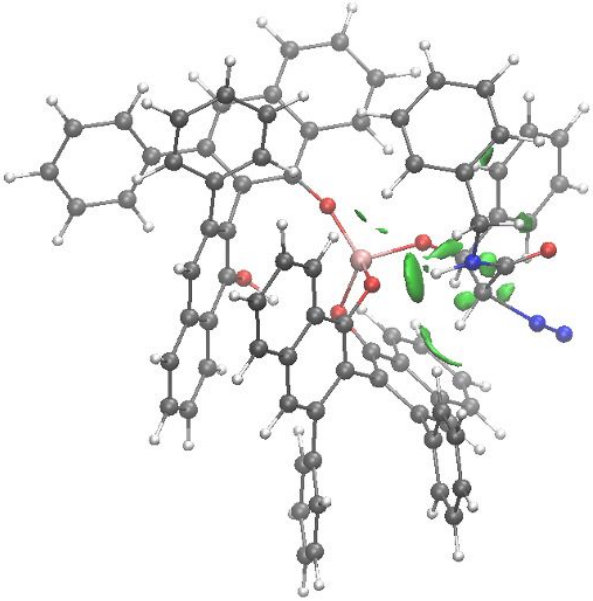

$TS_{RC\text{-}Al\text{-}BLA\text{-}maj}$
gives (S,S)-**24**

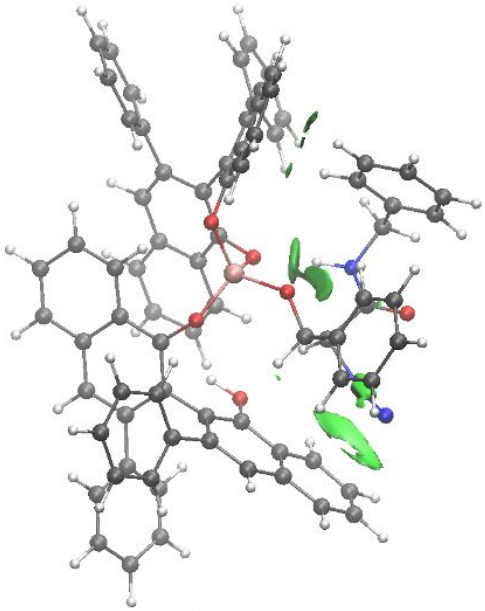

$TS_{RC\text{-}Al\text{-}LA\text{-}min}$
gives (R,R)-**24**

Figure S24: Non-covalent interaction plots for the transition states leading to the (*S,S*)-**24** and (*R,R*)-**24** products for both boron- and aluminum-catalyzed reactions are shown above. Dispersion interactions between the catalyst fragment (Brønsted Acid-assisted Lewis acid complex) and the reactant (the diazo acetamide) are depicted in green (isosurface of 0.01).

26. Energetics for different possible conformations

In this section, the energies of the all the calculated transition structures for all the described pathways in manuscript and supporting information for VANOL derived boron and aluminum catalyst are included. All the lowest energy transition structures discussed in manuscript/SI are highlighted (with same name) in red and corresponding higher energy conformations are also reported.

1. TS Geometry VANOL-Al – All the possible transition state conformations for different pathways calculated for VANOL-derived aluminum catalyst for epoxidation reaction

2. Extrapolated_SP_273K – qRRHO free-energy corrected single points at 233K

3. RE (kcal/mol) – All single point free energy differences are calculated relative to the lowest lying pre-reactive complex shown in Figure 1 in manuscript

Lowest-lying TSs for key carbon-carbon bond forming and ring-closing steps for each pathway described in the manuscript and supporting information are highlighted in red.

Table S8: Energetics of various conformations calculated for VANOL-Al catalyzed epoxidation of aldehydes (relative to the aluminum pre-reactive complex)

TS Geometry VANOL-Al[1]	Extrapolated_SP_273K – qRRHO[2]	RE[3]
TS-CC-Al-BA-maj	-3938.95864	8.5
TS-CC-Al-BA-maj-a	-3938.95864	8.5
TS-CC-Al-BA-maj-b	-3938.95767	9.1

TS-CC-Al-BLA-maj	-3938.96573	4.0
TS-CC-Al-BLA-maj-a	-3938.96409	5.0
TS-CC-Al-BLA-maj-b	-3938.95969	7.8
TS-CC-Al-BA-min	-3938.95795	8.9
TS-CC-Al-BA-min-a	-3938.95770	9.0
TS-CC-Al-BA-min-b	-3938.95526	10.6
TS-CC-Al-BA-min-c	-3938.95622	10.0
TS-CC-Al-BLA-min	-3938.95914	8.1
TS-CC-Al-BLA-min-a	-3938.94449	17.3
TS-CC-Al-BLA-min-b	-3938.94357	17.9
TS-CC-Al-BLA-min-c	-3938.94853	14.8
TS-CC-Al-BLA-min-d	-3938.94733	15.5
TS-RC-Al-BA-maj	-3938.95599	10.1
TS-RC-Al-BA-maj-a	-3938.95182	12.7
TS-RC-Al-BA-maj-b	-3938.95137	13.0
TS-RC-Al-BLA-maj	-3938.95868	8.4
TS-RC-Al-BLA-maj-a	-3938.95002	13.9
TS-RC-Al-BLA-maj-b	-3938.94196	18.9
TS-RC-Al-BLA-maj-c	-3938.95669	9.7
TS-RC-Al-BLA-maj-d	-3938.95542	10.5
TS-RC-Al-BLA-maj-e	-3938.95579	10.2
TS-RC-Al-BLA-maj-f	-3938.95460	11.0
TS-RC-Al-BLA-maj-g	-3938.95626	9.9
TS-RC-Al-BLA-maj-i	-3938.94694	15.8

TS-RC-Al-BLA-maj-j	-3938.94783	15.2
TS-RC-Al-BLA-maj-k	-3938.95392	11.4
TS-RC-Al-BLA-maj-l	-3938.95079	13.4
TS-RC-Al-BLA-maj-m	-3938.95455	11.0
TS-RC-Al-BLA-maj-n	-3938.95375	11.5
TS-RC-Al-BLA-maj-q	-3938.95604	10.1
TS-RC-Al-BLA-maj-r	-3938.95524	10.6
TS-RC-Al-BLA-maj-s	-3938.95174	12.8
TS-RC-Al-BLA-maj-t	-3938.95604	10.1
TS-RC-Al-BLA-maj-u	-3938.95694	9.5
TS-RC-Al-BLA-maj-v	-3938.95615	10.0
TS-RC-Al-BLA-maj-w	-3938.95659	9.7
TS-RC-Al-BLA-maj-x	-3938.95510	10.7
TS-RC-Al-BA-min	-3938.95468	10.9
TS-RC-Al-BA-min-a	-3938.95454	11.0
TS-RC-Al-BA-min-b	-3938.95454	11.0
TS-RC-Al-BLA-min	-3938.95287	12.1
TS-RC-Al-LA-min-a	-3938.95298	12.0
TS-RC-Al-BLA-min-b	-3938.94684	15.9
TS-RC-Al-BLA-min-c	-3938.94883	14.6
TS-RC-Al-BLA-min-d	-3938.95096	13.3
TS-RC-Al-BLA-min-e	-3938.94278	18.4
TS-RC-Al-BLA-min-f	-3938.94909	14.4
TS-RC-Al-BLA-min-g	-3938.95041	13.6

TS-RC-Al-BLA-min-h	-3938.94237	18.7
TS-RC-Al-BLA-min-i	-3938.94909	14.4
TS-RC-Al-BLA-min-j	-3938.95176	12.8
TS-RC-Al-BLA-min-k	-3938.94831	14.9
TS-RC-Al-BLA-min-l	-3938.94831	14.9
TS-RC-Al-BLA-maj-o	-3938.95460	11.0
TS-RC-Al-LA-maj-a	-3938.95170	12.8
TS-RC-Al-LA-maj	-3938.95193	12.7
TS-RC-Al-LA-min	-3938.95589	10.2
TS-RC-Al-LA-min-a	-3938.95254	12.3
TS-CC-Al-2-maj	-3938.94612	16.3
TS-RC-Al-2-maj	-3938.93672	22.2

1. TS Geometry VANOL-B – All the possible transition state conformations for different pathways calculated for VANOL-derived boron catalyst for epoxidation reaction

2. Extrapolated_SP_233K – qRRHO free-energy corrected single points at 233K

3.RE (kcal/mol) – All single point free energy differences are calculated relative to the lowest lying pre-reactive complex shown in Figure 1 in manuscript

Lowest-lying TSs for key carbon-carbon bond forming and ring-closing steps for each pathway described in the manuscript and supporting information are highlighted in red.

Table S9: Energetics of various conformations calculated for VANOL-B catalyzed epoxidation of aldehydes (relative to the boron pre-reactive complex)

TS Geometry VANOL-B[1]	Extrapolated_SP_233K – qRRHO[2]	RE[3]
TS-CC-B-BA-min	-3721.29772	7.2
TS-CC-B-BA-min-a	-3721.29755	7.3
TS-CC-B-BA-min-b	-3721.29772	7.2
TS-CC-B-BLA-min	-3721.30100	5.2
TS-CC-B-BLA-min-a	-3721.29895	6.5
TS-CC-B-BLA-min-b	-3721.29895	6.5
TS-CC-B-BA-maj	-3721.29609	8.2
TS-CC-B-BA-maj-a	-3721.29441	9.3
TS-CC-B-BA-maj-b	-3721.29442	9.3
TS-CC-B-BA-maj-c	-3721.29128	11.3
TS-CC-B-BLA-maj	-3721.30134	5.0
TS-CC-B-BLA-maj-a	-3721.27556	21.1
TS-CC-B-BLA-maj-b	-3721.28225	16.9
TS-CC-B-BLA-maj-c	-3721.28328	16.3
TS-CC-B-BLA-maj-d	-3721.28424	15.7
TS-CC-B-BLA-maj-e	-3721.29735	7.5
TS-CC-B-BLA-maj-f	-3721.29656	7.9
TS-RC-B-BA-min	-3721.29466	9.1
TS-RC-B-BA-min-a	-3721.29427	9.4
TS-RC-B-BA-min-b	-3721.29435	9.3
TS-RC-B-BLA-min	-3721.29315	10.1
TS-RC-B-BLA-min-a	-3721.29112	11.4

TS-RC-B-BLA-min-b	-3721.28633	14.4
TS-RC-B-BLA-min-c	-3721.28673	14.1
TS-RC-B-BLA-min-d	-3721.29314	10.1
TS-RC-B-BLA-min-e	-3721.28306	16.4
TS-RC-B-BLA-min-f	-3721.28571	14.8
TS-RC-B-BLA-min-g	-3721.27591	20.9
TS-RC-B-BLA-min-h	-3721.27929	18.8
TS-RC-B-BLA-min-i	-3721.28705	13.9
TS-RC-B-BLA-min-j	-3721.28706	13.9
TS-RC-B-BLA-min-k	-3721.29249	10.5
TS-RC-B-BA-maj	-3721.29426	9.4
TS-RC-B-BA-maj-a	-3721.29339	9.9
TS-RC-B-BA-maj-b	-3721.29475	9.1
TS-RC-B-BA-maj-c	-3721.29372	9.7
TS-RC-B-BLA-maj	-3721.29821	6.9
TS-RC-B-BLA-maj-a	-3721.27630	20.7
TS-RC-B-BLA-maj-b	-3721.27500	21.5
TS-RC-B-BLA-maj-c	-3721.27628	20.7
TS-RC-B-BLA-maj-e	-3721.27506	21.4
TS-RC-B-BLA-maj-f	-3721.28632	14.4
TS-RC-B-BLA-maj-g	-3721.28839	13.1
TS-RC-B-BLA-maj-h	-3721.28799	13.3
TS-RC-B-BLA-maj-i	-3721.28649	14.3
TS-RC-B-BLA-maj-k	-3721.27373	22.3

TS-RC-B-BLA-maj-m	-3721.27679	20.4
TS-RC-B-BLA-maj-n	-3721.27736	20.0
TS-RC-B-BLA-maj-o	-3721.27506	21.4
TS-RC-B-BLA-maj-p	-3721.29528	8.8
TS-RC-B-BLA-maj-q	-3721.29040	11.8
TS-RC-B-BLA-maj-r	-3721.29396	9.6
TS-RC-B-BLA-maj-s	-3721.28569	14.8
TS-RC-B-BLA-maj-t	-3721.28677	14.1
TS-RC-B-BLA-maj-u	-3721.28645	14.3
TS-RC-B-LA-maj	-3721.29040	11.8
TS-RC-B-LA-maj-a	-3721.28838	13.1
TS-RC-B-LA-maj-b	-3721.28701	13.9
TS-RC-B-LA-min	-3721.29019	11.9
TS-RC-B-LA-min-a	-3721.27946	18.7
TS-RC-B-LA-min-b	-3721.28083	17.8

27. References

1. Ding, Z.; Osminski, W. E. G.; Ren, H.; Wulff, W. D. "Scalable Syntheses of the Vaulted Biaryl Ligands VAPOL and VANOL via the Cycloaddition/Electrocyclization Cascade" *Org. Proc. Res. & Dev.* **2011**, *15*, 1089-1107.
2. Guan, Y.; Ding, Z.; Wulff, W. D. "Vaulted Biaryls in Catalysis: A Structure–Activity Relationship Guided Tour of the Immanent Domain of the VANOL Ligand" *Chemistry – A European Journal* **2013**, *19*, 15565-15571.
3. Guan, Y.; Lu, Z.; Yin, X.; Mohammadlou, A.; Staples, R. J.; Wulff, W. D. "Catalytic Asymmetric Aziridination of Benzhydryl Imines and Diazoacetate Esters with BOROX Catalysts from 3, 3′-Disubstituted VANOL Ligands" *Synthesis* **2020**, *52*, 2073-2091.

4. a) Guan, Y. PhD Dissertation. Michigan State University 2012 b) Yin, X. PhD Dissertation. Michigan State University 2018.
5. Arai, T.; Sasai, H.; Aoe, K.; Okamura, K.; Date, T.; Shibasaki, M., "A New Multifunctional Heterobimetallic Asymmetric Catalyst for Michael Additions and Tandem Michael- Aldol Reactions." *Angew. Chem. Int. Ed.* **1996**, *35,* 104–106.
6. Arai, T.; Sasai, H.; Yamaguchi, K.; Shibasaki, M., "Regioselective Catalytic Asymmetric Reaction of Horner−Wadsworth−Emmons Reagents with Enones: The Odyssey of Chiral Aluminum Catalysts." *J. Am. Chem. Soc.* **1998**, *120,* 441–442.
7. Gupta, A. K.; Yin, X.; Mukherjee, M.; Desai, A.; Mohammadlou, A.; Jurewicz, K.; Wulff, W. D.,"Catalytic Asymmetric Epoxidation of Aldehydes with Two VANOL-Derived Chiral Borate Catalysts." *Angew. Chem. Int. Ed.* **2019**, *58*, 3361–3367.
8. Cronan, J. M.; Cardellina, J. H., "A Novel δ-Lactam from the Sponge Tedania Ignis." *Nat.l Prod. Lett.* **1994**, *5*, 85–88.
9. Lago, J. H. G.; Kato, M. J., "3α,4α-Epoxy-2-Piperidone, a New Minor Derivative from Leaves of Piper Crassinervium Kunth (Piperaceae)." *Nat. Prod. Res.* **2007**, *21*, 910–914.
10. Han, J.; Liu, L.; Chang, Y.; Yue, G.; Guo, J.; Zhou, L.; Li, C.; Yang, Z., "Asymmetric Total Synthesis of Caribenol A via an Intramolecular Diels-Alder Reaction."*J. Org. Chem.* **2013**, *78*, 5492–5504.
11. Barry, C. S.; Bushby, N.; Harding, J. R.; Willis, C. L., "Stereoselective Synthesis of the Tetrahydropyran Core of Polycarvernoside A." *Org. Lett.* **2005**, *7*, 2683–2686.
12. Trost, Barry M., and Mark J. Bartlett. 2012. "Transition-Metal-Catalyzed Synthesis of Aspergillide B: An Alkyne Addition Strategy." *Org. Lett. 14*, 1322–1325.
13. Liu, X.; Deaton, T. M.; Haeffner, F.; Morken, J. P., "A Boron Alkylidene-Alkene Cycloaddition Reaction: Application to the Synthesis of Aphanamal." *Angew. Chem. Int. Ed.* **2017**, *56*, 11485–11489.
14. Wullschleger, C. W.; Gertsch, J.; Altmann, K., "Synthesis and Biological Activity of 7,8,9-Trideoxy- and 7 R DesTHP-Peloruside A." *Chem. Eur. J.* **2013**, *19,* 13105–13111.
15. Sanford, A. B.; Thane, T. A.; McGinnis, T. M.; Chen, P.; Hong, X.; and Jarvo, E. R., "Nickel-Catalyzed Alkyl-Alkyl Cross-Electrophile Coupling Reaction of 1,3-Dimesylates for the Synthesis of Alkylcyclopropanes." *J. Am. Chem. Soc.* **2020**, *142,* 5017–5023.
16. Li, X.; Borhan B. "Prompt Determination of Absolute Configuration for Epoxy Alcohols via Exciton Chirality Protocol" *J. Am. Chem. Soc.* **2008**, *130*, 16126–16127.
17. Gaussian 16, Revision A.03, Frisch, M. J.; Trucks, G. W.; Schlegel, H. B.; Scuseria, G. E.; Robb, M. A.; Cheeseman, J. R.; Scalmani, G.; Barone, V.; Petersson, G. A.; Nakatsuji, H.; Li, X.; Caricato, M.; Marenich, A. V.; Bloino, J.; Janesko, B. G.; Gomperts, R.; Mennucci, B.; Hratchian, H. P.; Ortiz, J. V.; Izmaylov, A. F.; Sonnenberg, J. L.; Williams-Young, D.; Ding, F.; Lipparini, F.; Egidi, F.; Goings, J.; Peng, B.; Petrone, A.; Henderson, T.; Ranasinghe, D.; Zakrzewski, V. G.; Gao, J.; Rega, N.; Zheng, G.; Liang, W.; Hada, M.; Ehara, M.; Toyota, K.; Fukuda, R.; Hasegawa, J.; Ishida, M.; Nakajima, T.; Honda, Y.; Kitao, O.; Nakai, H.; Vreven, T.; Throssell, K.; Montgomery, J. A., Jr.; Peralta, J. E.; Ogliaro, F.; Bearpark, M. J.; Heyd, J. J.; Brothers, E. N.; Kudin, K. N.; Staroverov, V. N.; Keith, T. A.; Kobayashi, R.; Normand, J.; Raghavachari, K.; Rendell, A. P.; Burant, J. C.; Iyengar, S. S.; Tomasi, J.; Cossi, M.; Millam, J. M.; Klene, M.; Adamo, C.; Cammi, R.; Ochterski, J. W.; Martin, R. L.; Morokuma, K.; Farkas, O.; Foresman, J. B.; Fox, D. J. Gaussian, Inc., Wallingford CT, 2016.

18. Zhao, Y.; Truhlar, D. G. The M06 suite of density functionals for main group thermochemistry, thermochemical kinetics, noncovalent interactions, excited states, and transition elements: two new functionals and systematic testing of four M06-class functionals and 12 other functionals. *Theor. Chem. Acc.* **2008**, *120,* 215-241.
19. a) Miertuš, S.; Scrocco, E.; Tomasi, J. Electrostatic interaction of a solute with a continuum. A direct utilizaion of AB initio molecular potentials for the prevision of solvent effects. *Chem. Phys.* **1981**, *55,* 117-129. (b) Tomasi, J.; Mennucci, B.; Cammi, R. Quantum mechanical continuum solvation models. *Chem. Rev.* **2005**, *105,* 2999-3094.
20. Becke, A. Density-Functional Thermochemistry. III. The Role of Exact Exchange. J. Chem. Phys., 98: 5648-5652. 1993.
21. Grimme, S.; Ehrlich, S.; Goerigk, L. Effect of the damping function in dispersion corrected density functional theory. *J. Comput. Chem.* **2011**, *32,* 1456-1465.
22. Hehre, W. J.; Stewart, R. F.; Pople, J. A. Self-Consistent Molecular-Orbital Methods. I. Use of Gaussian Expansions of Slater-Type Atomic Orbitals. *J. Chem. Phys.* **1969**, *51,* 2657-2664.
23. Grimme, S. Supramolecular binding thermodynamics by dispersion-corrected density functional theory. *Eur. J. Chem* **2012**, *18,* 9955-9964.
24. (a) Bickelhaupt, F. M.; Houk, K. N., Analyzing Reaction Rates with the Distortion/Interaction-Activation Strain Model. *Angew. Chem. Int. Ed. Engl.* **2017,** *56* (34), 10070-10086. (b) Ess, D. H.; Houk, K. N., Distortion/interaction energy control of 1,3-dipolar cycloaddition reactivity. *J. Am. Chem. Soc.* **2007,** *129* (35), 10646-7. (c) Maji, R.; Mallojjala, S. C.; Wheeler, S. E., Chiral phosphoric acid catalysis: from numbers to insights. *Chem. Soc. Rev.* **2018,** *47* (4), 1142-1158.
25. (a) Lockhart, Z.; Popescu, M.; Alegra-Requena, J.; Ahuja, J.; Paton, R.; Smith, M. A radical-polar crossover approach to complex nitrogen heterocycles via the triplet state. ChemRxiv. Cambridge: Cambridge Open engage; 2023. (b) Jones, B. A.; Solon, P.; Popescu, M. V.; Du, J-Y.; Paton, R.; Smith, M. D. Catalytic Enantioselective 6π Photocyclization of Acrylanilides. *J. Am. Chem. Soc.* **2023,** *145*, 171-178.
26. Lu, T.; Chen, Q., Independent gradient model based on Hirshfeld partition: A new method for visual study of interactions in chemical systems. J. Comput. Chem. 2022, 43 (8), 539-555.
27. Lu, T.; Chen, F. Multiwfn: A multifunctional wavefunction analyzer. J. Comput. Chem. 2011, 33 (5), 580-592.
28. Humphrey, W., Dalke, A. and Schulten, K., "VMD - Visual Molecular Dynamics", J. Molec. Graphics, 1996, vol. 14, pp. 33-38.

(*2S,3S*)-**11**-^{1}H-NMR (500 MHz -$CDCl_3$); $^{13}C\{^{1}H\}$ (126 MHz, $CDCl_3$)

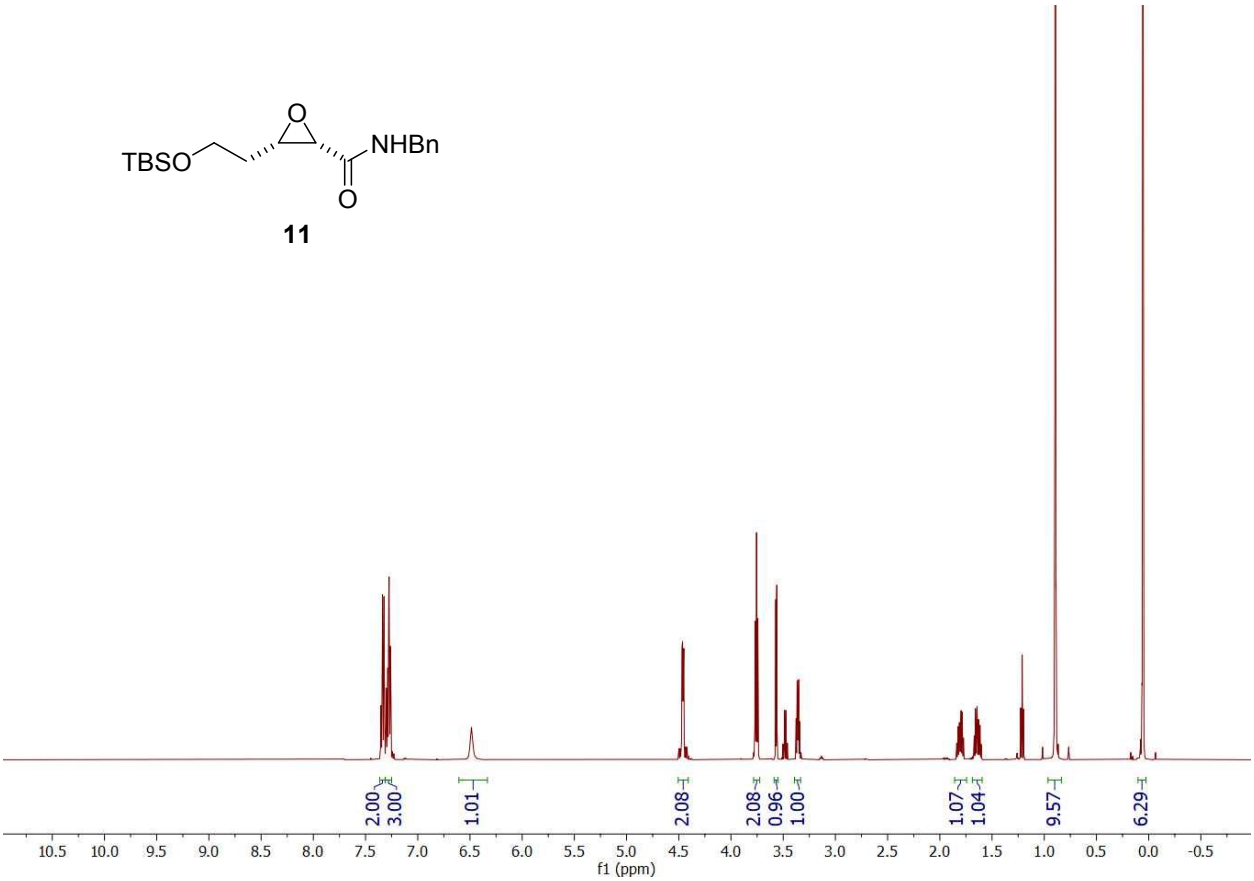

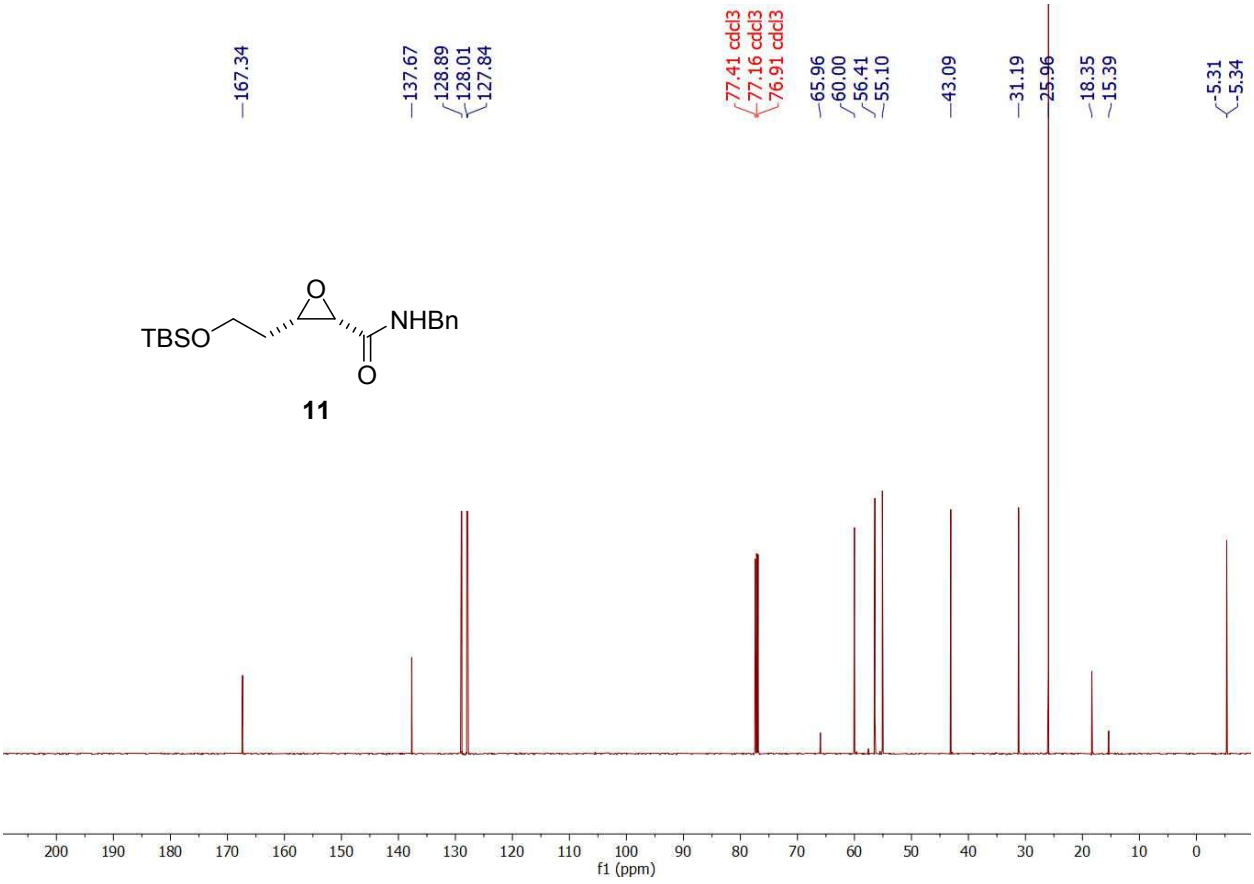

(*2S,3S*)-**13**-^{1}H-NMR (500 MHz -$CDCl_3$); $^{13}C\{^{1}H\}$ (126 MHz, $CDCl_3$)

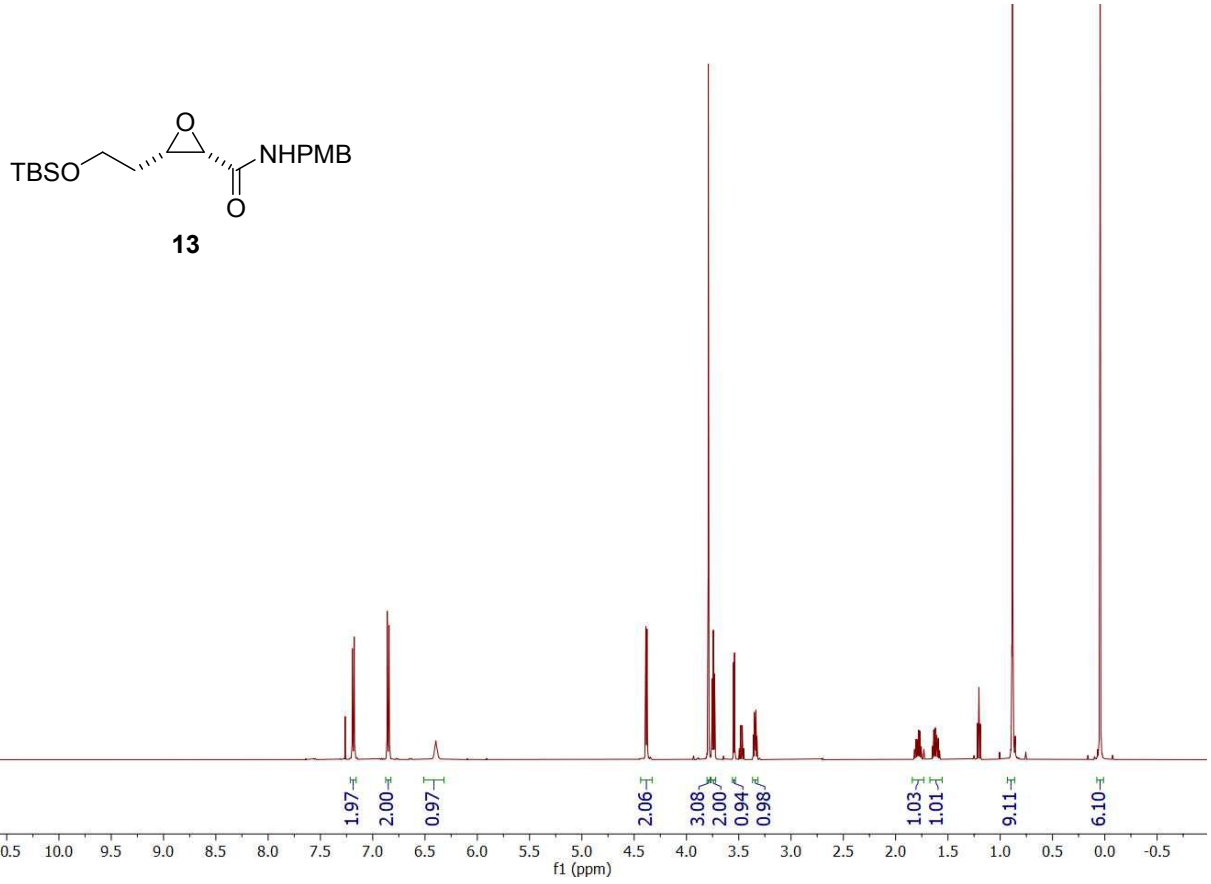
TBSO
O
NHPMB
O
13
1.97
2.00
0.97
2.06
3.08
2.00
0.94
0.98
1.03
1.01
9.11
6.10
10.5 10.0 9.5 9.0 8.5 8.0 7.5 7.0 6.5 6.0 5.5 5.0 4.5 4.0 3.5 3.0 2.5 2.0 1.5 1.0 0.5 0.0 -0.5
f1 (ppm)

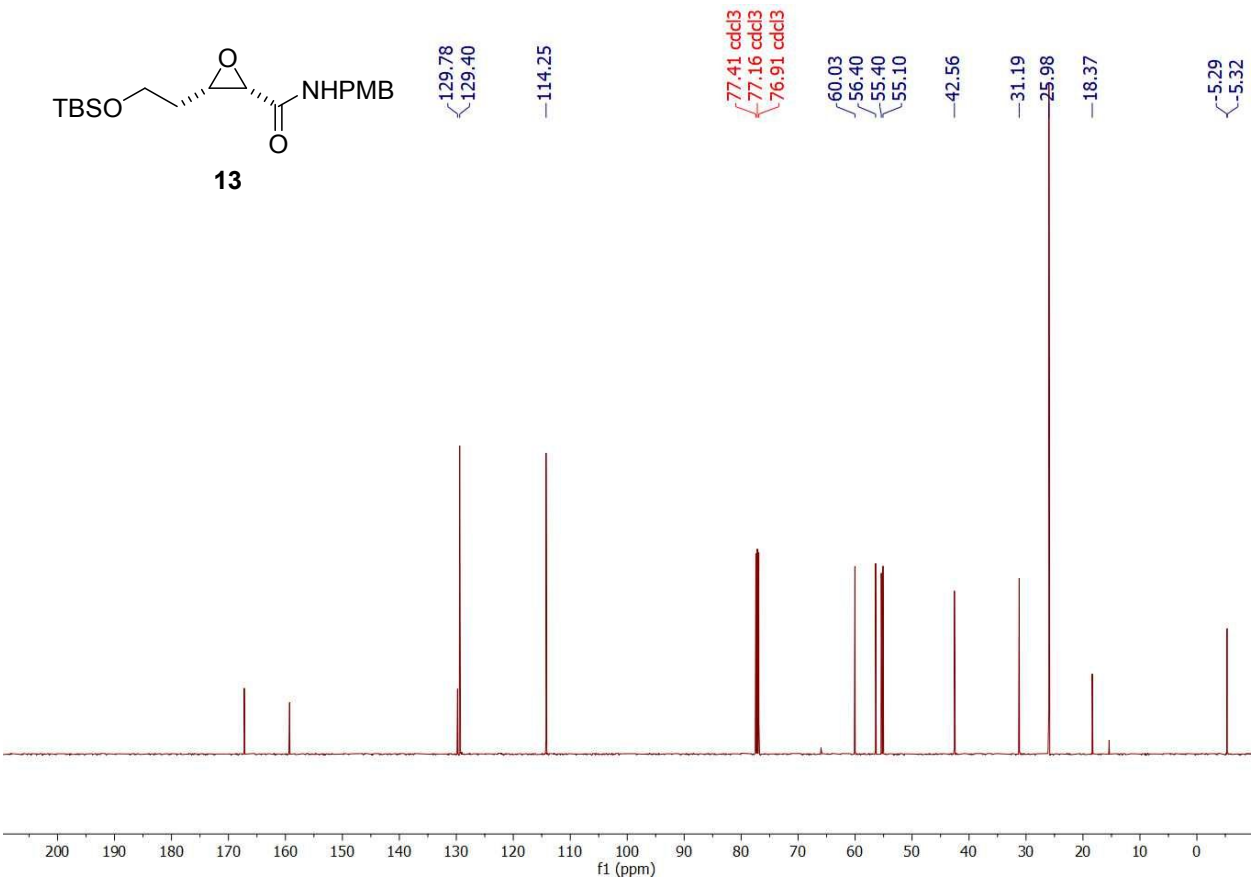

(*2S,3S*)-**14**-^{1}H-NMR (500 MHz -$CDCl_3$); $^{13}C\{^{1}H\}$ (126 MHz, $CDCl_3$)

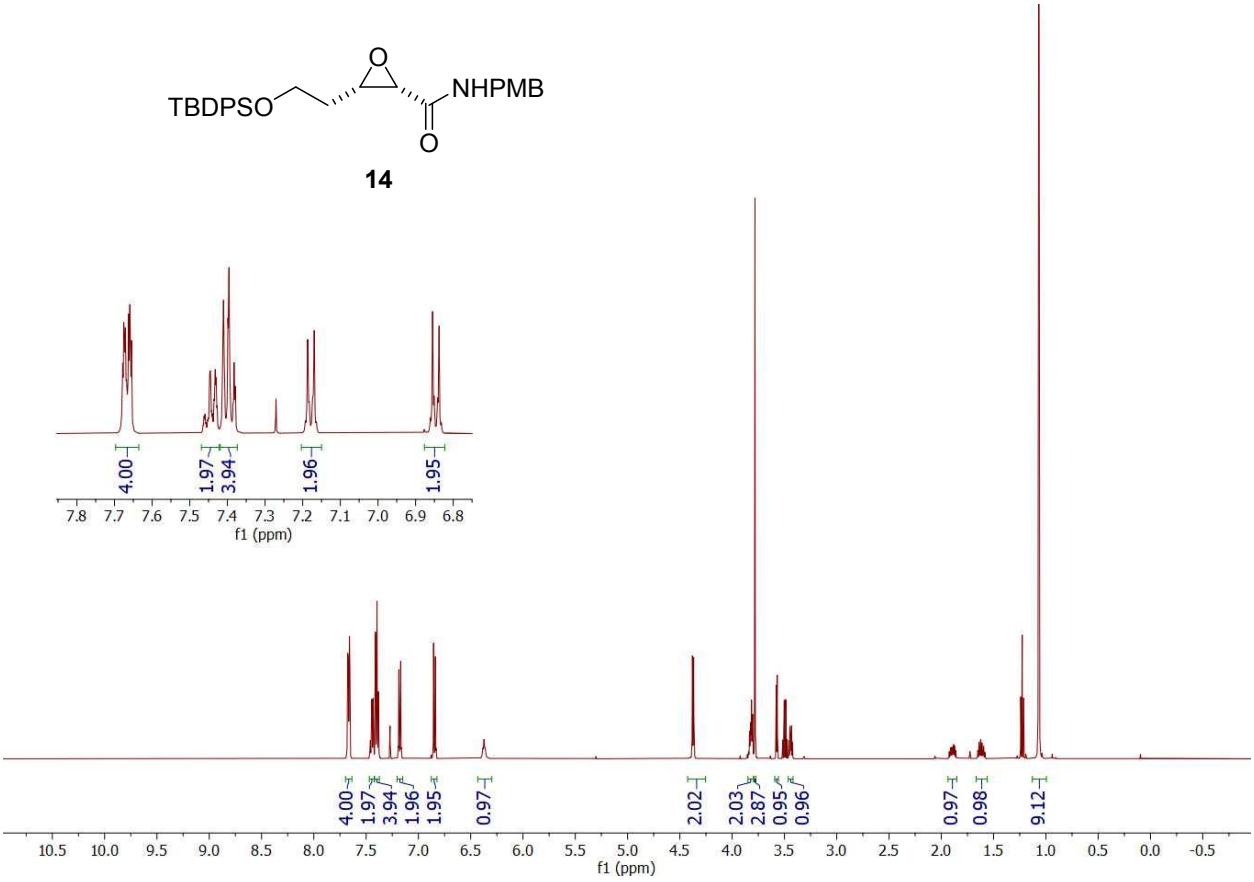
TBDPSO
NHPMB
O
O
14
4.00
1.97
3.94
1.96
1.95
7.8 7.7 7.6 7.5 7.4 7.3 7.2 7.1 7.0 6.9 6.8
f1 (ppm)
4.00
1.97
3.94
1.96
1.95
0.97
2.02
2.03
2.87
0.95
0.96
0.97
0.98
9.12
10.5 10.0 9.5 9.0 8.5 8.0 7.5 7.0 6.5 6.0 5.5 5.0 4.5 4.0 3.5 3.0 2.5 2.0 1.5 1.0 0.5 0.0 -0.5
f1 (ppm)

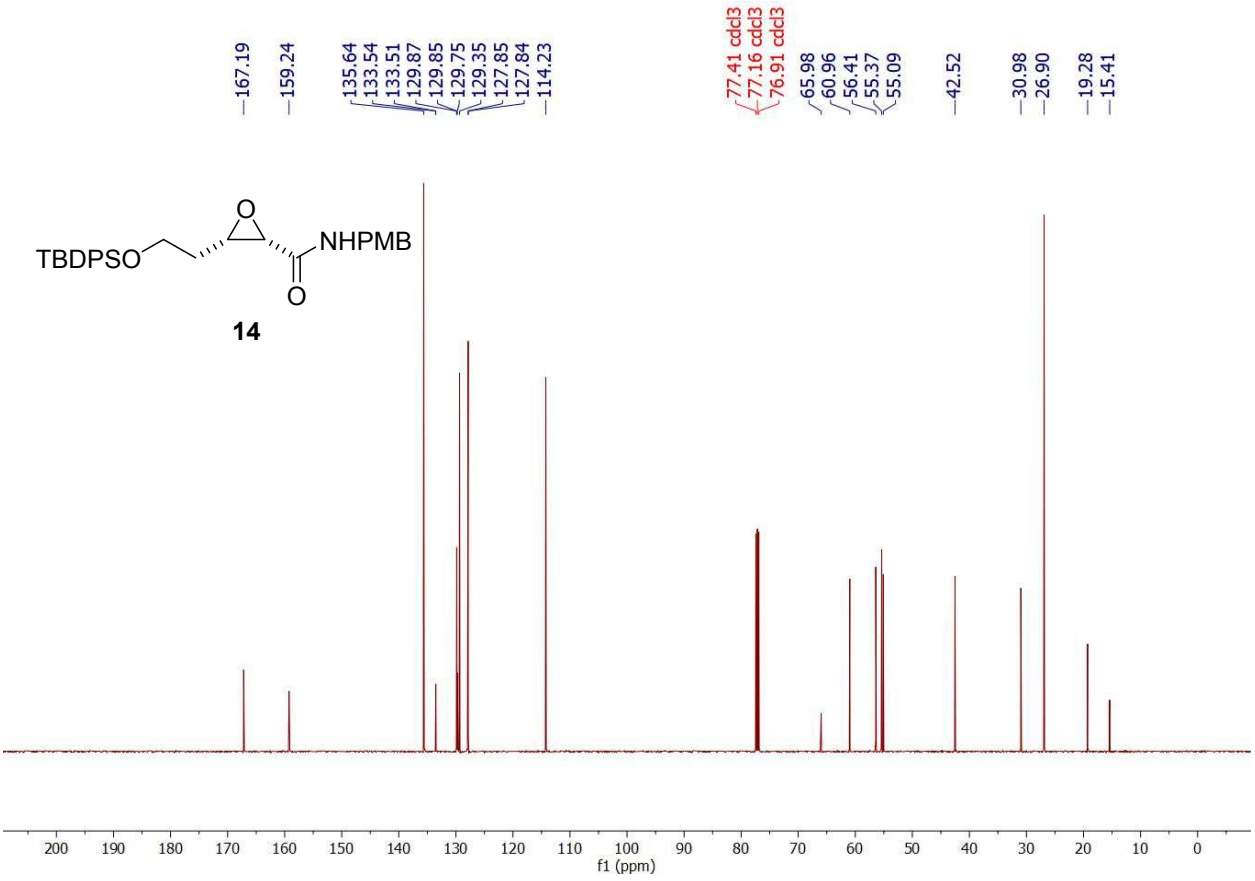
167.19
159.24
135.64
133.54
133.51
129.87
129.85
129.75
129.35
127.85
127.84
114.23
77.41 cdcl3
77.16 cdcl3
76.91 cdcl3
65.98
60.96
56.41
55.37
55.09
42.52
30.98
26.90
19.28
15.41
TBDPSO
O
NHPMB
O
14
200
190
180
170
160
150
140
130
120
110
100
90
80
70
60
50
40
30
20
10
0
f1 (ppm)

(*2S,3S*)-**24a**-^{1}H-NMR (500 MHz -$CDCl_3$); $^{13}C\{^{1}H\}$ (126 MHz, $CDCl_3$)

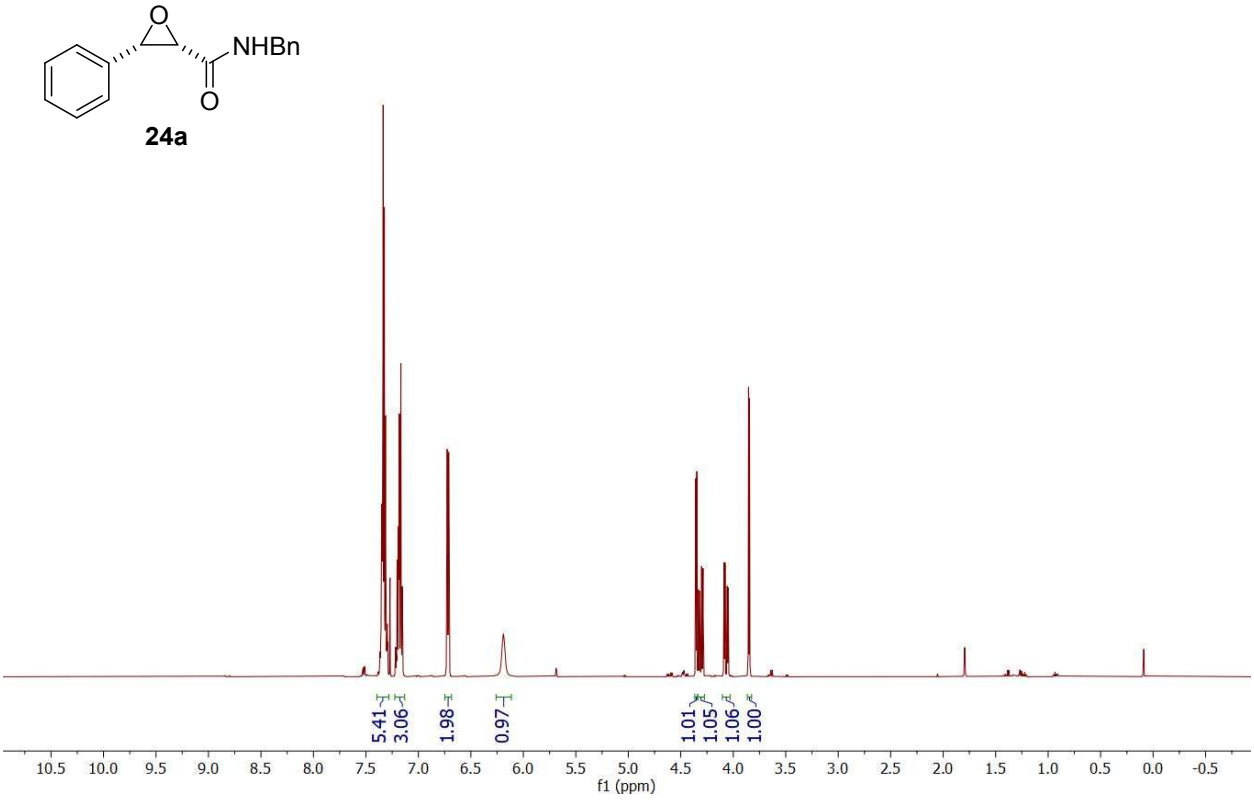

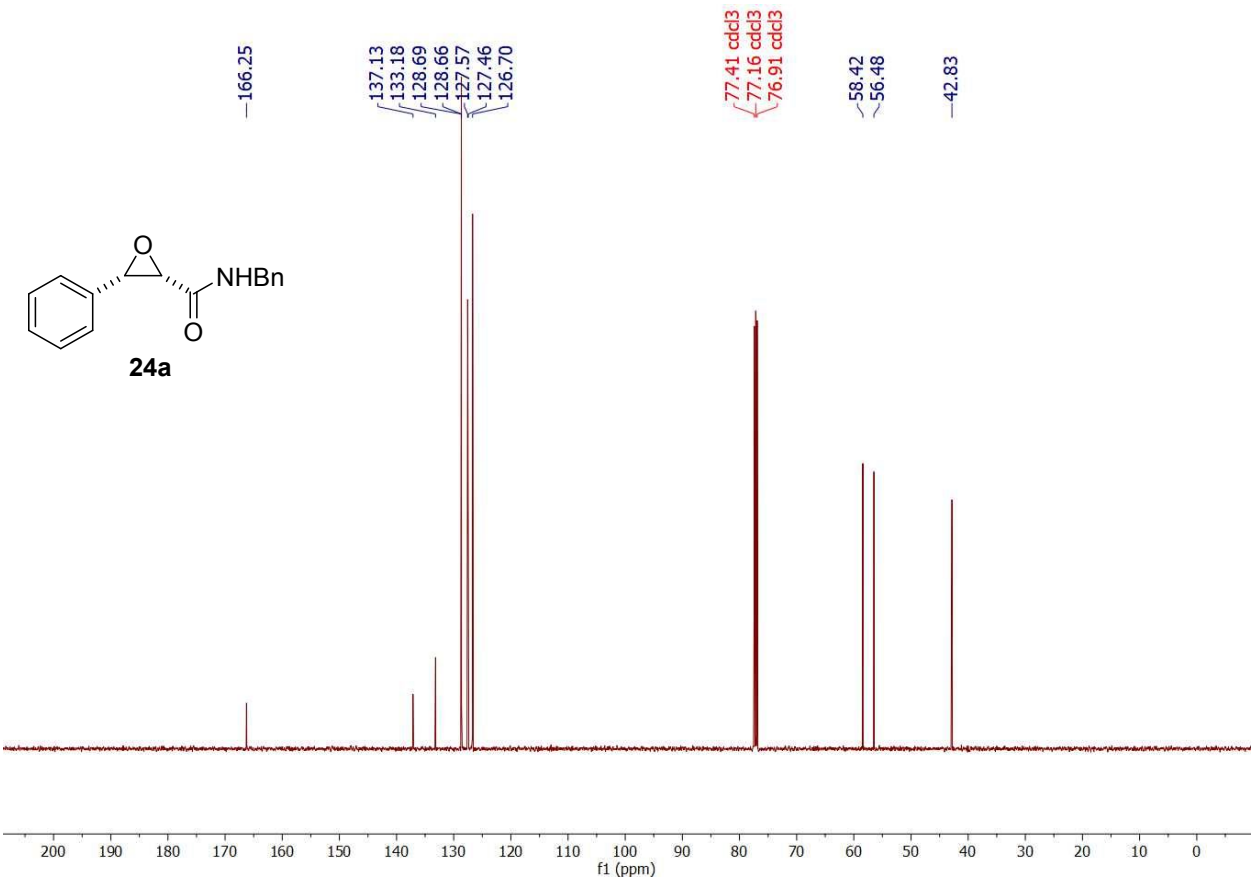
166.25
137.13
133.18
128.69
128.66
127.57
127.46
126.70
77.41 cdcl3
77.16 cdcl3
76.91 cdcl3
58.42
56.48
42.83
O
NHBn
O
24a
200
190
180
170
160
150
140
130
120
110
100
90
80
70
60
50
40
30
20
10
0
f1 (ppm)

(*2S,3S*)-**24a**-^{1}H-NMR (500 MHz -$CDCl_3$); $^{13}C\{^{1}H\}$ (126 MHz, $CDCl_3$)

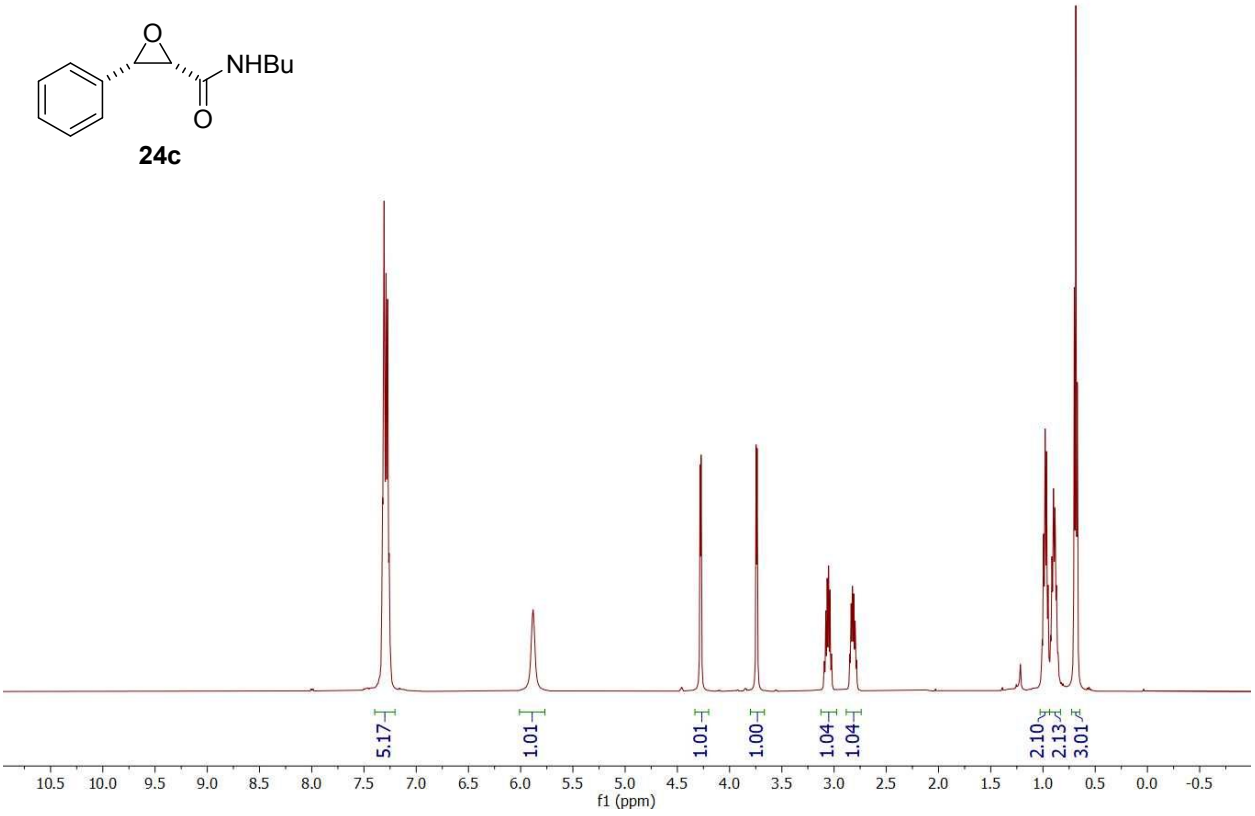

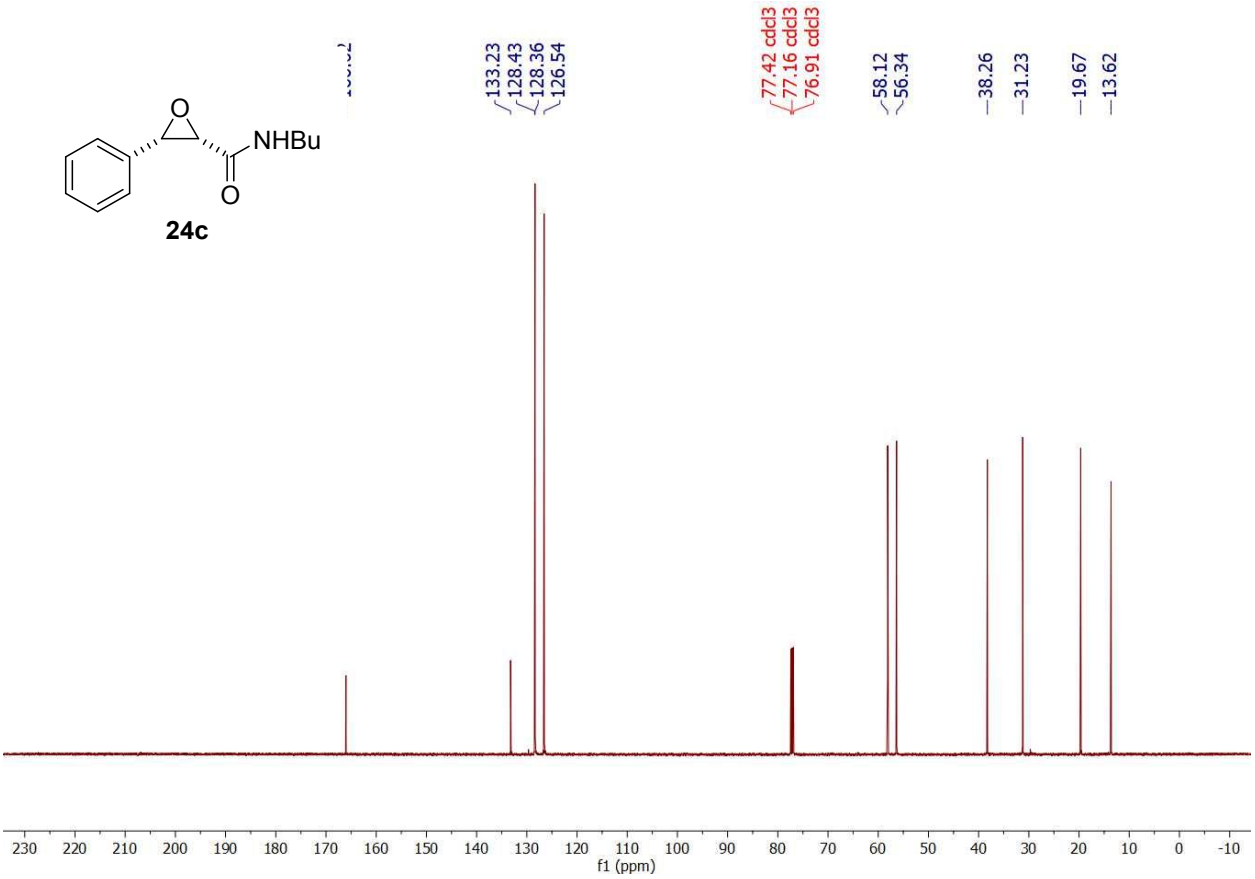
O
NHBu
O
24c
133.23
128.43
128.36
126.54
77.42 cdcl3
77.16 cdcl3
76.91 cdcl3
58.12
56.34
38.26
31.23
19.67
13.62
230 220 210 200 190 180 170 160 150 140 130 120 110 100 90 80 70 60 50 40 30 20 10 0 -10
f1 (ppm)

(*2S,3S*)-**25a**-^{1}H-NMR (500 MHz -$CDCl_3$); $^{13}C\{^{1}H\}$ (126 MHz, $CDCl_3$)

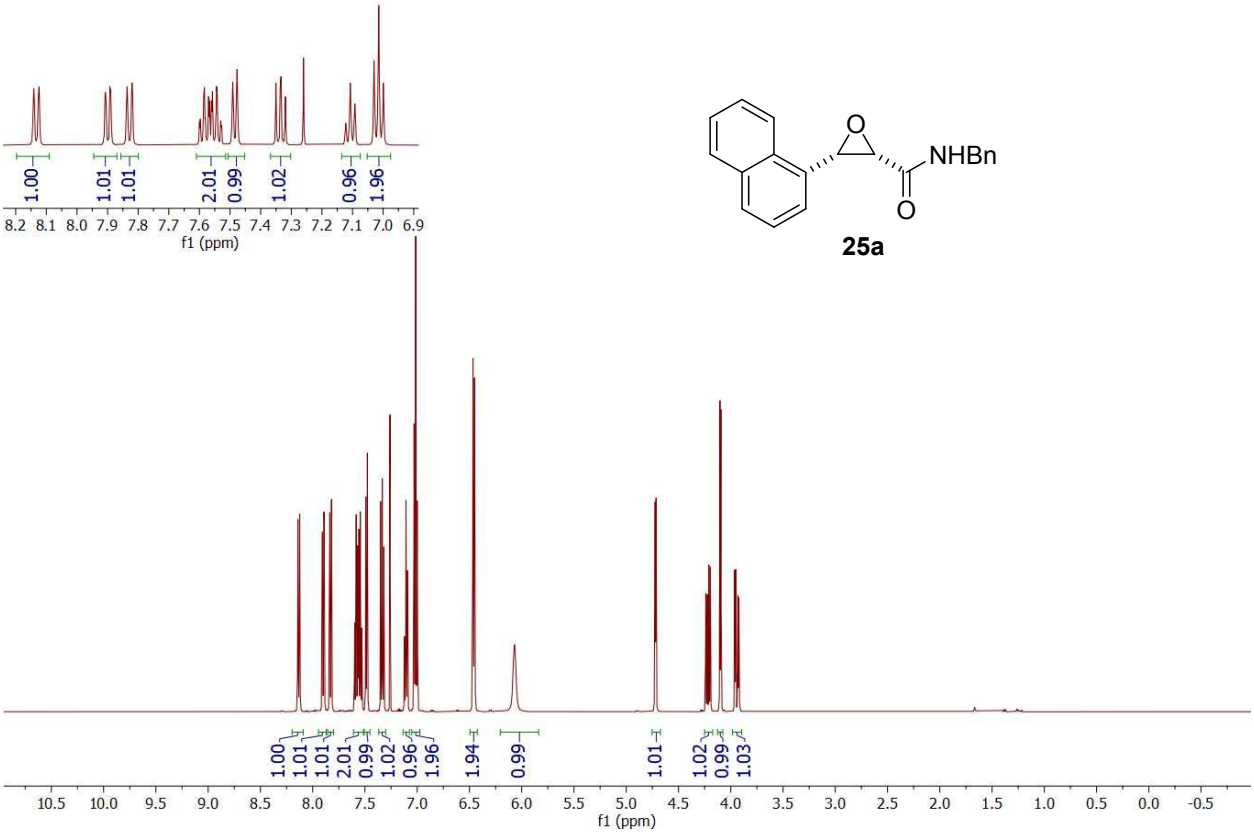

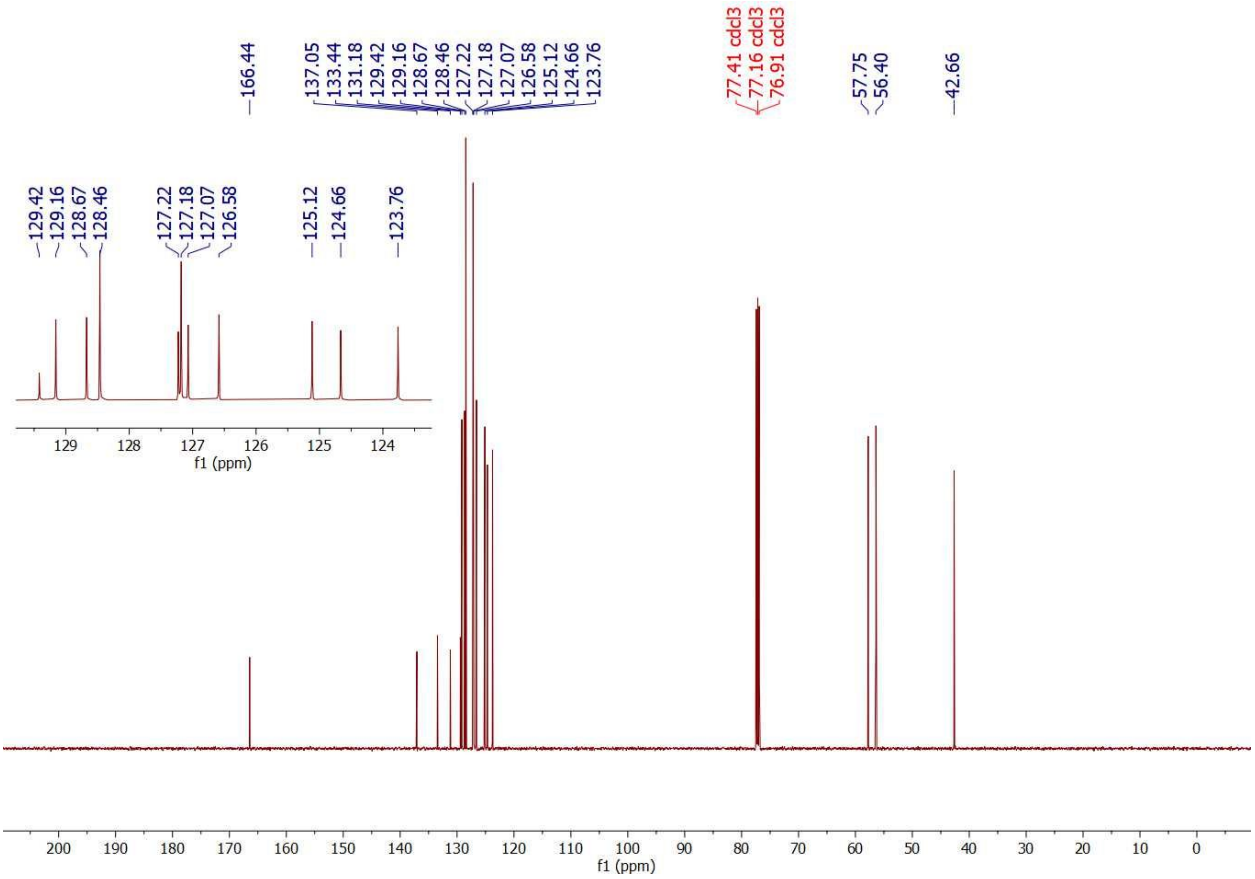
166.44
137.05
133.44
131.18
129.42
129.16
128.67
128.46
127.22
127.18
127.07
126.58
125.12
124.66
123.76
77.41 cdcl3
77.16 cdcl3
76.91 cdcl3
57.75
56.40
42.66
f1 (ppm)
f1 (ppm)

(*2S,3S*)-**26a**-^{1}H-NMR (500 MHz -$CDCl_3$); $^{13}C\{^{1}H\}$ (126 MHz, $CDCl_3$)

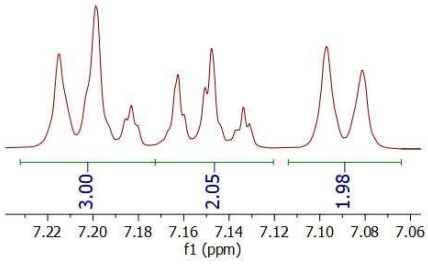

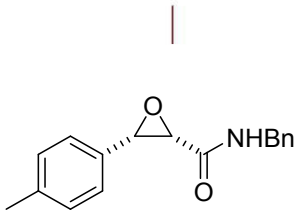

26a

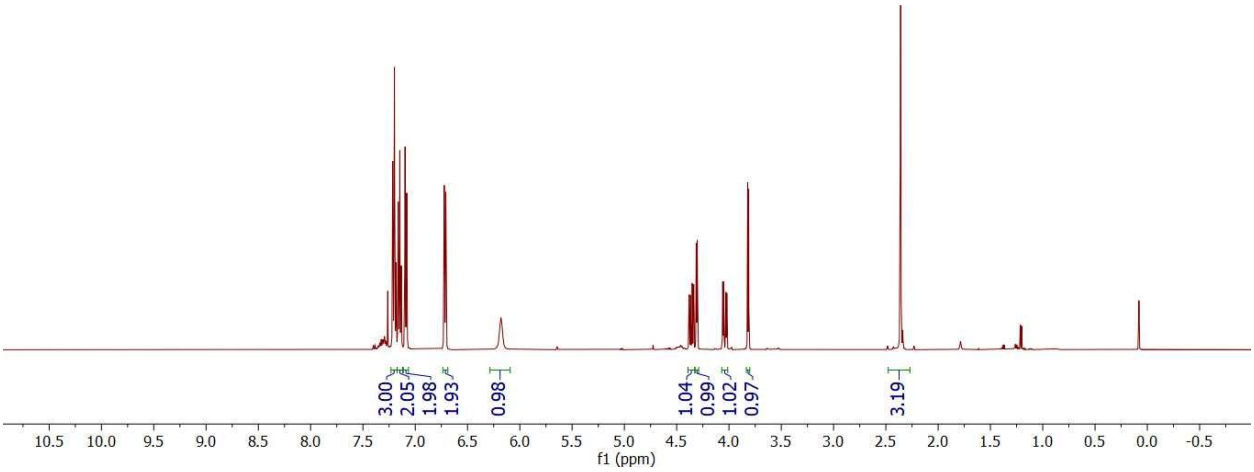

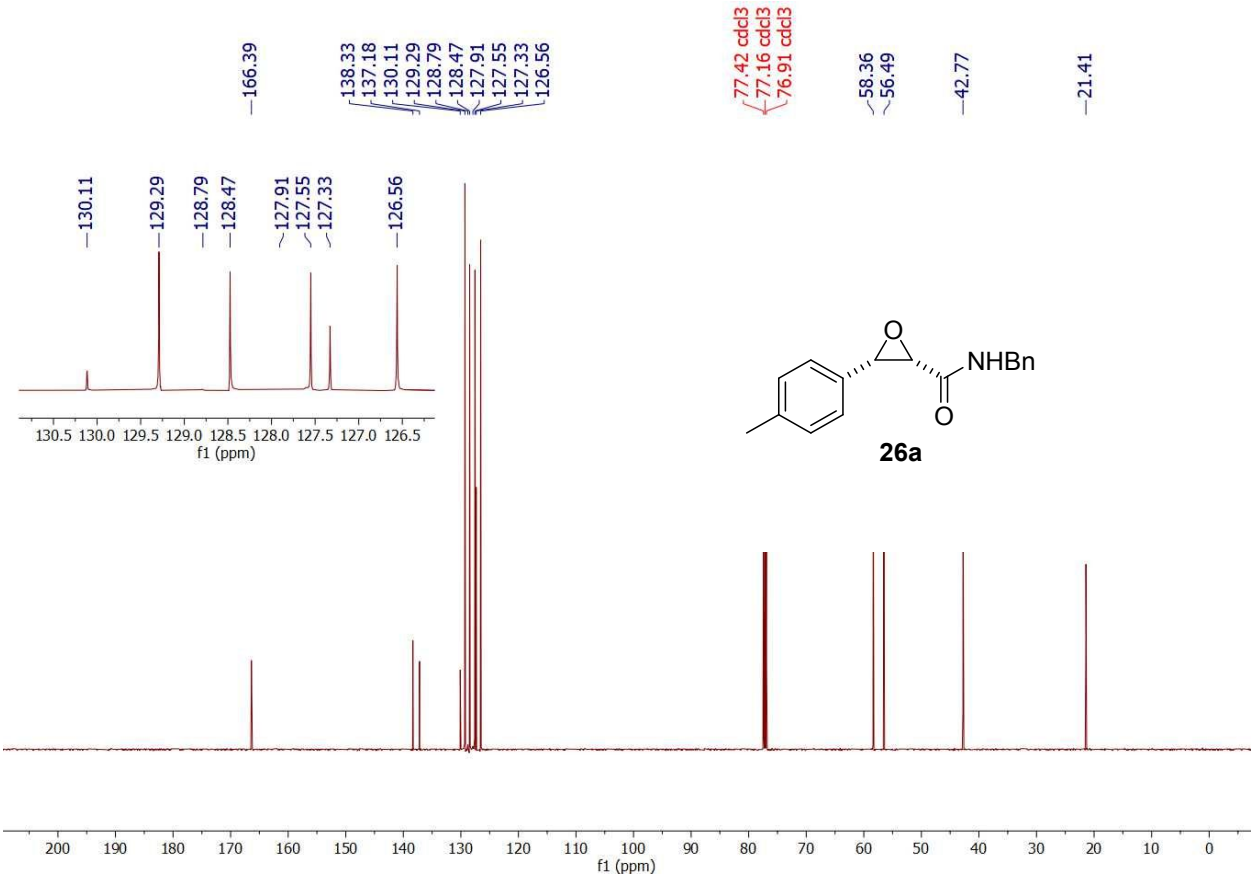
166.39
138.33
137.18
130.11
129.29
128.79
128.47
127.91
127.55
127.33
126.56
77.42 cdcl3
77.16 cdcl3
76.91 cdcl3
58.36
56.49
42.77
21.41
130.11
129.29
128.79
128.47
127.91
127.55
127.33
126.56
130.5 130.0 129.5 129.0 128.5 128.0 127.5 127.0 126.5
f1 (ppm)
O
NHBn
O
26a
200 190 180 170 160 150 140 130 120 110 100 90 80 70 60 50 40 30 20 10 0
f1 (ppm)

(*2S,3S*)-**26c**-^{1}H-NMR (500 MHz -$CDCl_3$); $^{13}C\{^{1}H\}$ (126 MHz, $CDCl_3$)

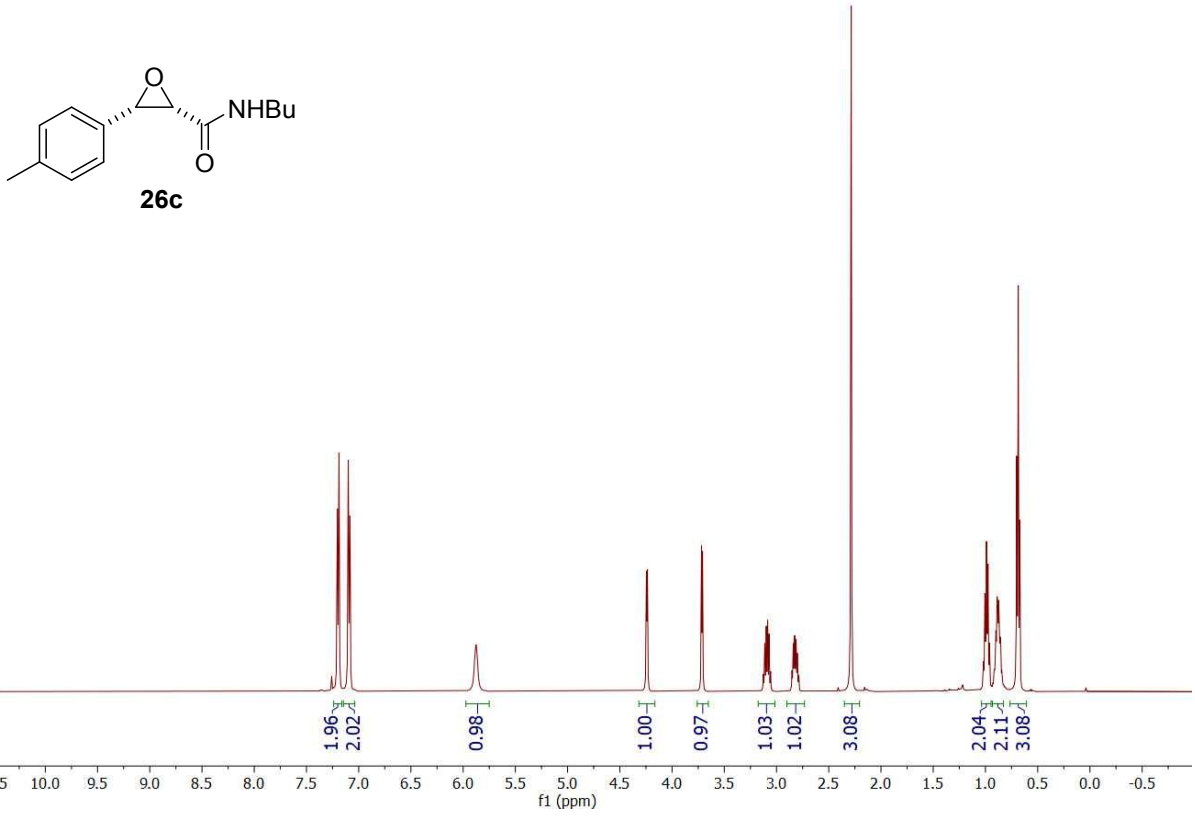

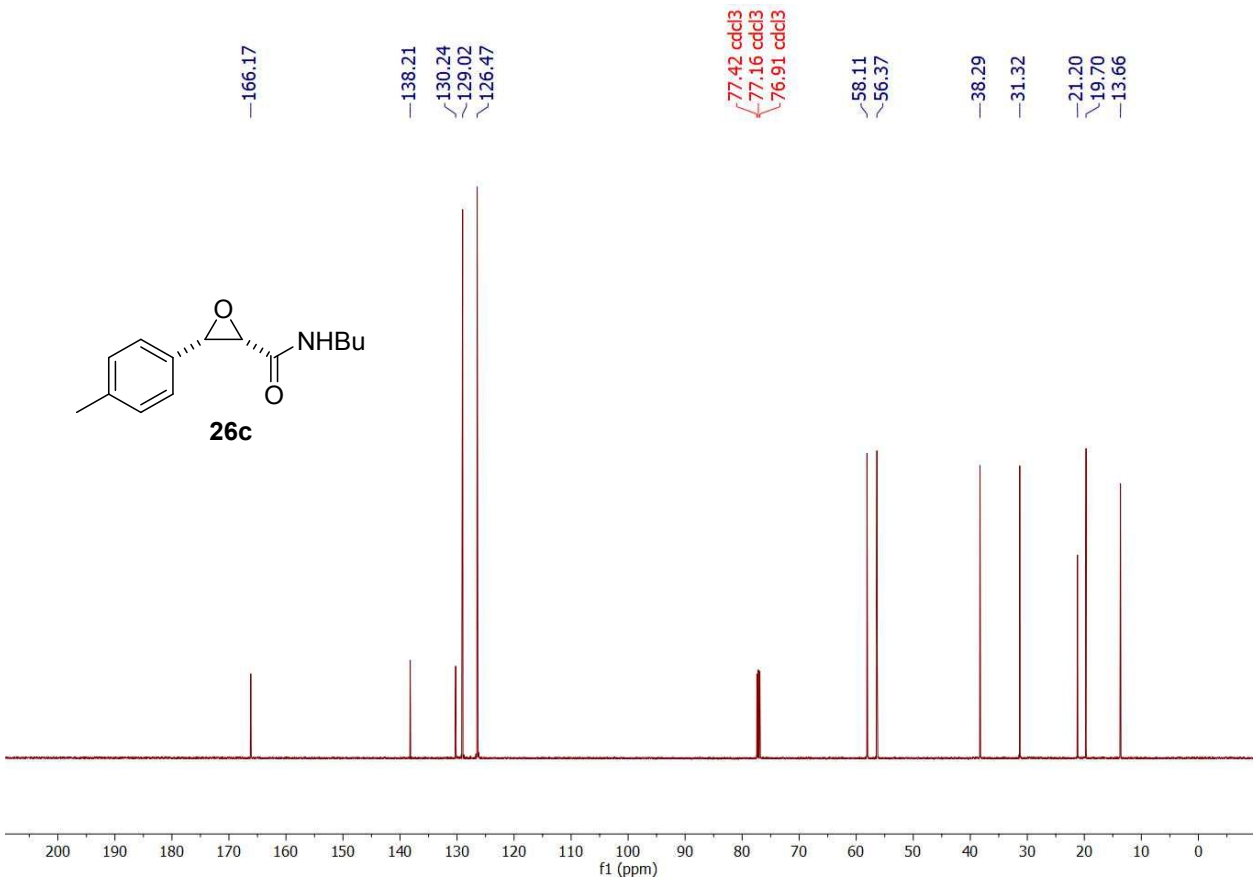
166.17
138.21
130.24
129.02
126.47
77.42 cdcl3
77.16 cdcl3
76.91 cdcl3
58.11
56.37
38.29
31.32
21.20
19.70
13.66
O
NHBu
O
26c
200 190 180 170 160 150 140 130 120 110 100 90 80 70 60 50 40 30 20 10 0
f1 (ppm)

(*2S,3S*)-**28a**-^{1}H-NMR (500 MHz -$CDCl_3$); $^{13}C\{^{1}H\}$ (126 MHz, $CDCl_3$)

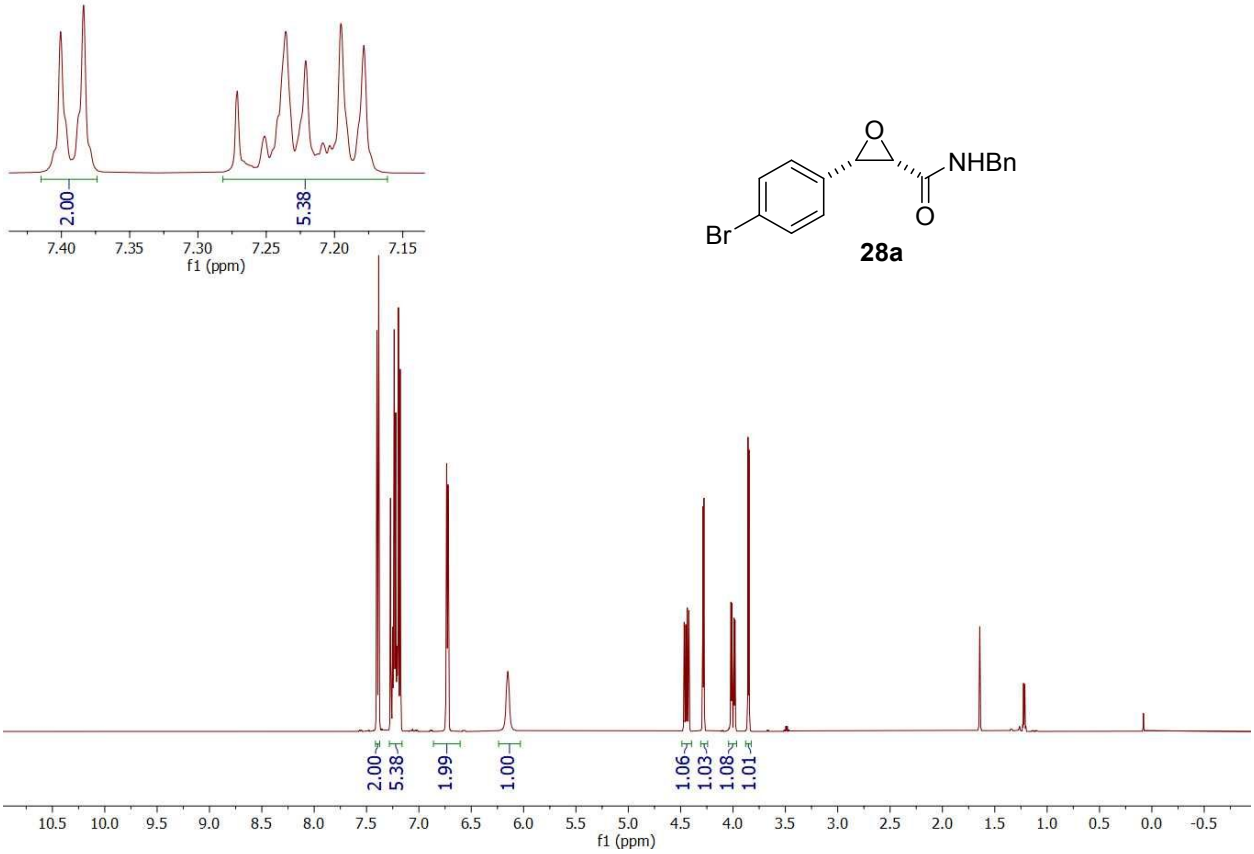

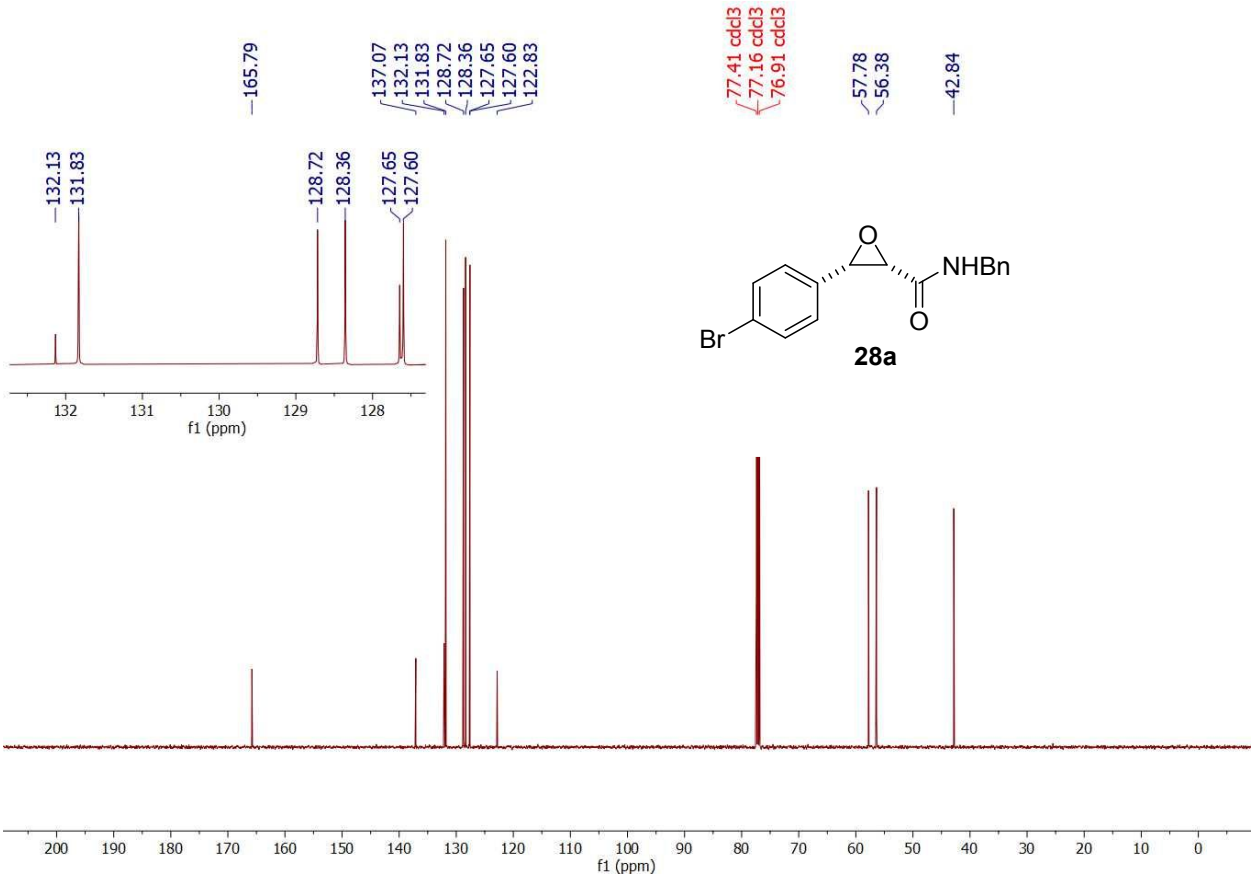
165.79
137.07
132.13
131.83
128.72
128.36
127.65
127.60
122.83
77.41 cdcl3
77.16 cdcl3
76.91 cdcl3
57.78
56.38
42.84
132.13
131.83
128.72
128.36
127.65
127.60
132
131
130
129
128
f1 (ppm)
O
NHBn
O
Br
28a
200
190
180
170
160
150
140
130
120
110
100
90
80
70
60
50
40
30
20
10
0
f1 (ppm)

(*2S,3S*)-**28c**-^{1}H-NMR (500 MHz -$CDCl_3$); $^{13}C\{^{1}H\}$ (126 MHz, $CDCl_3$)

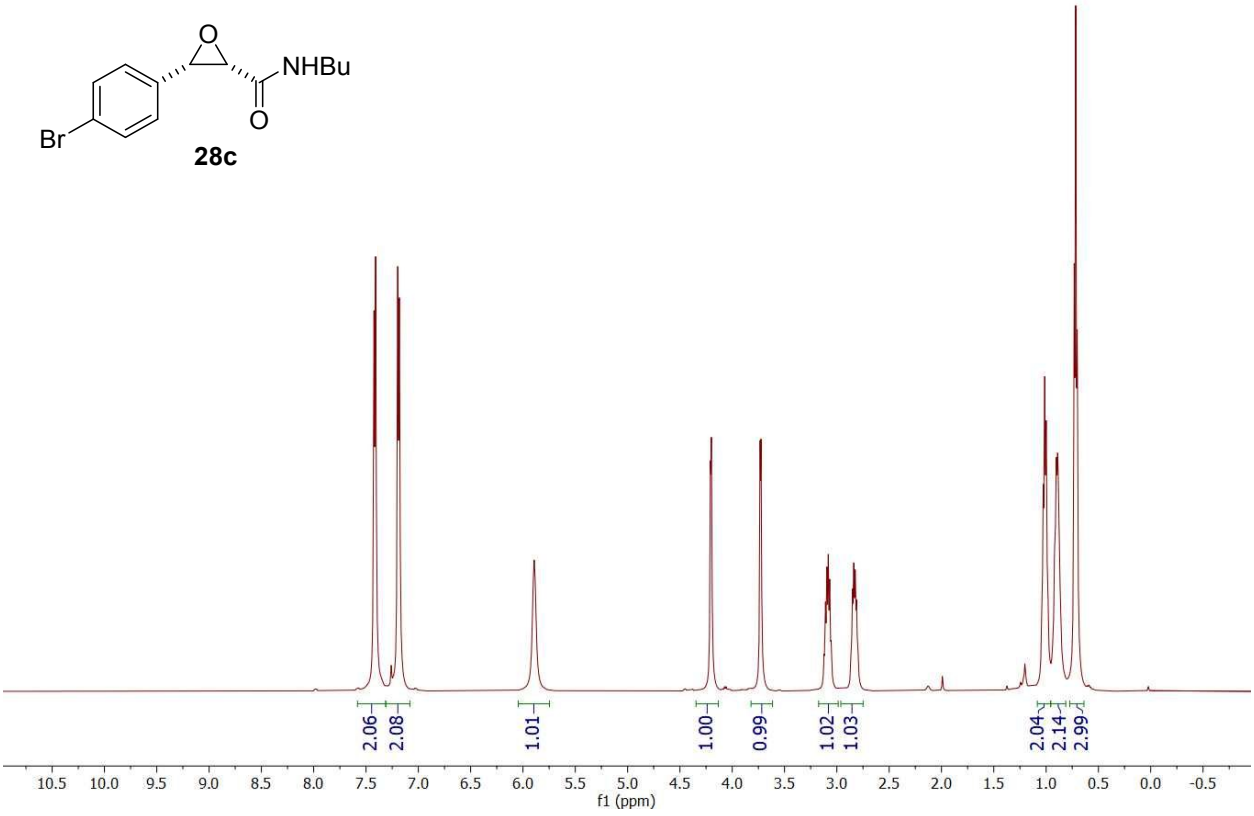

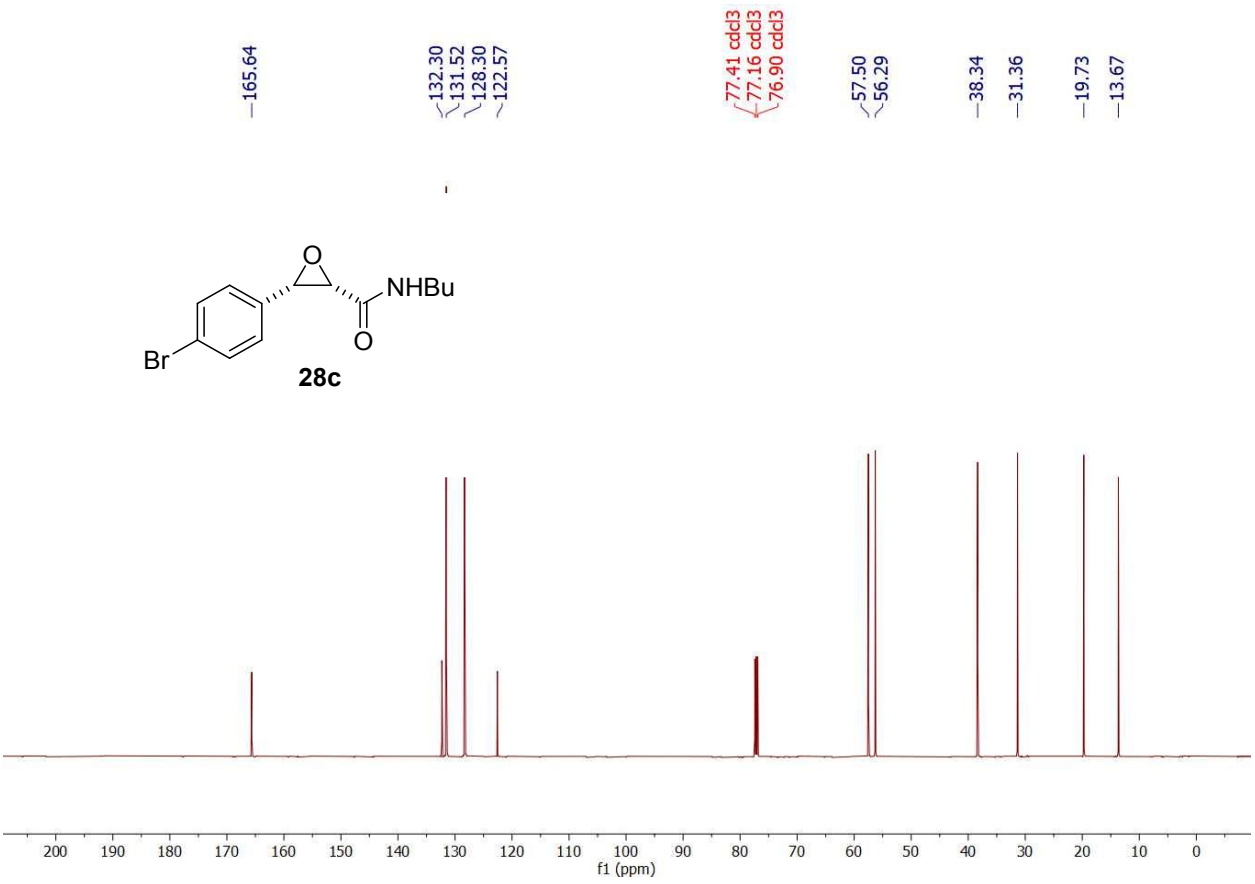
165.64
132.30
131.52
128.30
122.57
77.41 cdcl3
77.16 cdcl3
76.90 cdcl3
57.50
56.29
38.34
31.36
19.73
13.67
NHBu
O
O
Br
28c
200
190
180
170
160
150
140
130
120
110
100
90
80
70
60
50
40
30
20
10
0
f1 (ppm)

(*2S,3S*)-**29a**-^{1}H-NMR (500 MHz -$CDCl_3$); $^{13}C\{^{1}H\}$ (126 MHz, $CDCl_3$)

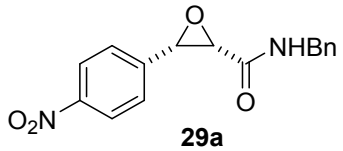

29a

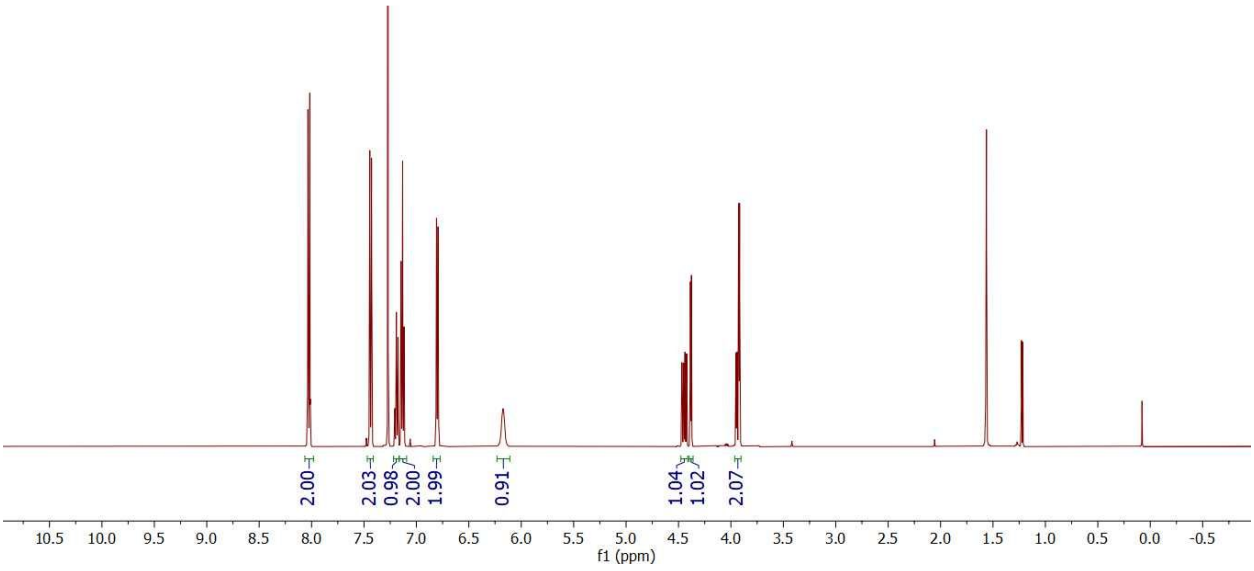

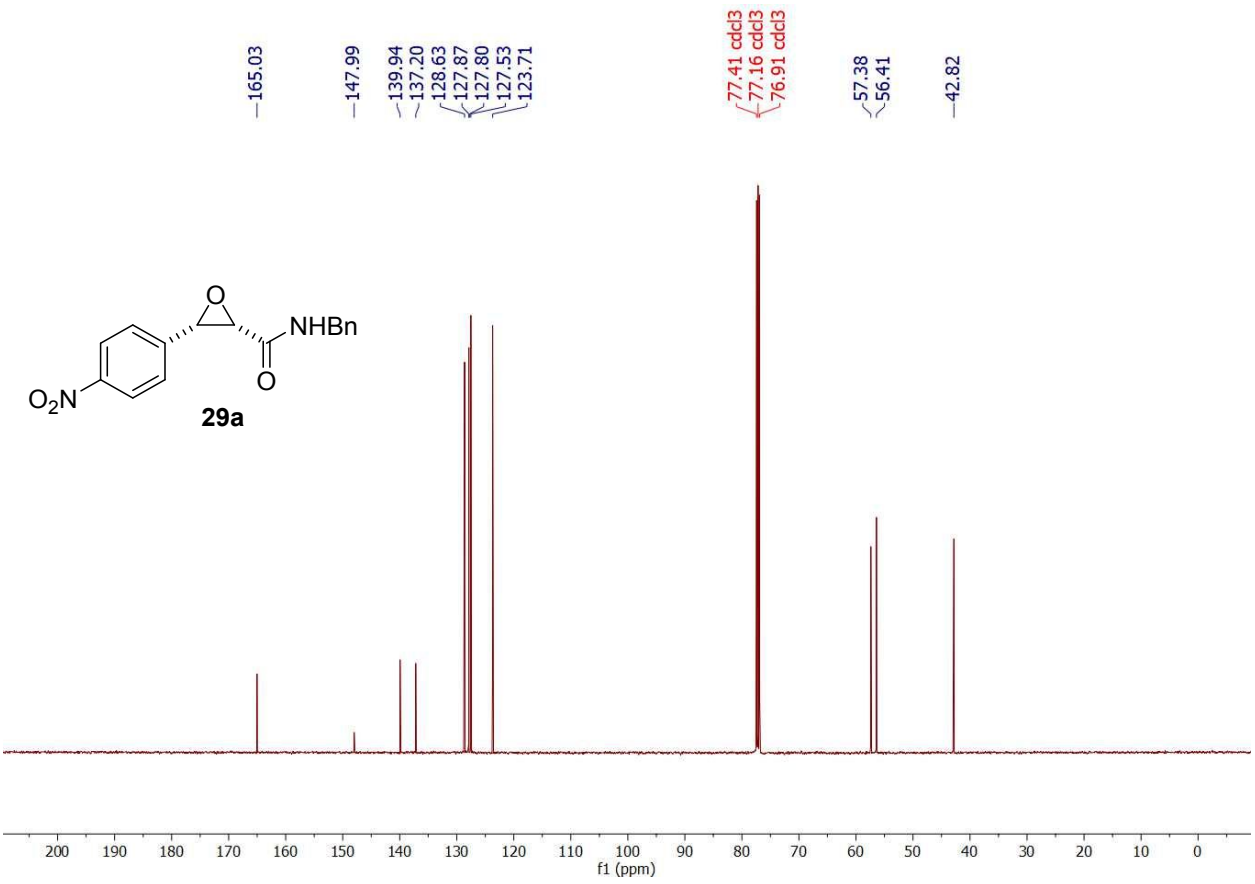
165.03
147.99
139.94
137.20
128.63
127.87
127.80
127.53
123.71
77.41 cdcl3
77.16 cdcl3
76.91 cdcl3
57.38
56.41
42.82
O
NHBn
O
O2N
29a
200
190
180
170
160
150
140
130
120
110
100
90
80
70
60
50
40
30
20
10
0
f1 (ppm)

(*2S,3S*)-**29c**-^{1}H-NMR (500 MHz -$CDCl_3$); $^{13}C\{^{1}H\}$ (126 MHz, $CDCl_3$)

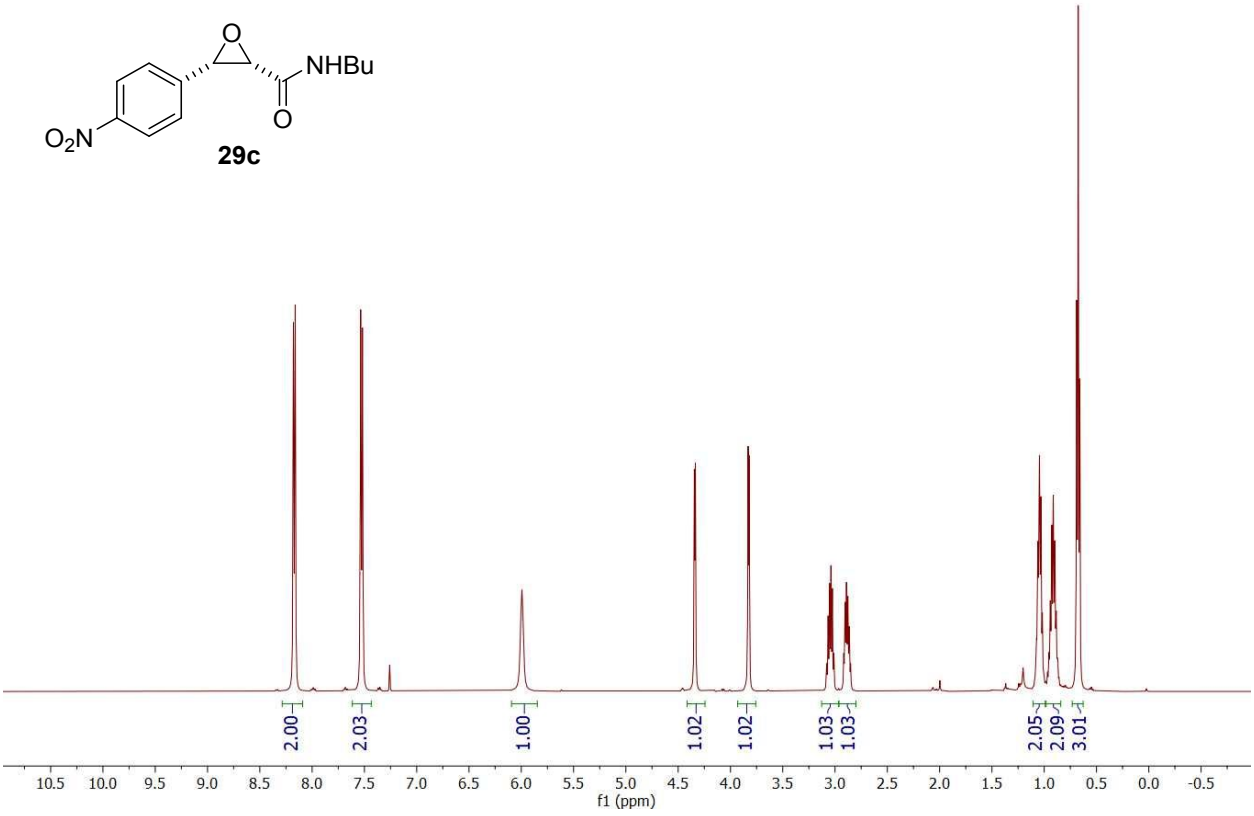

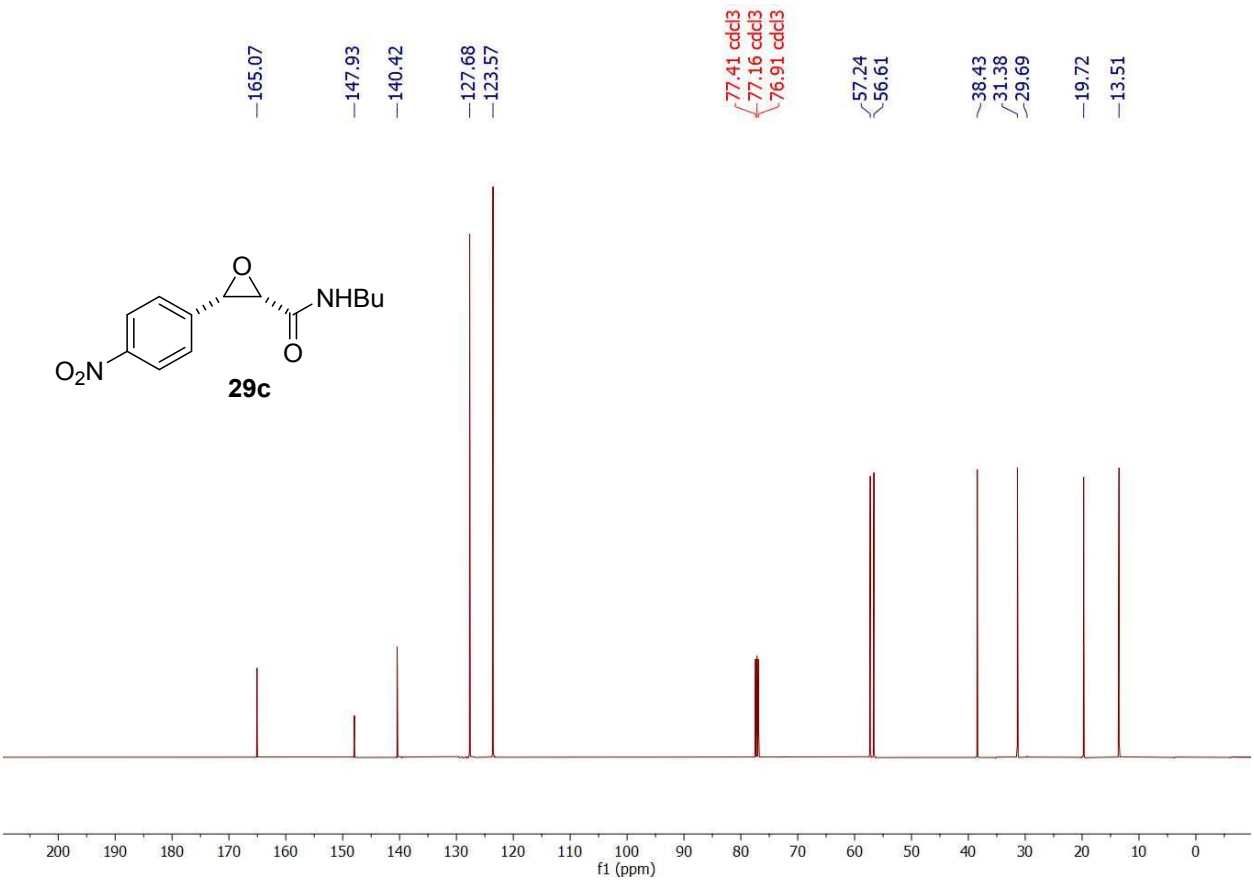
165.07
147.93
140.42
127.68
123.57
77.41 cdcl3
77.16 cdcl3
76.91 cdcl3
57.24
56.61
38.43
31.38
29.69
19.72
13.51
O
NHBu
O
O2N
29c
200
190
180
170
160
150
140
130
120
110
100
90
80
70
60
50
40
30
20
10
0
f1 (ppm)

(*2S,3S*)-**36a**-^{1}H-NMR (500 MHz -$CDCl_3$); $^{13}C\{^{1}H\}$ (126 MHz, $CDCl_3$)

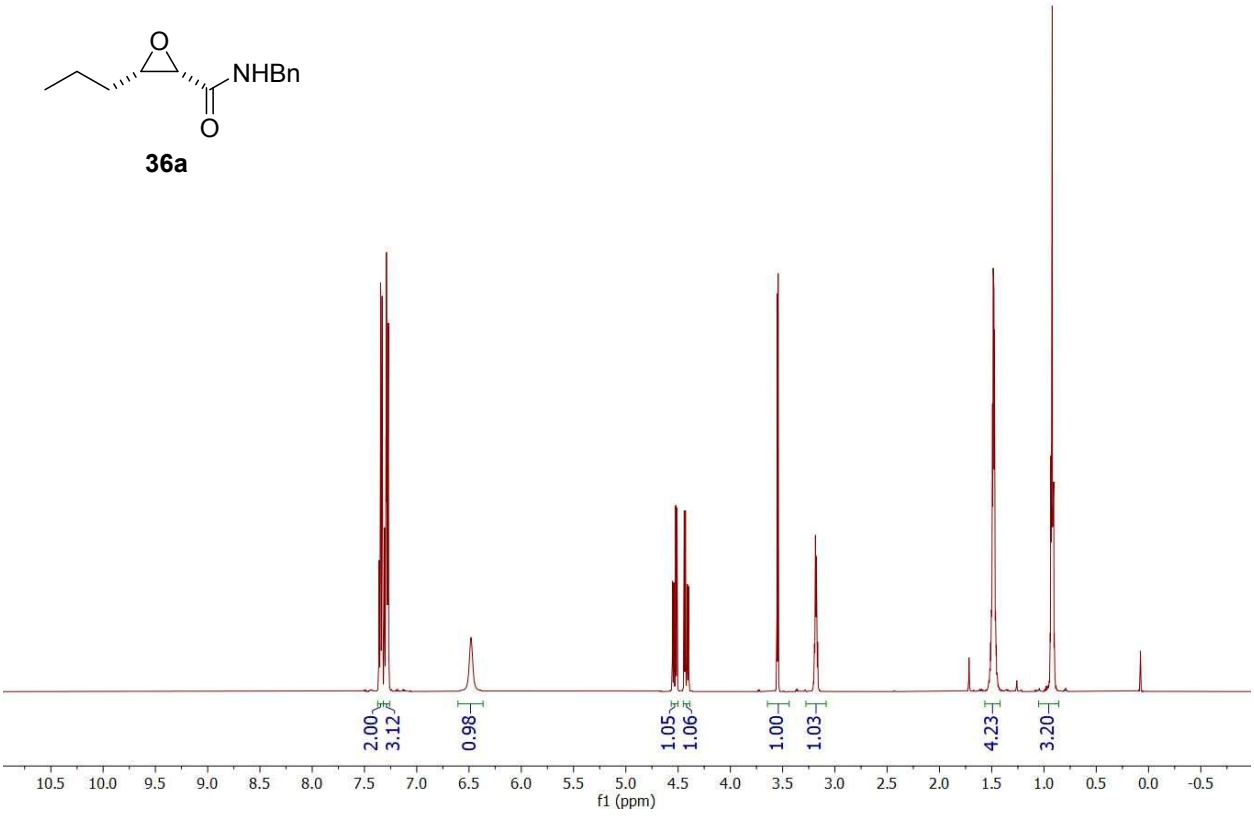

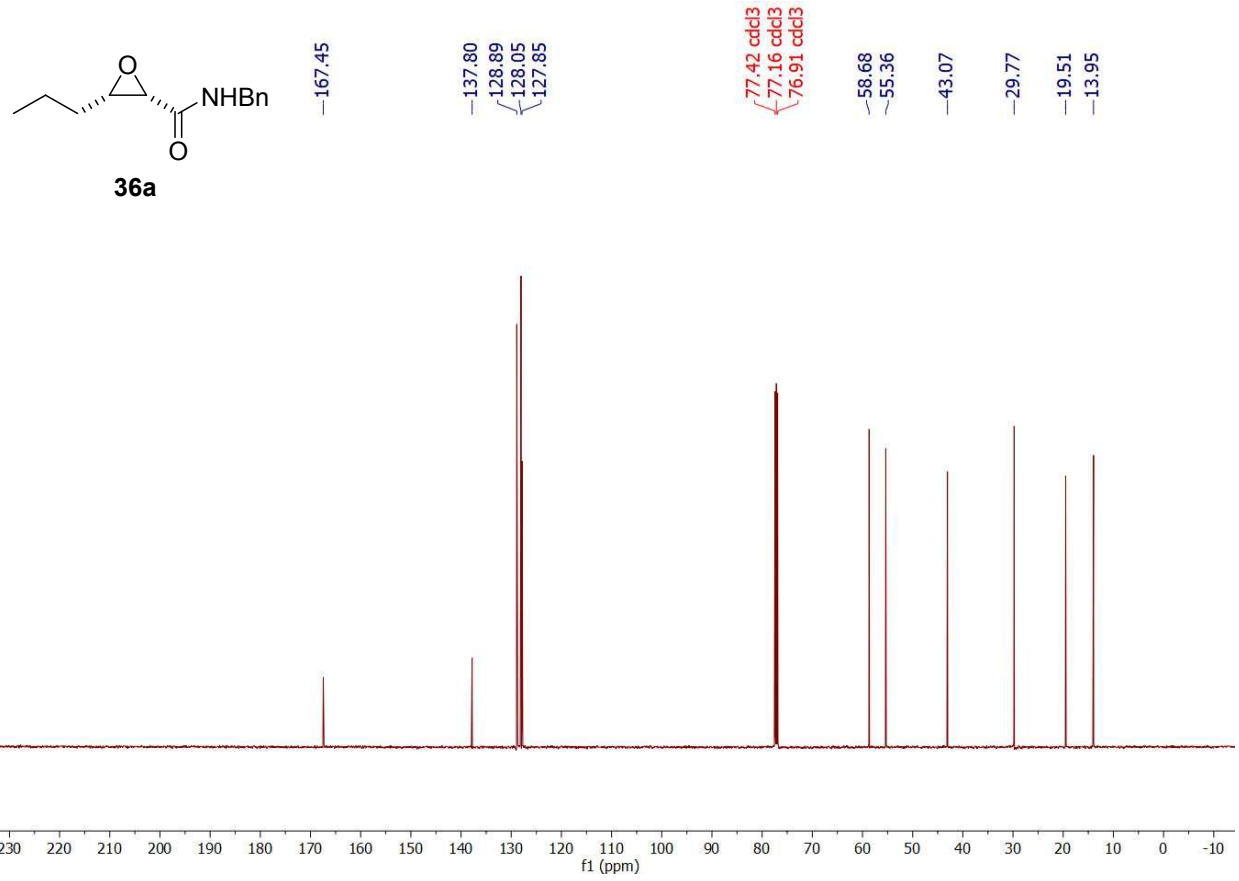
NHBn
O
O
167.45
137.80
128.89
128.05
127.85
77.42 cdcl3
77.16 cdcl3
76.91 cdcl3
58.68
55.36
43.07
29.77
19.51
13.95
230 220 210 200 190 180 170 160 150 140 130 120 110 100 90 80 70 60 50 40 30 20 10 0 -10
f1 (ppm)

36a

(*2S,3S*)-**36b**-^{1}H-NMR (500 MHz -$CDCl_3$); $^{13}C\{^{1}H\}$ (126 MHz, $CDCl_3$)

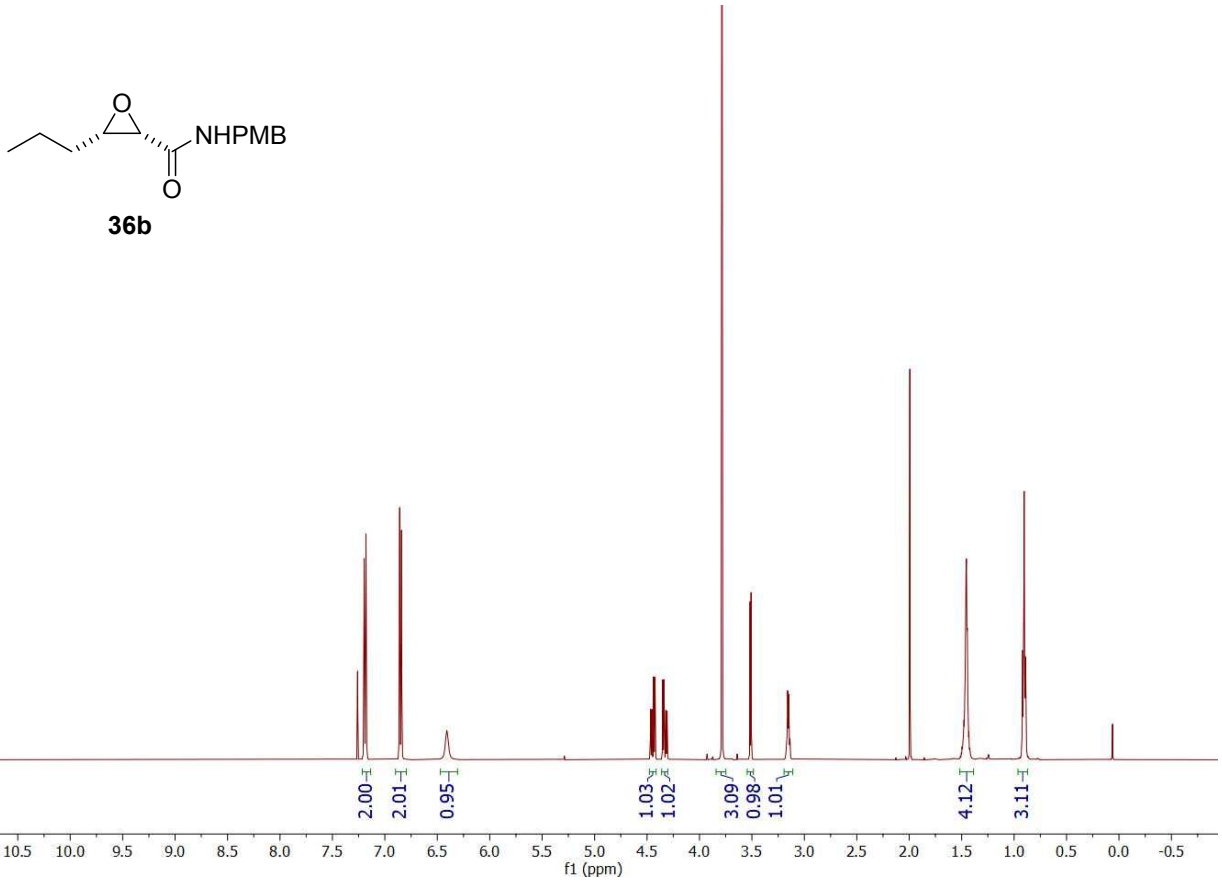

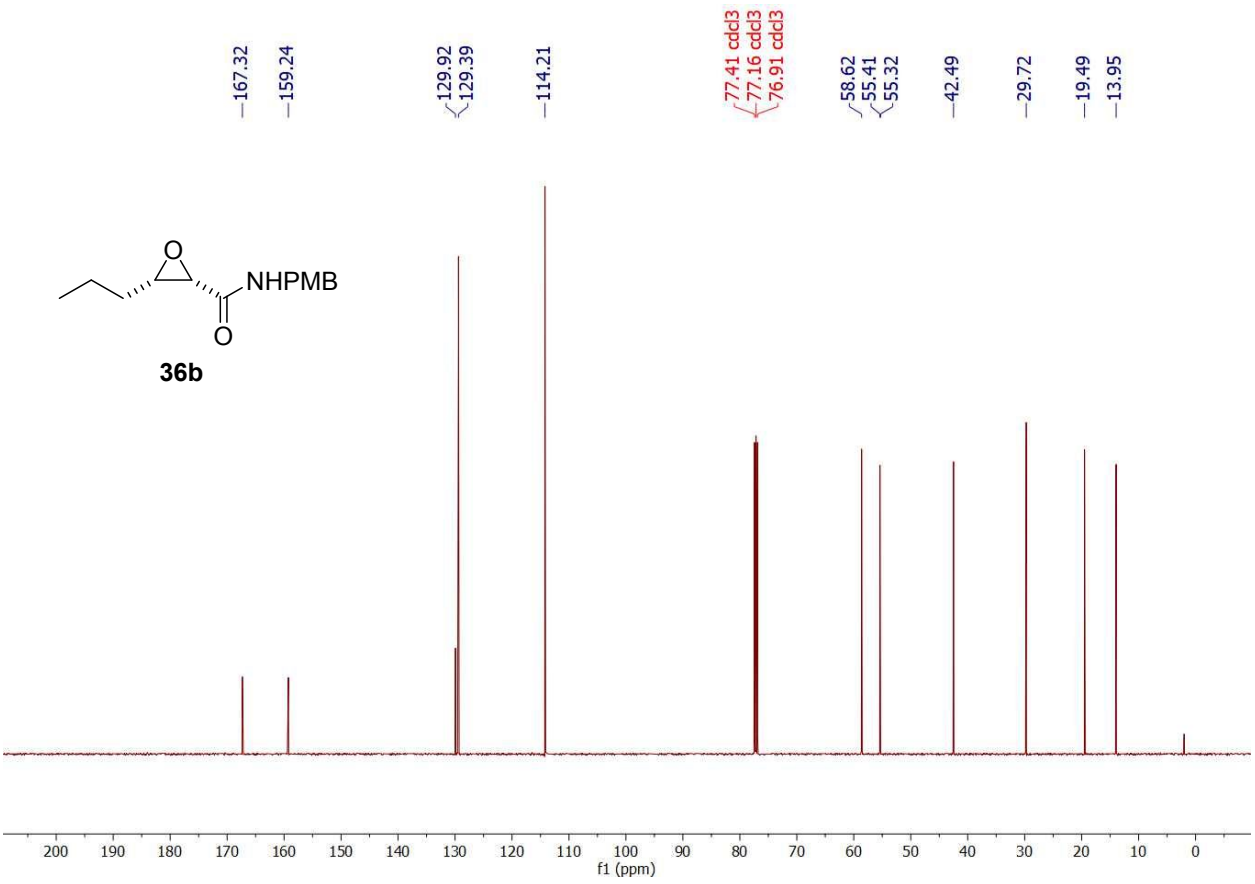
167.32
159.24
129.92
129.39
114.21
77.41 cdcl3
77.16 cdcl3
76.91 cdcl3
58.62
55.41
55.32
42.49
29.72
19.49
13.95
NHPMB
O
O
36b
200
190
180
170
160
150
140
130
120
110
100
90
80
70
60
50
40
30
20
10
0
f1 (ppm)

(*2S,3S*)-**37a**-^{1}H-NMR (500 MHz -$CDCl_3$); $^{13}C\{^{1}H\}$ (126 MHz, $CDCl_3$)

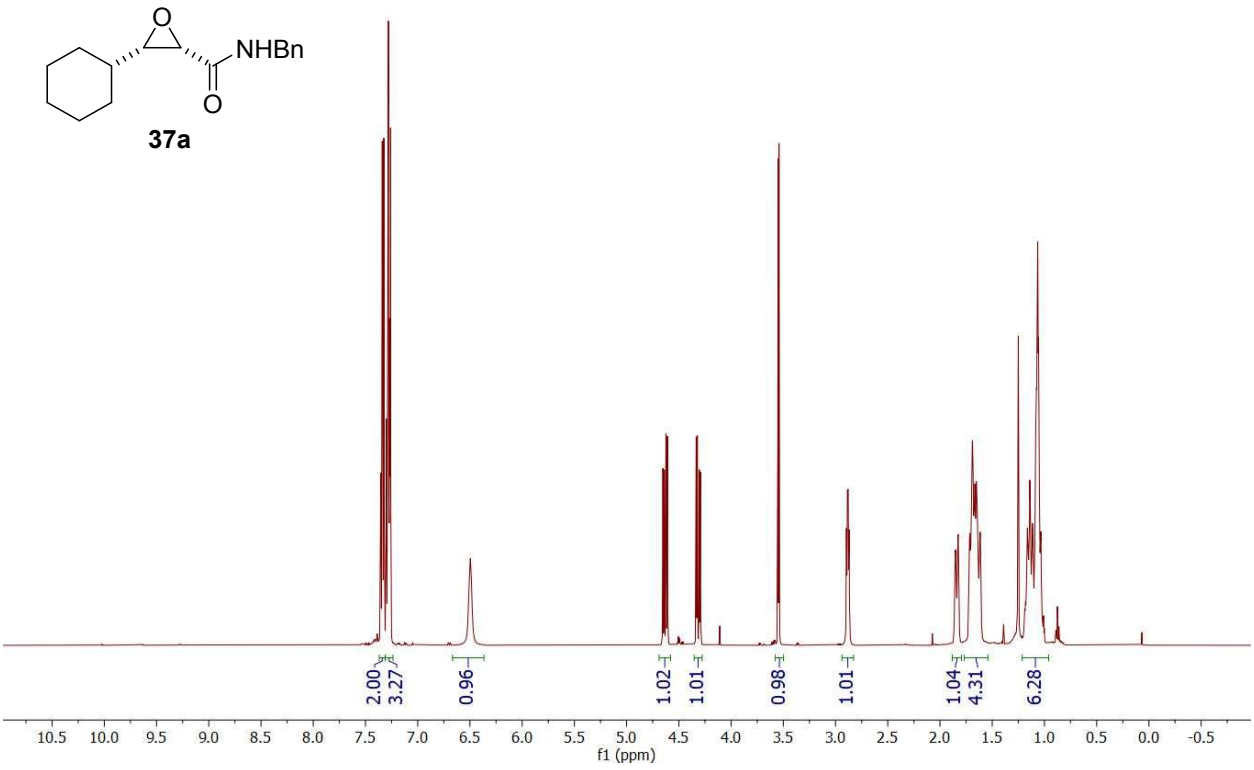

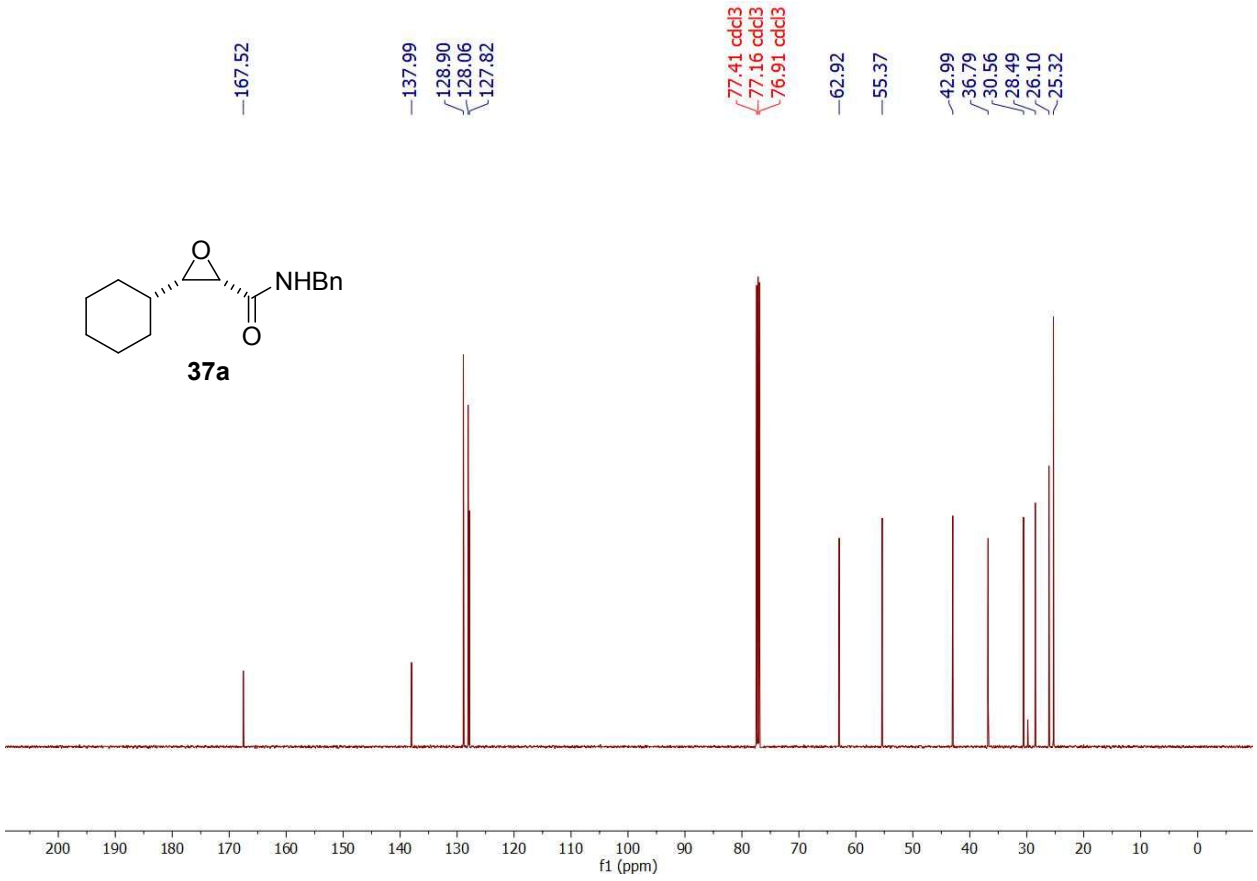
167.52
137.99
128.90
128.06
127.82
77.41 cdcl3
77.16 cdcl3
76.91 cdcl3
62.92
55.37
42.99
36.79
30.56
28.49
26.10
25.32
O
NHBn
O
37a
200
190
180
170
160
150
140
130
120
110
100
90
80
70
60
50
40
30
20
10
0
f1 (ppm)

(*2S,3S*)-**38a**-^{1}H-NMR (500 MHz -$CDCl_3$); $^{13}C\{^{1}H\}$ (126 MHz, $CDCl_3$)

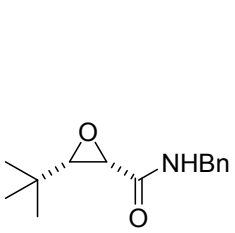

38a

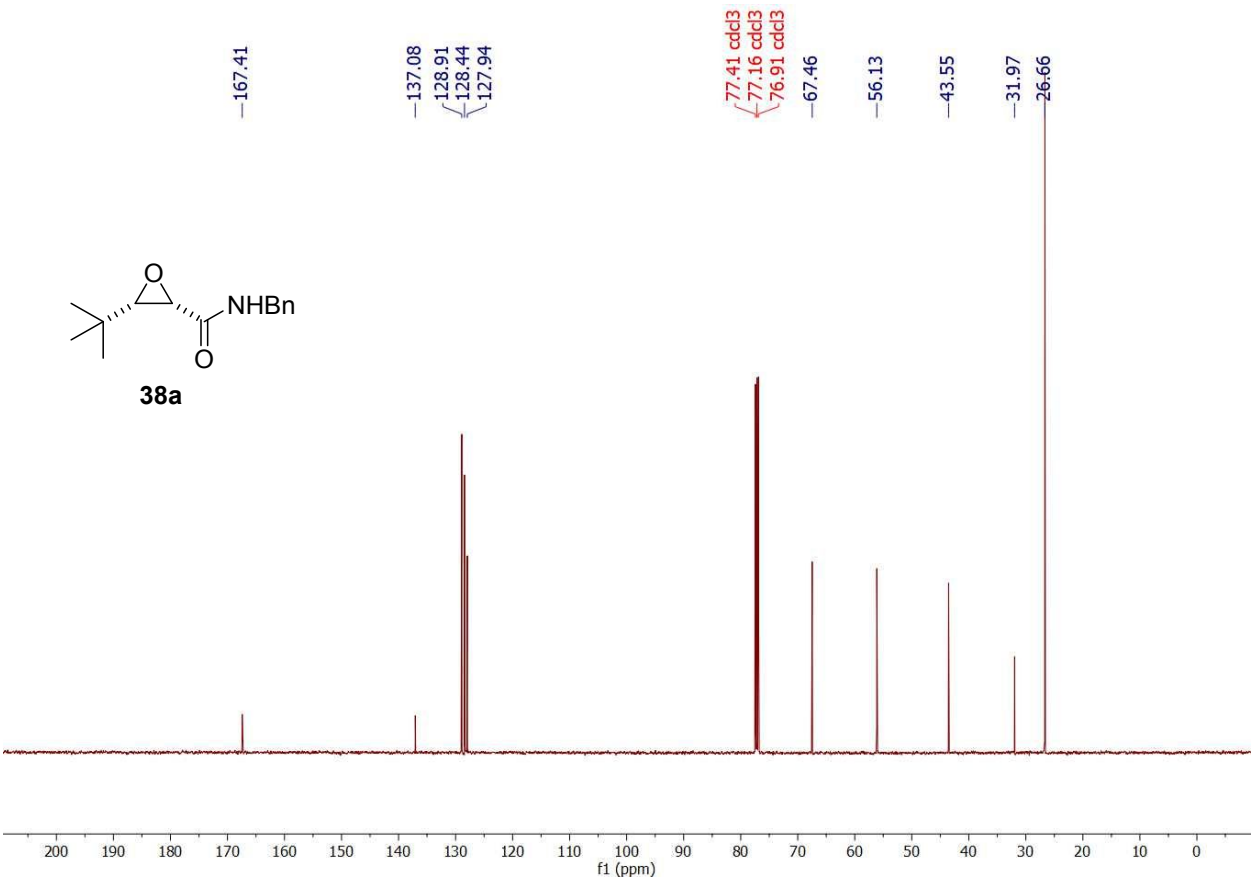
167.41
137.08
128.91
128.44
127.94
77.41 cdcl3
77.16 cdcl3
76.91 cdcl3
67.46
56.13
43.55
31.97
26.66
O
NHBn
O
38a
200
190
180
170
160
150
140
130
120
110
100
90
80
70
60
50
40
30
20
10
0
f1 (ppm)

(*2S,3S*)-**39a**-^{1}H-NMR (500 MHz -$CDCl_3$); $^{13}C\{^{1}H\}$ (126 MHz, $CDCl_3$)

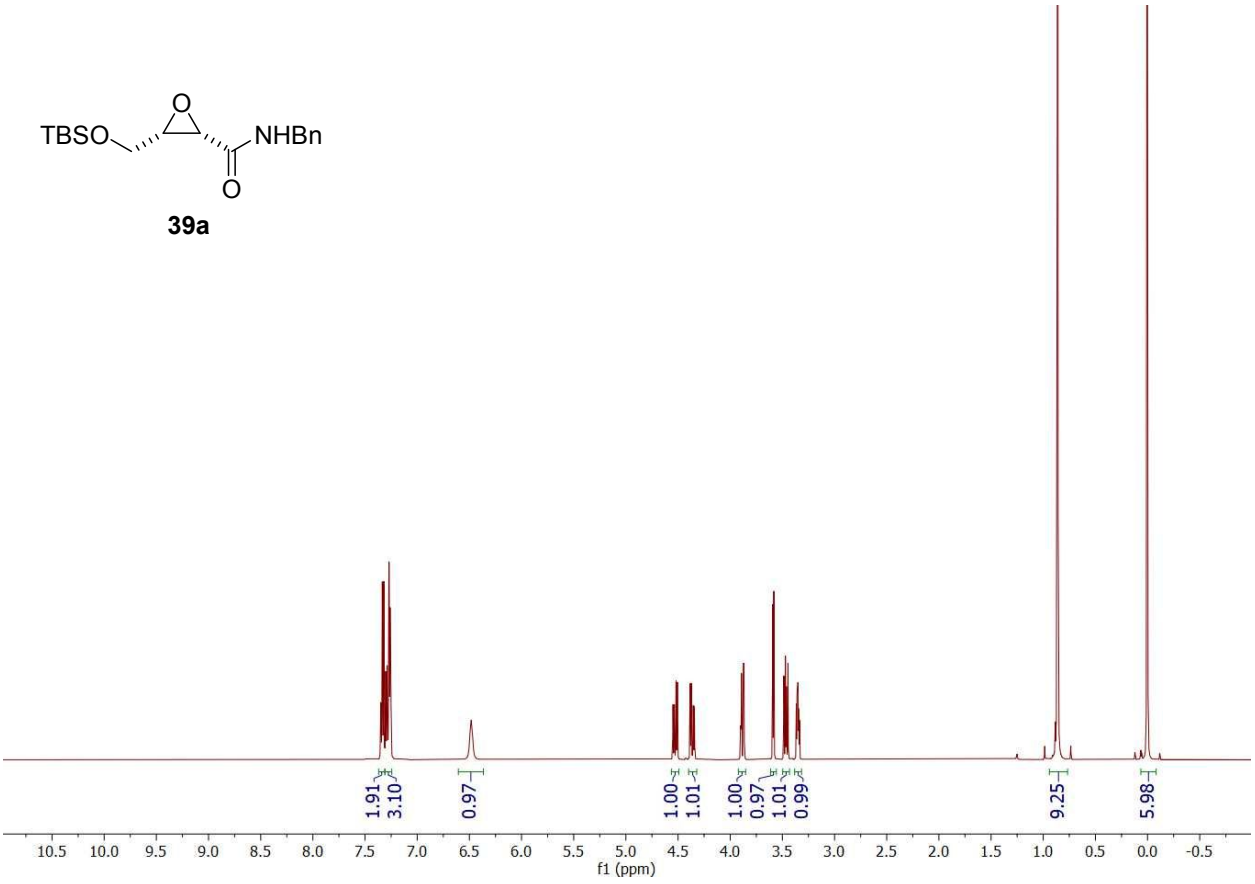

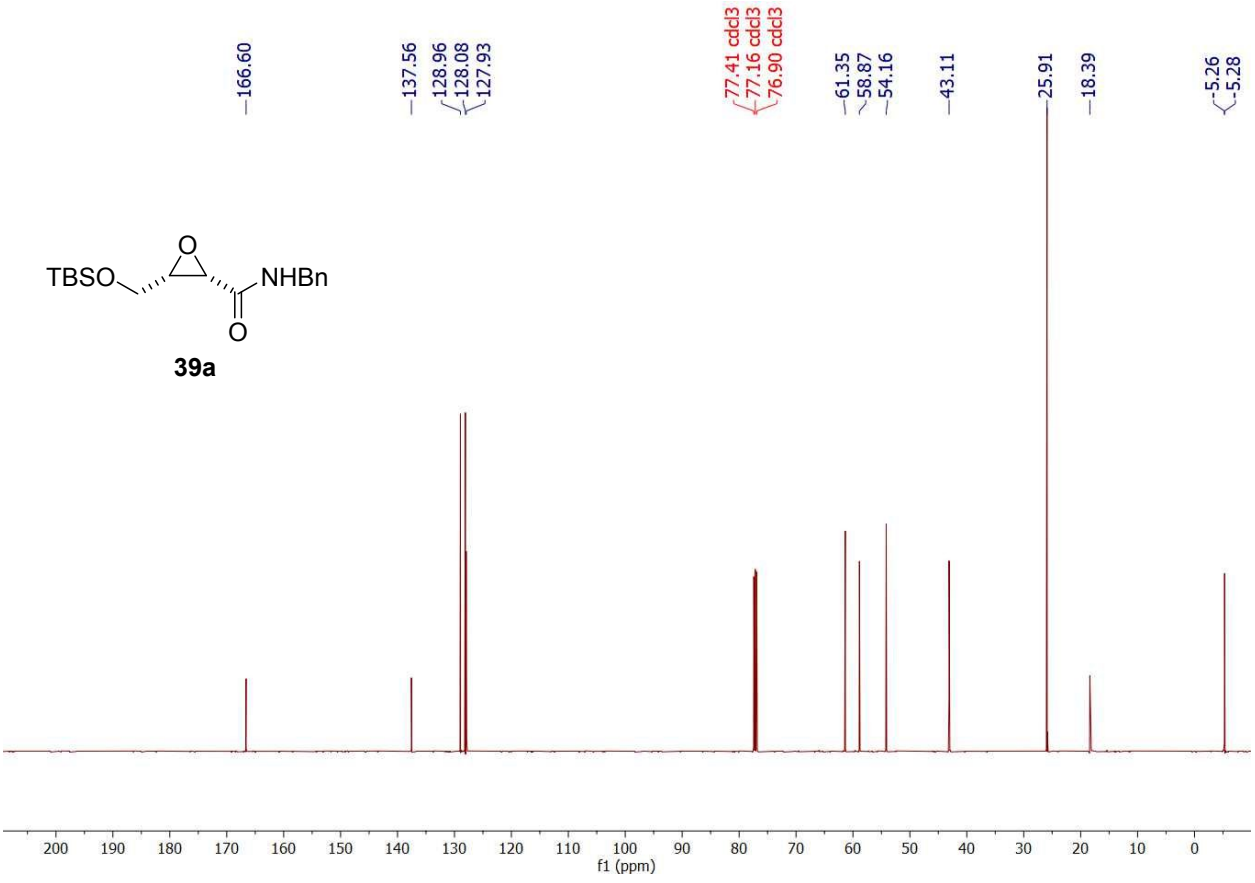
166.60
137.56
128.96
128.08
127.93
77.41 cdcl3
77.16 cdcl3
76.90 cdcl3
61.35
58.87
54.16
43.11
25.91
18.39
-5.26
-5.28
TBSO
NHBn
O
O
39a
200 190 180 170 160 150 140 130 120 110 100 90 80 70 60 50 40 30 20 10 0
f1 (ppm)

(*2S,3S*)-**39b**-^{1}H-NMR (500 MHz -$CDCl_3$); $^{13}C\{^{1}H\}$ (126 MHz, $CDCl_3$)

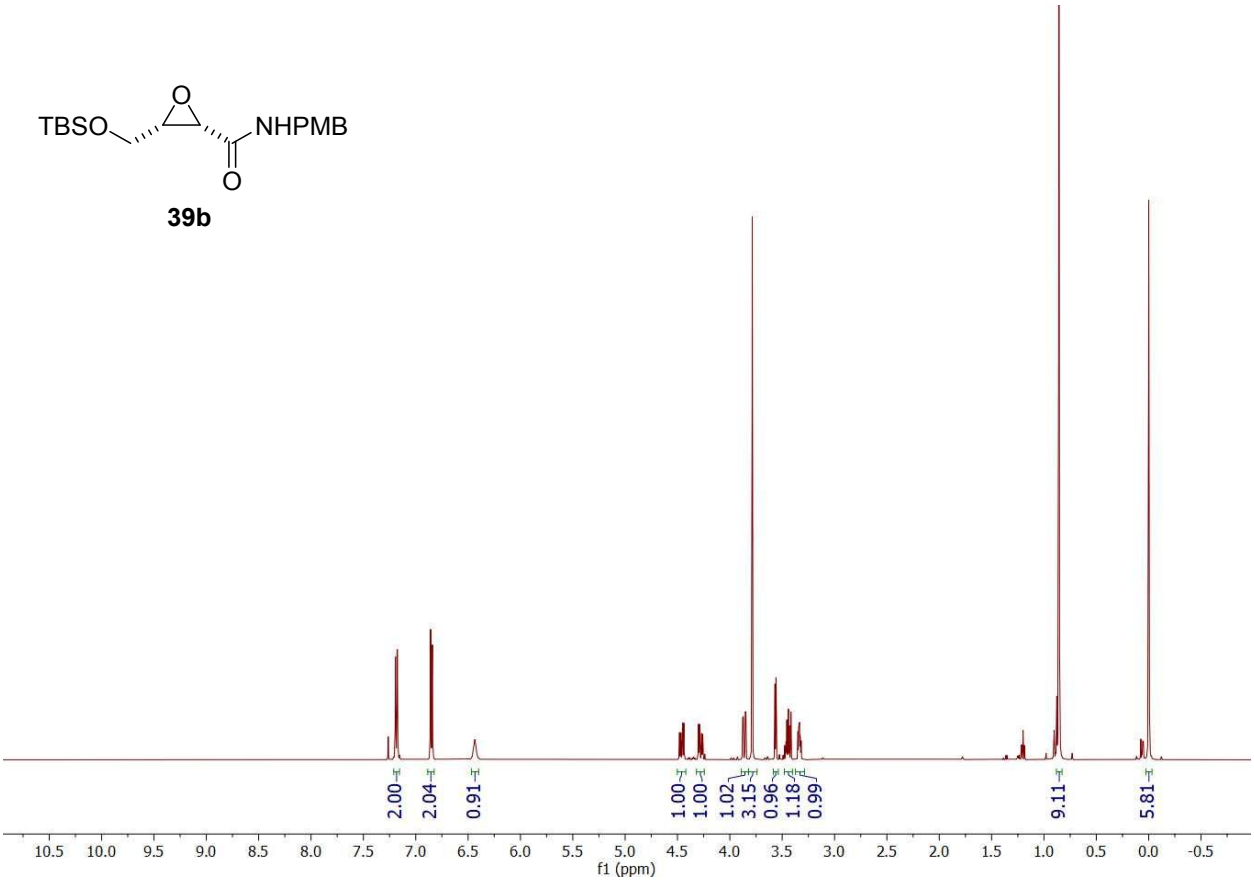

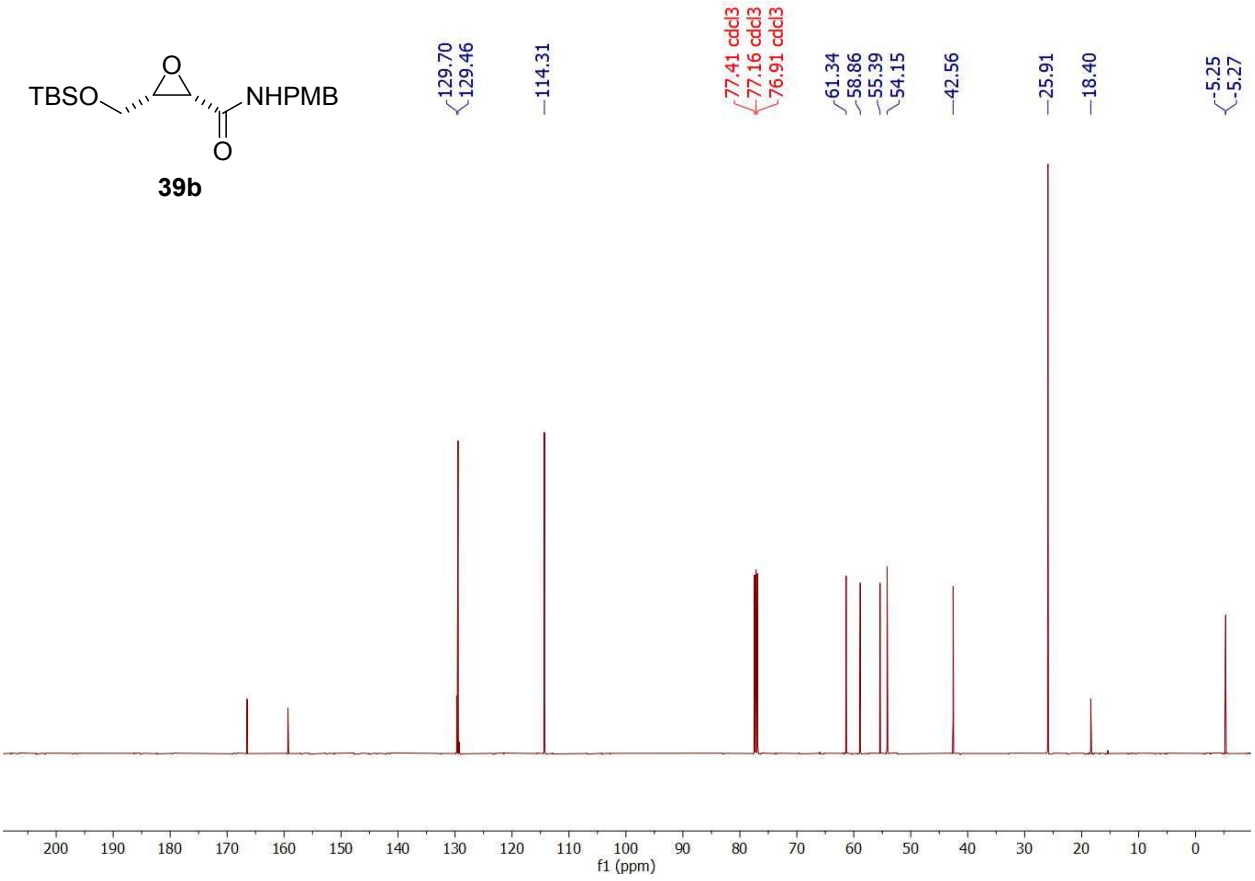
TBSO
NHPMB
O
O
39b
129.70
129.46
114.31
77.41 cdcl3
77.16 cdcl3
76.91 cdcl3
61.34
58.86
55.39
54.15
42.56
25.91
18.40
-5.25
-5.27
200 190 180 170 160 150 140 130 120 110 100 90 80 70 60 50 40 30 20 10 0
f1 (ppm)

(*2S,3S*)-**40a**-^{1}H-NMR (500 MHz -$CDCl_3$); $^{13}C\{^{1}H\}$ (126 MHz, $CDCl_3$)

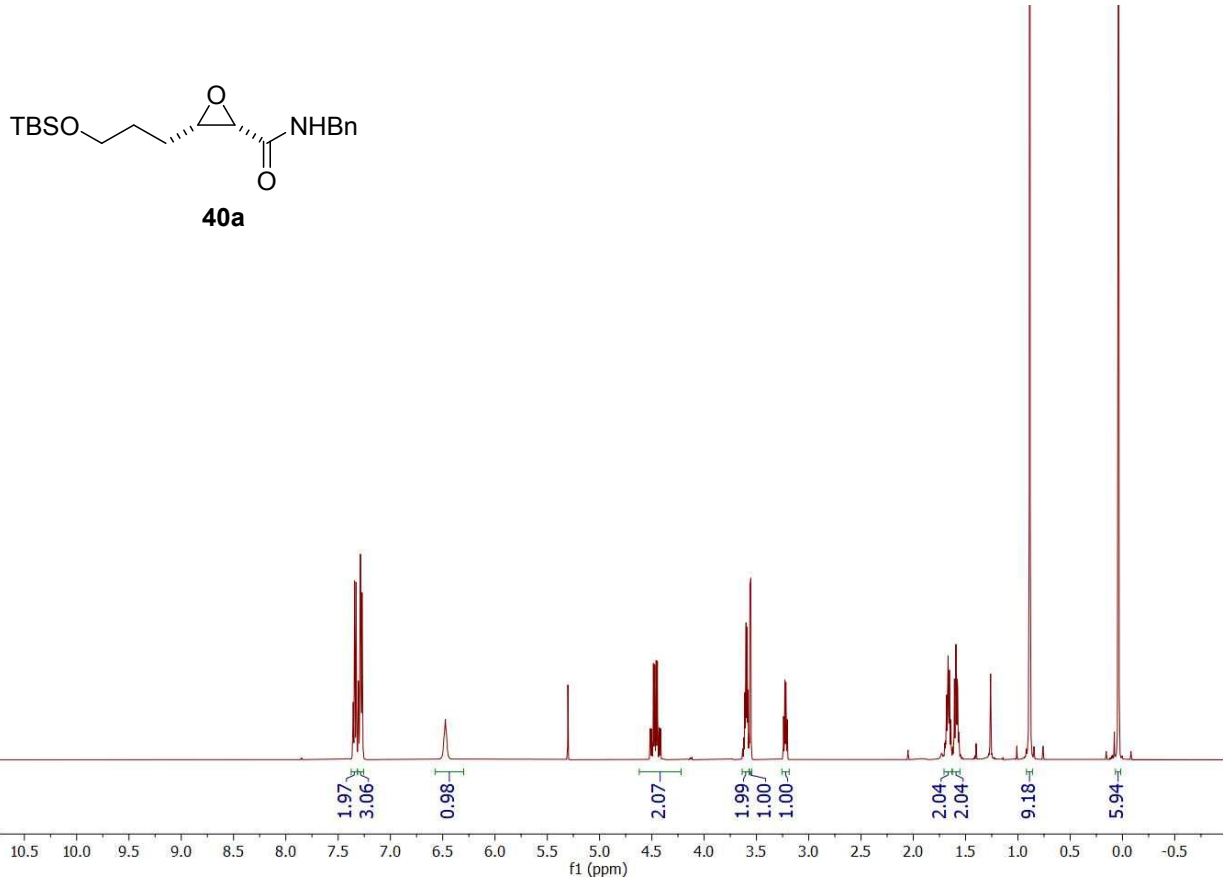

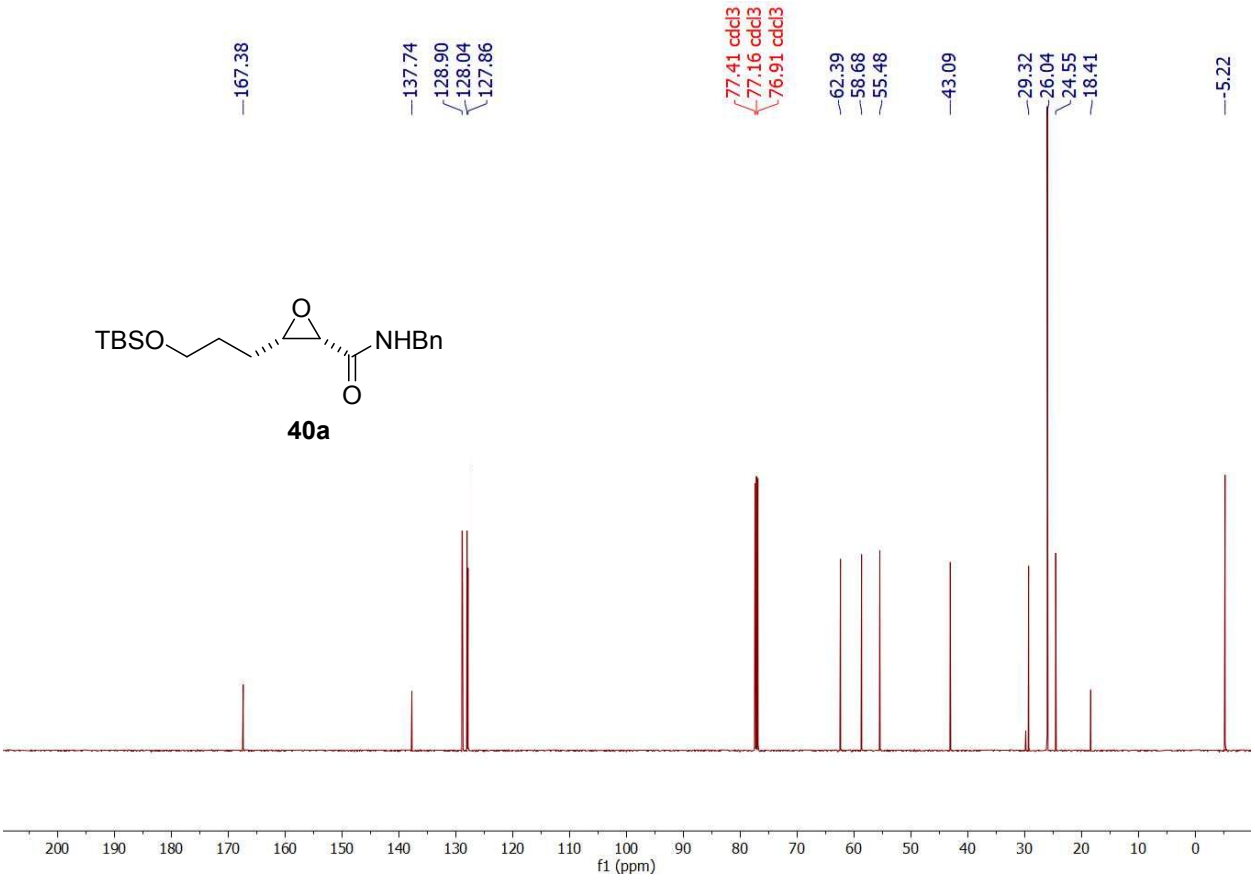
167.38
137.74
128.90
128.04
127.86
77.41 cdcl3
77.16 cdcl3
76.91 cdcl3
62.39
58.68
55.48
43.09
29.32
26.04
24.55
18.41
-5.22
TBSO
NHBn
O
O
40a
200
190
180
170
160
150
140
130
120
110
100
90
80
70
60
50
40
30
20
10
0
f1 (ppm)

(*2S,3S*)-**40b**-^{1}H-NMR (500 MHz -$CDCl_3$); $^{13}C\{^{1}H\}$ (126 MHz, $CDCl_3$)

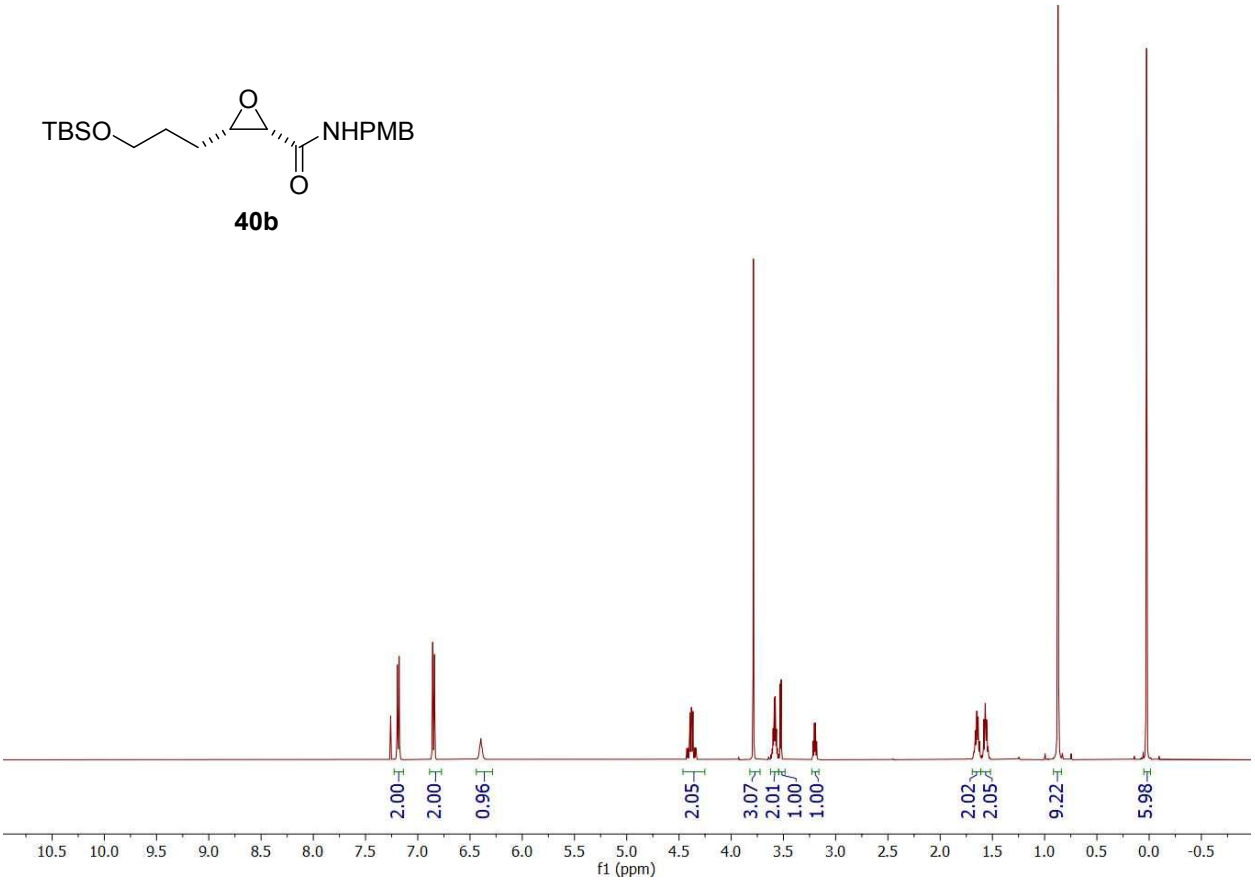

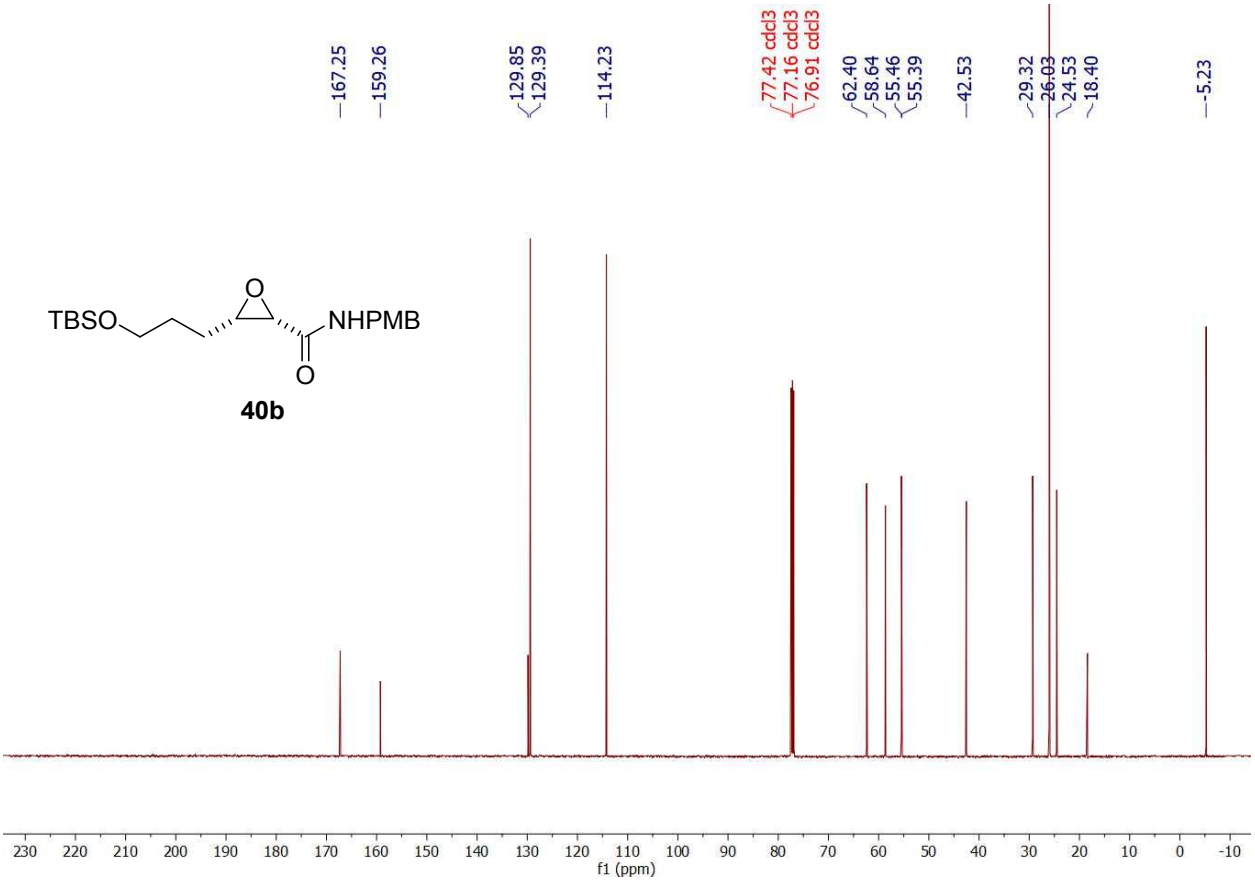
167.25
159.26
129.85
129.39
114.23
77.42 cdcl3
77.16 cdcl3
76.91 cdcl3
62.40
58.64
55.46
55.39
42.53
29.32
26.03
24.53
18.40
-5.23
TBSO
O
NHPMB
O
40b
230 220 210 200 190 180 170 160 150 140 130 120 110 100 90 80 70 60 50 40 30 20 10 0 -10
f1 (ppm)

(*2S,3S*)-**41a**-^{1}H-NMR (500 MHz -$CDCl_3$); $^{13}C\{^{1}H\}$ (126 MHz, $CDCl_3$)

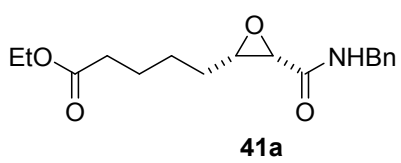

41a

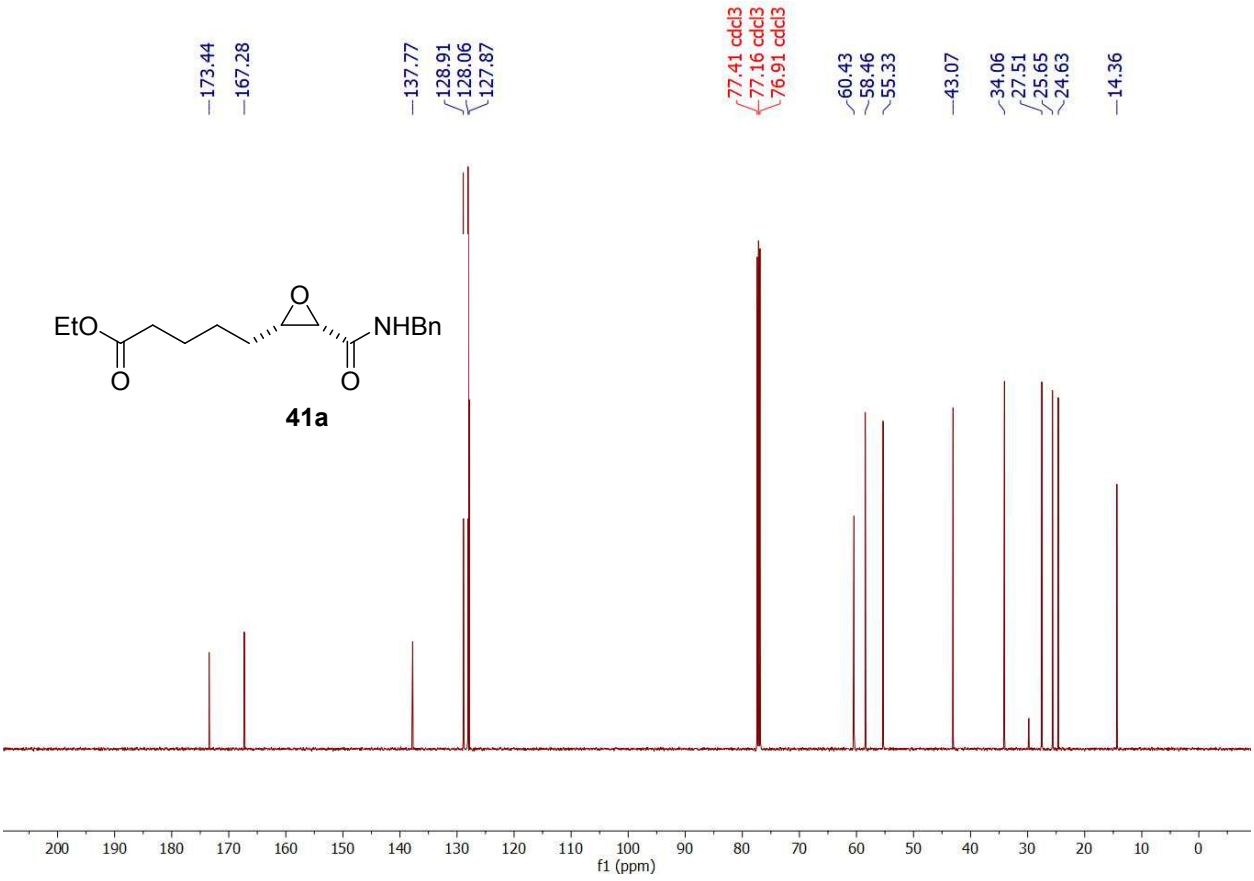
173.44
167.28
137.77
128.91
128.06
127.87
77.41 cdcl3
77.16 cdcl3
76.91 cdcl3
60.43
58.46
55.33
43.07
34.06
27.51
25.65
24.63
14.36
EtO
O
O
O
NHBn
41a
200
190
180
170
160
150
140
130
120
110
100
90
80
70
60
50
40
30
20
10
0
f1 (ppm)

(*2S,3S*)-**44**-^{1}H-NMR (500 MHz -$CDCl_3$); $^{13}C\{^{1}H\}$ (126 MHz, $CDCl_3$)

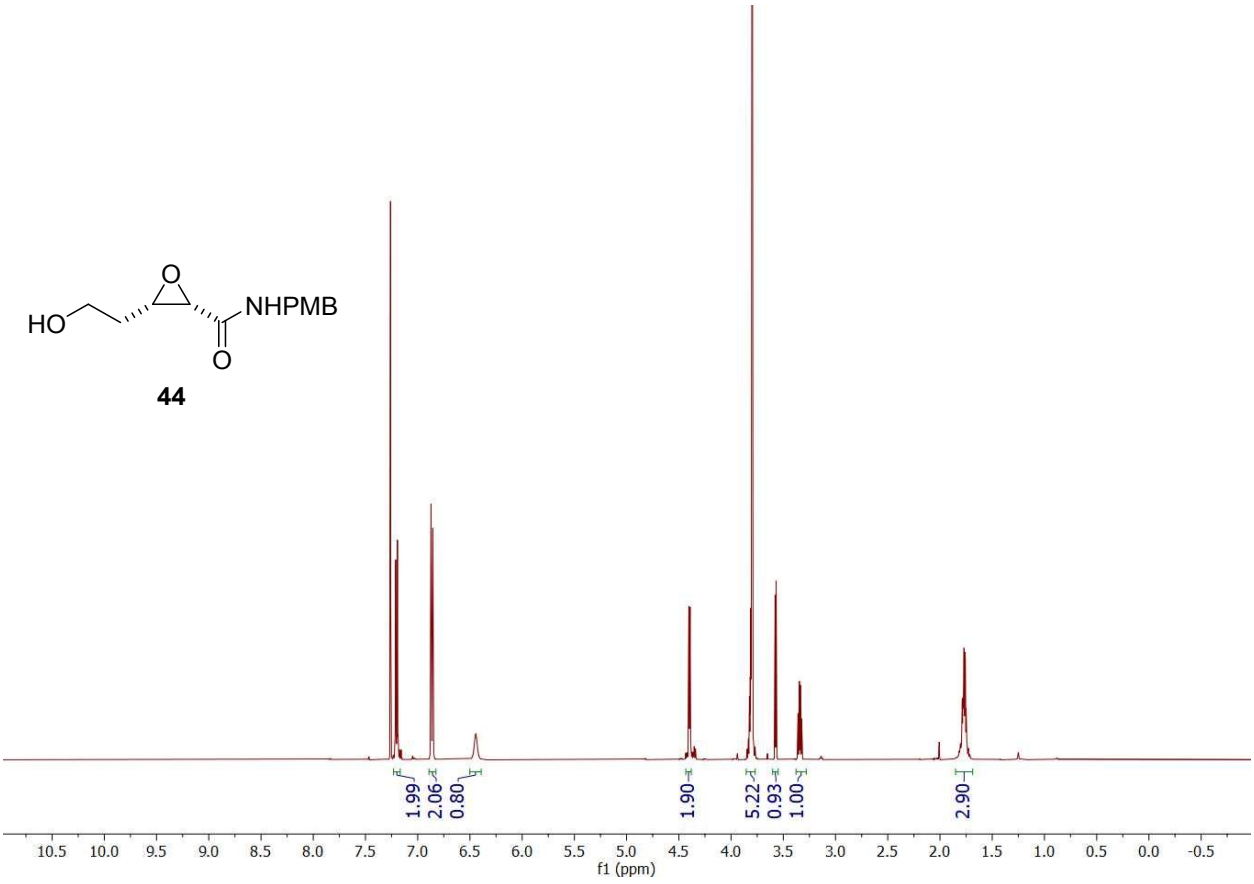

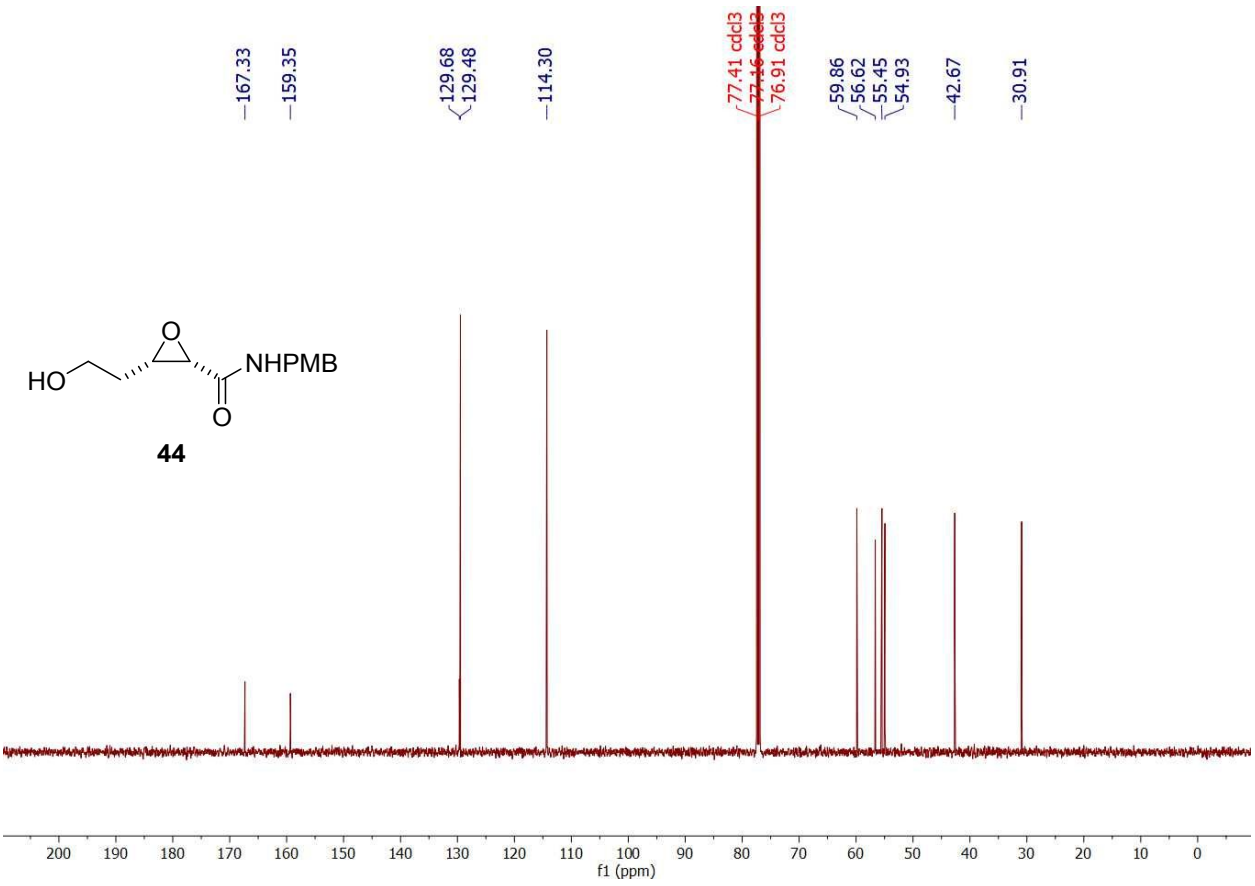
167.33
159.35
129.68
129.48
114.30
77.41 cdcl3
77.16 cdcl3
76.91 cdcl3
59.86
56.62
55.45
54.93
42.67
30.91
HO
O
NHPMB
O
44
200
190
180
170
160
150
140
130
120
110
100
90
80
70
60
50
40
30
20
10
0
f1 (ppm)

(*2S,3S*)-**45**-^{1}H-NMR (500 MHz -$CDCl_3$); $^{13}C\{^{1}H\}$ (126 MHz, $CDCl_3$)

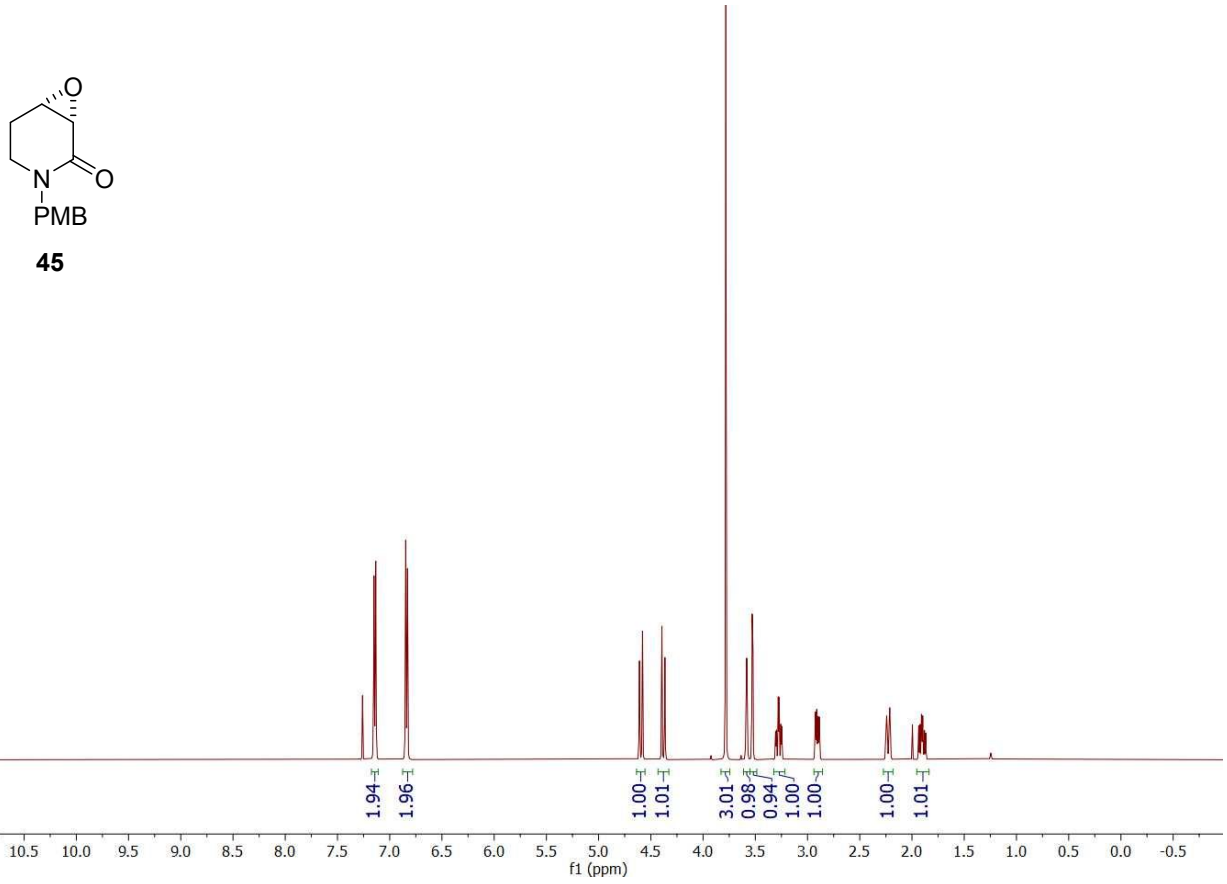

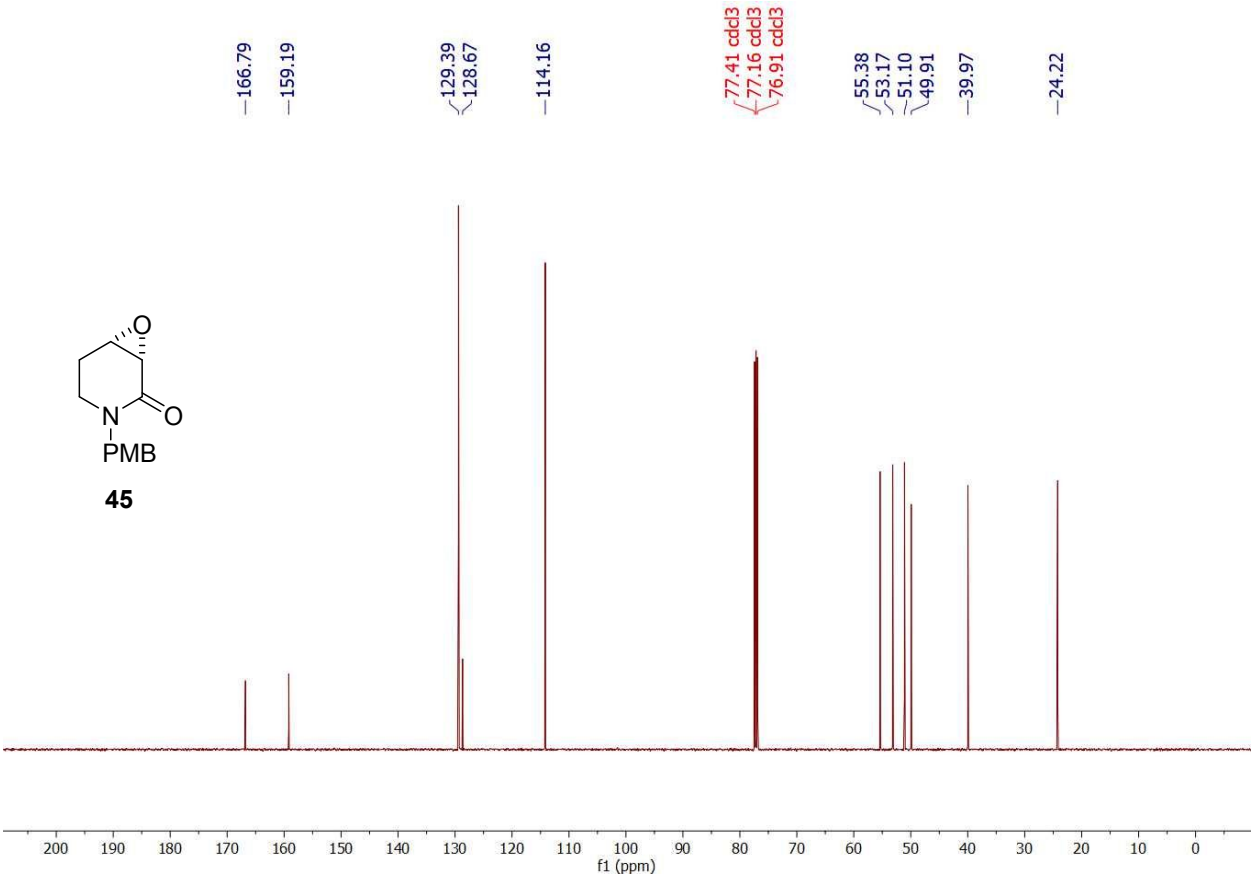
166.79
159.19
129.39
128.67
114.16
77.41 cdcl3
77.16 cdcl3
76.91 cdcl3
55.38
53.17
51.10
49.91
39.97
24.22
O
N
O
PMB
45
200 190 180 170 160 150 140 130 120 110 100 90 80 70 60 50 40 30 20 10 0
f1 (ppm)

(*2S,3S*)-**5**-^{1}H-NMR (500 MHz -$CDCl_3$); $^{13}C\{^{1}H\}$ (126 MHz, $CDCl_3$)

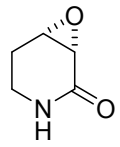

5

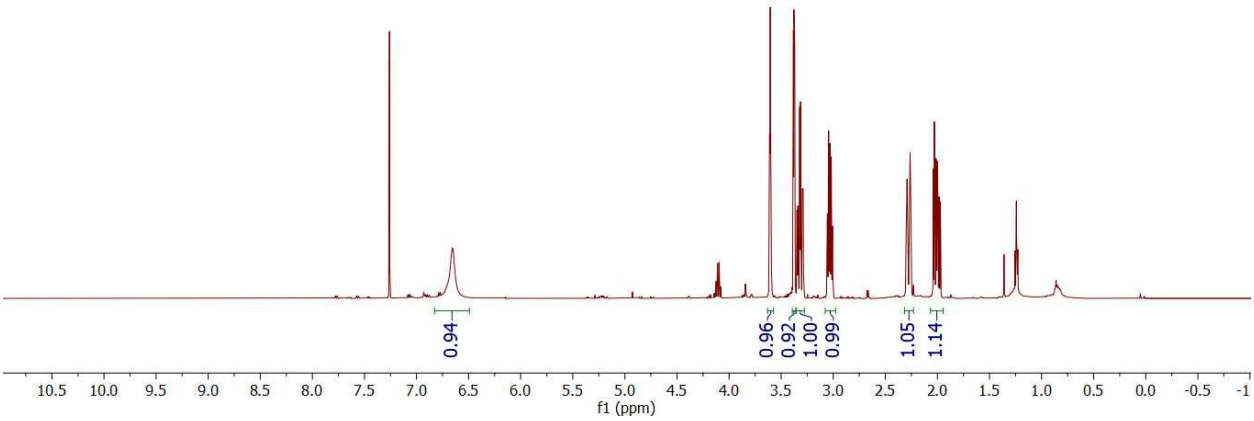

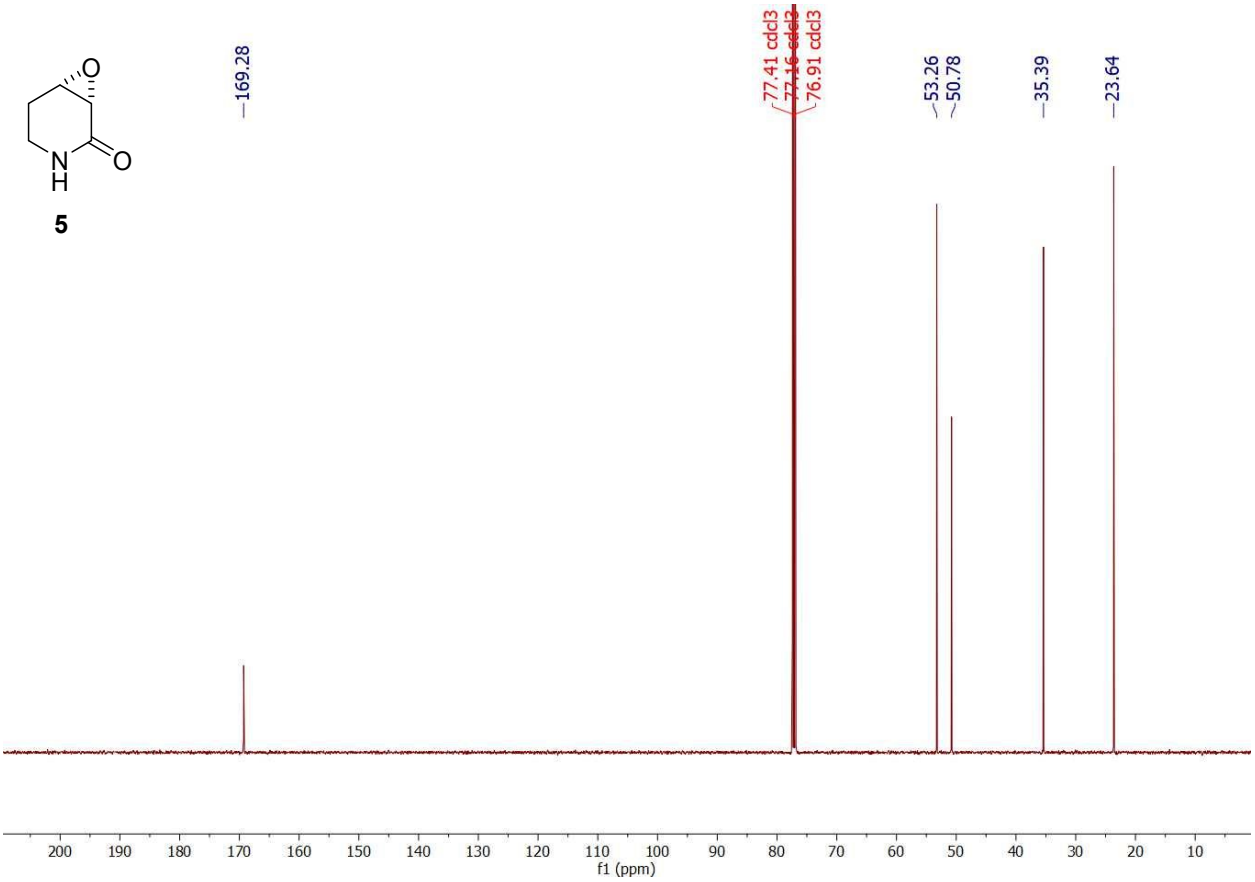
5
169.28
77.41 cdcl3
77.16 cdcl3
76.91 cdcl3
53.26
50.78
35.39
23.64
200 190 180 170 160 150 140 130 120 110 100 90 80 70 60 50 40 30 20 10
f1 (ppm)

1b-^{1}H-NMR (500 MHz -$CDCl_3$); $^{13}C\{^{1}H\}$ (126 MHz, $CDCl_3$)

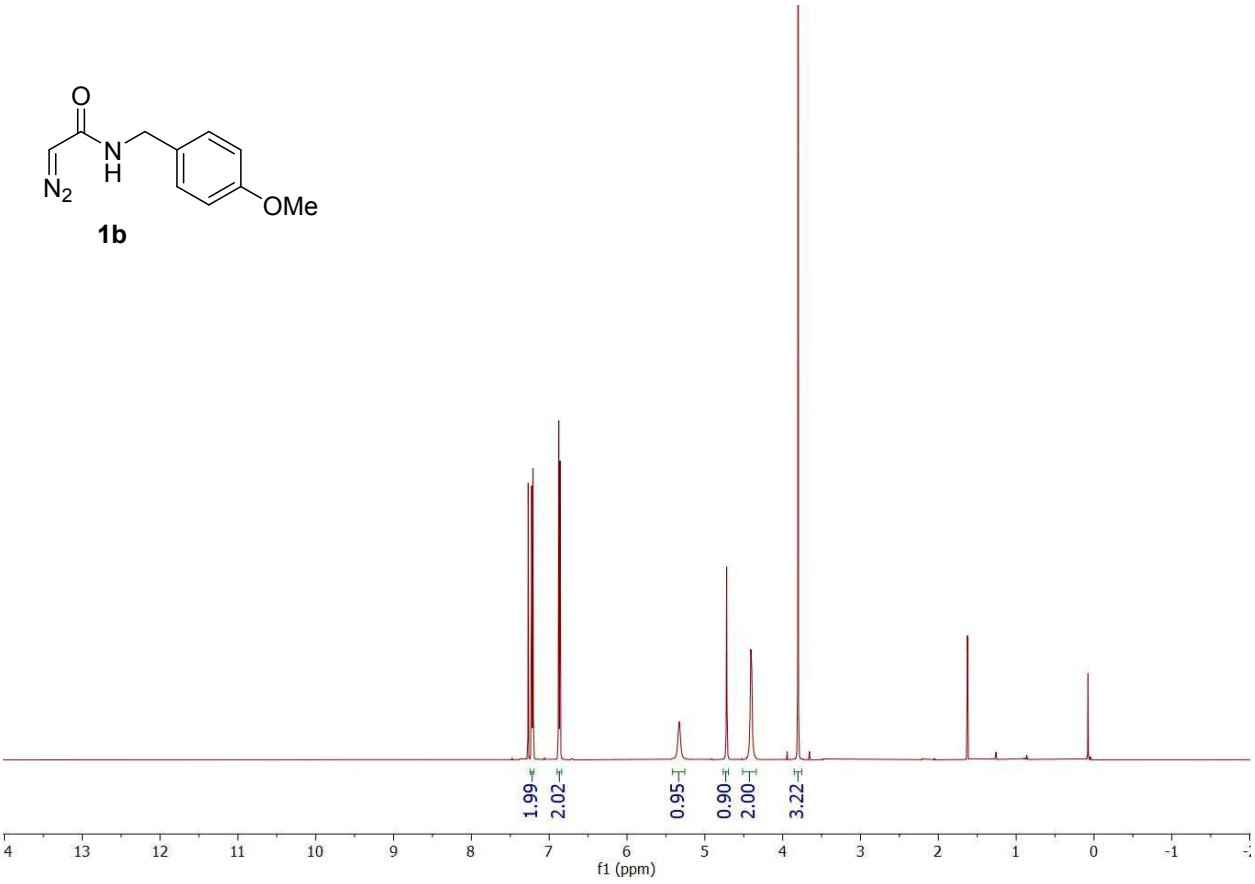

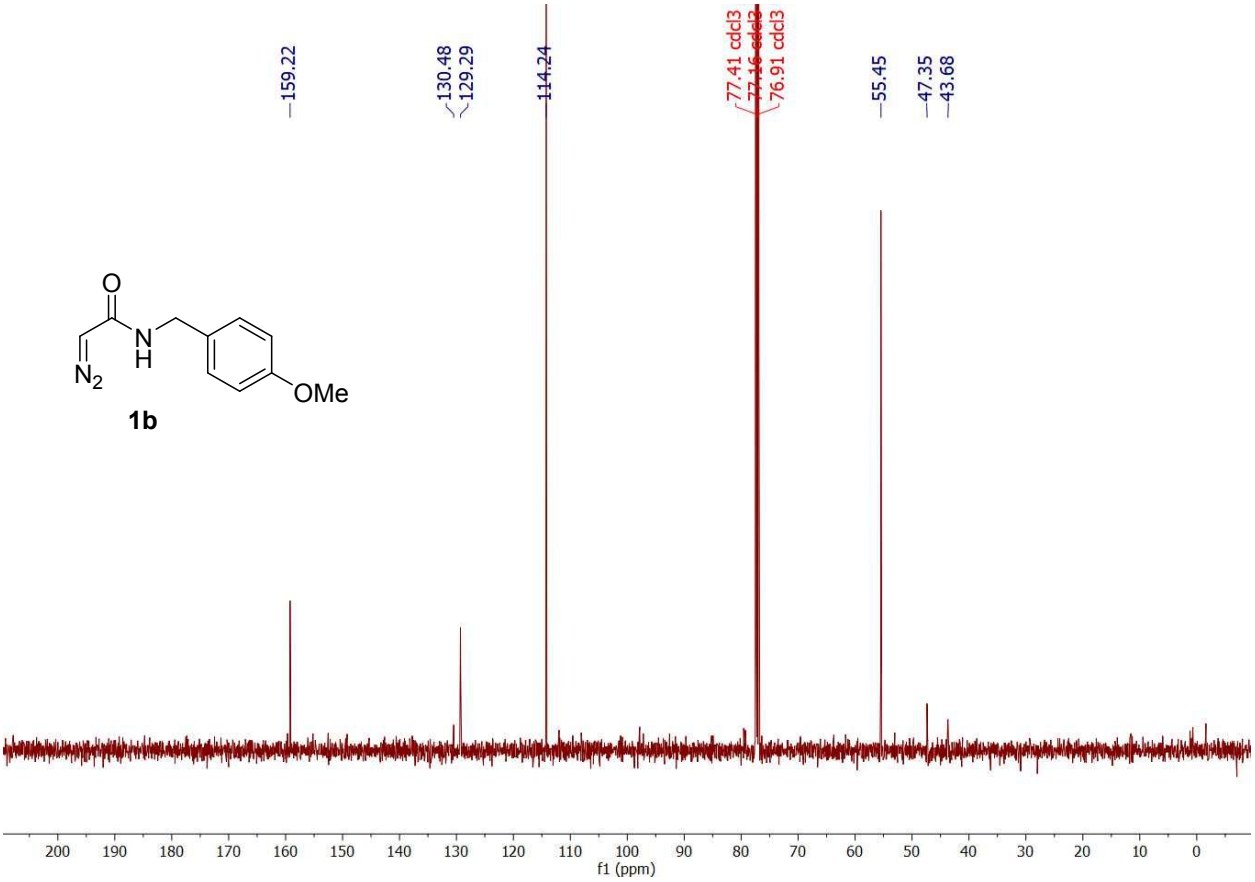
159.22
130.48
129.29
114.24
77.41 cdcl3
77.16 cdcl3
76.91 cdcl3
55.45
47.35
43.68
O
N
H
N2
OMe
1b
200 190 180 170 160 150 140 130 120 110 100 90 80 70 60 50 40 30 20 10 0
f1 (ppm)